NONLINEAR CONTROL OF UNMANNED AIRCRAFT FORMATIONS

A THESIS SUBMITTED TO
THE GRADUATE SCHOOL OF NATURAL AND APPLIED SCIENCES
OF
MIDDLE EAST TECHNICAL UNIVERSITY

BY

SEGUN ARIYIBI

IN PARTIAL FULFILMENT OF THE REQUIREMENTS
FOR
THE DEGREE OF MASTERS OF SCIENCE
IN
AEROSPACE ENGINEERING

FEBRUARY 2014

Approval of the thesis:

NONLINEAR CONTROL OF UNMANNED AIRCRAFT FORMATIONS

Submitted by **SEGUN ARIYIBI** in partial fulfillment of the requirements for the degree of **Master of Science in Aerospace Engineering Department, Middle East Technical University** by,

Prof. Dr. Canan Özgen   _____
Dean, Graduate School of **Natural and Applied Sciences**

Prof. Dr. Ozan Tekinalp   _____
Head of Department, **Aerospace Engineering**

Prof. Dr. Ozan Tekinalp   _____
Supervisor, **Aerospace Engineering Dept., METU**

Examining Committee Members:

Prof. Dr. Serkan Özgen
Aerospace Engineering Dept., METU   _____

Prof. Dr. Ozan Tekinalp
Aerospace Engineering Dept., METU   _____

Assoc. Prof. Dr. Melin Şahin
Aerospace Engineering Dept., METU   _____

Asst. Prof. Dr. Ali Türker Kutay
Aerospace Engineering Dept., METU   _____

Prof. Dr. Reşit Soylu
Mechanical Engineering Dept., METU   _____

                                                 Date: **February 06, 2014**

I hereby declare that all information in this document has been obtained and presented in accordance with academic rules and ethical conduct. I also declare that, as required by these rules and conduct, I have fully cited and referenced all materials and results that are not original to this work.

Name, Last Name: SEGUN ARIYIBI

Signature   :

ABSTRACT

NONLINEAR CONTROL OF UNMANNED AIRCRAFT FORMATIONS

Ariyibi, Segun

M.S, Department of Aerospace Engineering

Supervisor: Prof. Dr. Ozan Tekinalp

February 2014, 114 pages

In this thesis, a leader-follower approach is employed to make two unmanned aircrafts fly in a fixed geometrical formation. The first aircraft in the formation is designated as leader and the second is treated as the follower. The leader maintains a prescribed trajectory while the follower tracks and maintains a fixed relative distance from its leader. Since the associated kinematic equations are nonlinear, the relative guidance of the follower using two nonlinear control approaches, the Lyapunov based control algorithm and the State Dependent Riccati Equation, (SDRE) based algorithms are proposed. After the formation control problem has been solved, the follower must fly in certain attitudes for it to realize the desired flight paths needed to fly in the desired geometrical formation. This is called the attitude control problem.

Simulations and tests of our proposed algorithms were carried out using a linear model of the SIG RASCAL 110 UAV for both the leader and follower UAV. Lyapunov and SDRE algorithm were used to solve the formation control problem, while linear quadratic tracking, (LQT) controllers were used on the linear models for the attitude control problems.

Keywords: UAV, Autonomous Formation flight, SDRE, Lyapunov, Leader-follower approach

ÖZ

İNSANSIZ HAVA ARAÇLARININ KOL UÇUŞUNUN DOĞRUSAL OLMAYAN KONTROLÜ

Ariyibi, Segun

Yüksek Lisans, Havacilik ve Uzay Mühendisliği Bölümü

Tez Yöneticisi: Prof. Dr. Ozan Tekinalp

Şubat 2014, 114 sayfa

Bu tezde iki insansız uçağı sabit geometrik bir formasyonda uçurmak için bir lider-takipçi yaklaşımı çalışılmıştır. Formasyondaki ilk uçak lider olarak ikincisi ise takipçi olarak belirlenmiştir. Lider önceden belirlenmiş bir rotayı takip ederken takipçi lidere göre sabit bir konumu korumayı hedeflemektedir. İlgili kinematik denklemler doğrusal olmadığından takipçinin göreceli güdümü için Lyapunov tabanlı ve Duruma Bağlı Ricatti Denklemi (SDRE) olmak üzere iki doğrusal olmayan kontrol yöntemi önerilmiştir. Formasyon kontrol problemi çözüldükten sonra takipçinin istenen göreceli konumu koruması için takip etmesi gereken rota belirlenir. Bu rotayı takip edebilmesi için takipçinin belli açısal konumlara sahip olması gerekmektedir. Takipçinin gereken açısal konumlara getirilmesi yönelim kontrol problemi olarak adlandırılmaktadır.

Önerilen algoritmaların simülasyonu ve testi lider ve takipçi için SIG RASCAL 110 İnsansız Hava Aracının (İHA) doğrusal modeli kullanılarak gerçekleştirilmiştir. Doğrusal İHA modellerinin yönelim kontrolü için LQT kontrolcüler kullanılırken formasyon kontrol problemi Lyapunov ve SDRE algoritmaları ile çözülmüştür.

Anahtar Kelimeler: İnsansız Hava Aracı, Otonom Kol Uçuşu, Duruma Bağlı Ricatti Denklemi, Lyapunov, Lider-Takipçi Yaklaşımı

To my family

ACKNOWLEDGEMENT

I would like to express my deepest and sincerest gratitude to my thesis supervisor, Prof. Dr. Ozan Tekinalp. Without his devotion, I would not have been able to complete this thesis; we practically wrote the thesis together. He provided invaluable ideas and shared with me his wealth of knowledge which facilitated the completion of the thesis.

TABLE OF CONTENTS

LIST OF TABLES

TABLES

LIST OF FIGURES

FIGURES

LIST OF SYMBOLS AND ABBREVIATIONS

ABBREVIATION DEFINITIONS

UAV   Unmanned Aerial Vehicle

SDRE   State Dependent Riccati Equation

FGC   Formation Geometry Center

LQT   Linear Quadratic Tracker

UCAV Unmanned Combat Aerial Vehicle

SDC   State Dependent Coefficient

ARE   Algebraic Riccati Equation

ROMAN SYMBOLS

v_{hL} , v_{hf} Leader and follower aircraft velocities

h_L , h_f Leader and follower aircraft altitudes

(x,y,z) Actual relative position of the follower UAV with respect to the leader UAV

(x_f,y_f,z_f) Coordinate axes of the follower reference frame

h_{fc} Reference altitude for follower aircraft to track desired formation geometry

v_{fc} Reference velocity for follower UAV to track desired formation geometry

r_{fc} Reference yaw rate for a coordinated turn for Φ_{fc}

$(x_{ref},y_{ref},z_{ref})$ Desired relative position of the follower UAV with respect to the leader UAV

GREEK SYMBOLS

ψ_L , ψ_f Leader and follower aircraft heading angles

$\dot{\psi}_f$ Follower heading rate

Φ_{fc} Reference altitude for follower aircraft to track desired formation geometry

Ψ_e Leader heading minus follower heading

CHAPTER 1

INTRODUCTION

1.1   Overview

Interests in unmanned aerial vehicles (UAV) have been growing over recent years and for the right reasons. An unmanned aerial vehicle is an aircraft without a human pilot on board. They can be controlled autonomously by computers on board or remotely controlled by a pilot situated on the ground or in another vehicle [1]. Since UAVs do not require an aircrew, they are much smaller in size than manned aircrafts. Their small size as well as an absence of an aircrew thereby reduce manufacturing and operational costs and provide various advantages over manned aircrafts. The elimination of the aircrew means that UAVs are able to fly longer, faster and perform tighter and faster maneuvers as opposed to a manned aircraft due to the absence of human physical limitations. The can also perform dangerous missions without the risk of losing human lives [2]. UAVs find their use in military and civilian operations. Civilian applications include domestic policing, oil and gas exploration, scientific research, search and rescue, and surveillance missions like livestock monitoring, wildfire mapping and forest fire detection. Military applications include intelligence, surveillance and reconnaissance, maritime operations, combat missions (Unmanned Combat Air Vehicle, UCAV), electronic warfare [1], [2].

When two or more aircraft fly together by keeping the relative distances among each other the same, such a flight is called formation flight. There are a number of advantages of a formation flight. Using formation flights in surveillance missions enables the synthesis of antennas with dimensions far larger than using a single aircraft thereby leading to an increased sensitivity of the antennas and consequently leading to better information gathering. Flying aircrafts in a V-flight formation leads to a reduction in the induced drag of each of the aircrafts in the formation. NASA Dryden Research Center carried out a formation flight test on two F/A-18 aircrafts. The results obtained from this formation flight test showed reduction in induced drag of more than 20% and a reduction in fuel consumption by more than 18% at a flight condition of Mach 0.56 and altitude of 25000ft [3]. Fowler, J.M. and Andrea, R.D. conducted an experiment on a large formation of 31 wings; the result showed an induced drag reduction of up to 41% is possible [4]. This reduction in drag leads to a reduction in fuel or power needed to operate the UAVs. Military use formation flight for defensive reasons as well as concentration of offensive power. A formation flight could also be employed in an aerial refueling scenario.

There are numerous types of formation geometries of aircrafts depending on the number of aircrafts in the formation and the purpose of the formation flight. The V-formation flight as discussed earlier has the beneficial effect of reducing the induced drag on the individual aircrafts in the formation consequently leading to an increased flight range. In military operations, especially in World War 2, the 3-aircraft V-formation geometry was the standard formation geometry used. It afforded a concentration of offensive power for bombers and

also improved visual contact with enemy aircrafts. This formation geometry is still been used in the modern era as well.
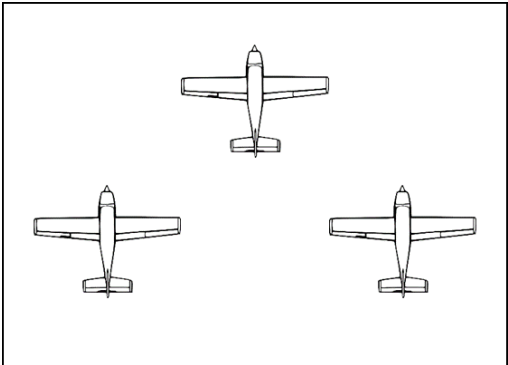
Figure 1.1: V-Formation Geometry

There are several other formation geometries such as the finger-four formation geometry, wall formation geometry, ladder formation geometry, missing man formation geometry and so on. However, this thesis focuses on the formation flight of two aircrafts. For a 2-aircraft formation flight, there are three basic formation geometries. They include the echelon formation geometry (left or right), line abreast formation geometry and the trail formation geometry. In all the three formation geometries mentioned above, one aircraft is designated as the leader and the other is designated as the follower. The job of the follower is to maintain its relative position to the leader while the leader directs the formation as a whole. In the echelon formation geometry, the follower is behind and to the side of the leader. If the follower is to the left, it is called an echelon left formation, and if the follower is to the right of the leader, it is called an echelon right formation.
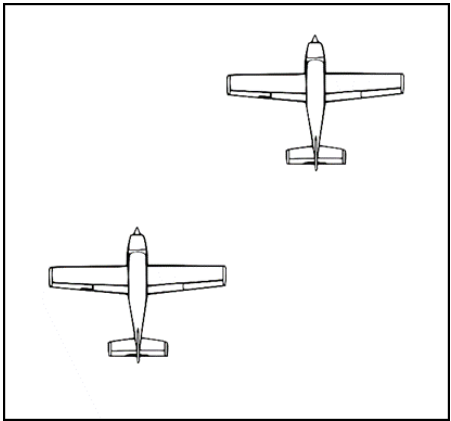
Figure 1.2: Echelon Left Formation Geometry
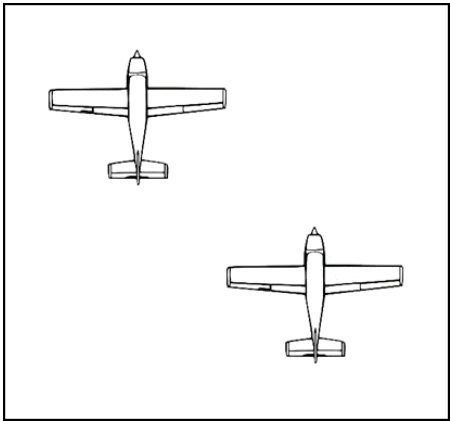
Figure 1.3: Echelon Right Formation Geometry

2

In the line abreast formation geometry, the leader and the follower fly side by side. The follower can be either to the left side or the right side of the leader.
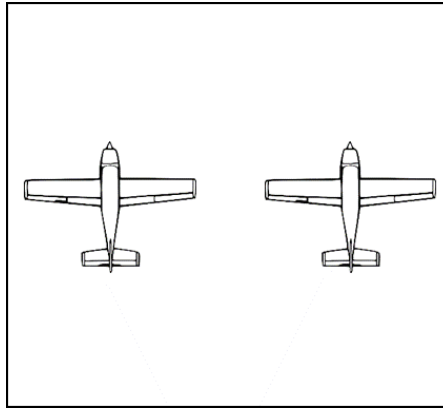
Figure 1.4: Line Abreast Formation Geometry

In the trail formation geometry, the follower is directly behind the leader.
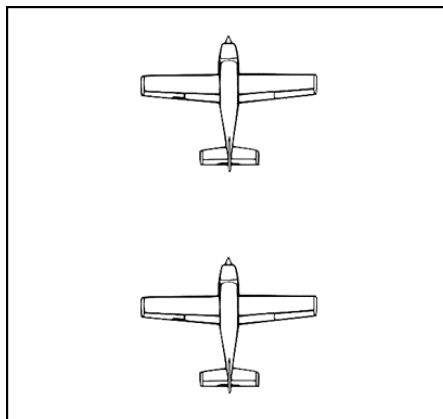
Figure 1:5: Trail formation geometry

Any of these three basic formation geometries described above can also be stepped. In other words, the leader and follower fly at different altitudes. If the follower flies at a higher altitude than the leader, it is called a stepped up formation geometry and if the follower flies at a lower altitude, it is called a stepped down formation geometry.

1.2 Purpose of the Thesis

The aim of this thesis is to design an algorithm for an autonomous formation flight of two unmanned aerial vehicles. Full linear dynamics of the SIG RASCAL 110 UAV is used in testing the algorithm.

1.3   Literature Survey

Several researches have been carried out to tackle the problem of creating an efficient autonomous formation flight. Individual members of the formation must avoid colliding with one another as well as with obstacles in their path. If required, formation's geometry should be maintained during maneuvering. For example, a multitude of UAVs must fly in a V-flight formation to take full advantage of the reduction in induced drag that comes with such formation. To tackle the problems listed above as well as several other problems that come with an autonomous formation flight, several proposals have been made. Most of the existing literature deal with the problem of automatic formation control while fixed formation geometry is assumed.

There are six main approaches in the literature to tackle the problem of autonomous formation flight. These approaches are:

1)   Leader-Follower approach
2)   Virtual Leader approach
3)   Virtual Structure approach
4)   Virtual Reference Point approach
5)   Behavioral Approach
6)   Formation Graph Approach

The leader-follower approach exists predominantly in the literature because of the ease in implementing it and also because its approach is similar the approach employed in real life manned formation flights. In the leader-follower approach, some of the aircrafts in the formation are designated as leader and the rest of the aircrafts are treated as followers. The leaders maintain a prescribed trajectory while the followers track a fixed relative distance from the neighboring aircraft. Thus, the formation behavior is prescribed by specifying the relative distances that the followers must maintain. The followers have the formation-hold autopilot implemented on them. The downside of this approach is that a rear aircraft usually exhibits a poorer response than its reference due to error propagation and it is not robust to leader's failure. [5], [6]. The Virtual Leader approach was introduced to counter the problems of the Leader-Follower approach. In this approach, to create robustness to leader's failure, all the aircrafts in the formation receive the trajectory of a virtual leader. This trajectory is usually an ideal point in the formation that the corresponding aircraft must track. The downside of this approach is that the individual members of the formation have no idea about their relative distances to one another and subsequently, collision avoidance might be impossible [6]. In the virtual structure approach, the concept of leaders and followers is non-existent. The constituent aircrafts of the formation are treated as if they were particles of a rigid body. In other words, the entire formation is treated like a single rigid body structure, hence the name virtual structure [7], [8]. In [8], a virtual structure is defined as *"A virtual structure is a collection of elements, e.g. robots, which maintain a (semi) rigid geometric relationship to each other and a frame of reference"*. Due to the fact that the entire formation move as a single rigid body and the individual members of the formation always maintain a fixed geometric relationship with one another, it is impossible to use this approach for formations that vary with time. In the virtual reference point approach, all

UAVs in the formation try to maintain prescribed relative distances and angles from a virtual reference point. This reference point is usually a moving point on a pre-designed reference trajectory. The upside of this approach is that formation reconfiguration is easy to implement just by changing the coordinates of the reference point and the reference trajectory [9]. The behavioral approach entails prescribing desired behaviors for each vehicle in the formation; these behaviors may be formation keeping, collision avoidance, obstacle avoidance. The control action of each aircraft is a weighted average of the control for each behavior [6]. This approach also makes use of an imaginary point in the formation called a Formation Geometry Center (FGC), this FGC method was introduced by Giulietti et al. [10]. Each aircraft in the formation maintains a prescribed distance from the FGC. This distance depends on the relative distances among the aircrafts in the formation. This FGC approach ensures that individual members of the formation are aware of the positions of other members in the formation and it also provides some sort of feedback to the formation. In the formation graph approach, the relative positions of the aircrafts in the formation are determined using graph theory [11]. In [11], formation graph is defined as "*The formation graph of n aircraft is defined as an undirected graph* $G = (V, \varepsilon)$*, where* $V = \{1, 2, ..., n\}$ *is a finite set of vertices (nodes) in correspondence with the n aircraft in the group, and* $\varepsilon \subseteq VxV$ *is a set of edges* (i, j) *representing interaircraft position specifications. The neighborhood set of the aircraft* $i, N_i = \{j \mid (i, j) \in \varepsilon, j \neq i\}$*, includes all other aircraft which communicate with it.*"

After selecting an approach to the formation problem, a control scheme has to be adopted. Lots of control schemes have been implemented. In [5], proportional and integral control was used on a leader-follower approach. First-order dynamics were used to model both the leader and the follower UAVs. A kinematic relationship for the relative distance of the follower UAV with respect to the leader UAV was derived. The resulting equations were then linearized and a PI controller was designed using the resulting linearized kinematic relations. In [11], Constraint forces control approach were used on a formation graph approach. Constraint forces control approach involves determining the total force required on each aircraft in the formation to maintain the desired formation geometry. The constraint force control approach involved imposing geometric constraints on the system of aircrafts by adding a set of constraint forces to the governing equations that keep the constraints satisfied. The overall control input required for each aircraft to achieve or maintain a formation is the sum of the applied force per unit mass and the constraint force per unit mass that limits the motion of the system to be consistent with the constraints. In [12], potential field method was used on a virtual leader approach. The potential field method involves generating a potential field for each vehicle in the formation based on the desired and actual formation geometry. These fields are used to avoid obstacles in the path of the formation as well as to avoid collision among the aircrafts in the formation. A number of factors influence the potential field generated on a particular aircraft in the formation. These factors include the virtual leader since a virtual leader approach was employed, the other aircrafts in the formation, the presence of obstacles in the path of that aircraft and the proximity of the other aircrafts in the formation to it. In [13], High order sliding mode control scheme was implemented on a leader-follower approach. In [14], an adaptive output feedback control scheme is used. Various other control schemes exist in literature as well.

In this thesis, SDRE control algorithm as well as a Lyapuvov based control scheme is implemented on a leader-follower approach. Full linear dynamics of the UAVs are used in testing the formation-control algorithm. The state dependent ricatti equation (SDRE) control method has become quite popular over the last decade. It is a nonlinear control technique for synthesizing nonlinear feedback controls by allowing nonlinearities in the system states while also offering great design flexibility through state-dependent weighting matrices [15]. This method has been extensively studied by pearson [16], Wernli and Cook [17], and Mracek and Cloutier [18]. The SDRE algorithm captures the nonlinearities of a system by converting the nonlinear system to a linear-like structure using state-dependent coefficient (SDC) matrices. In this way, the controller gains are frequently computed ensuring the stability and performance of the nonlinear system. Thus, an Algebraic Riccati equation, (ARE) with SDC matrices is then solved on-line to obtain the control gains. Consequently, algebraic Riccati equation becomes state-dependent Riccati equation, or SDRE. SDRE control algorithm is used predominantly in spacecraft attitude control problems as well as in the development of flight control systems for quadrotors. However, the SDRE control algorithm has not been extensively utilized for the nonlinear flight regimes of fixed wing aircrafts as well as unmanned aerial vehicles.

In this thesis, the simulations and tests of our proposed algorithms are carried out using a linear model of the SIG RASCAL 110 UAV for both the leader and follower UAV. Lyapunov and SDRE algorithm are used to solve the formation control problem, i.e., the determination of the required guidance law for the follower UAV to maintain the desired formation. Linear quadratic optimal tracking controllers (LQT) are implemented on the linear models for the attitude control problems. The formation-hold controllers determine the required reference signals required to track the desired formation geometry. These reference signals are then sent to the follower, tracking this reference signals by the follower is the attitude control problem of the follower.

1.4   Contributions of the Thesis

An SDRE based nonlinear controller as a guidance loop is the main contribution of this thesis. In addition a Lyapunov based guidance scheme is also proposed and the effectiveness of both guidance schemes are demonstrated.

1.5   Contents of the Thesis

In chapter 1, the definition and advantages of formation flight are discussed. Also, various approaches to tackle the autonomous formation flight of UAVs as well as the control algorithms used are discussed. The various types of formation geometries for a 2-aircraft formation flight are also discussed.

In chapter 2, the formulation of the problem is discussed. The derivation of the formation kinematics and the control algorithms chosen are discussed. The overall structure of the

formation-hold control system to be designed is also discussed. The design of the formation control algorithm's inner loop controllers are discussed.

Chapter 3 presents the SDRE based controller. The approach used in the application of the SDRE to the formation flight is also given. The SDRE tuning technique and the impact of its update rate is discussed as well. Three formation flight scenarios are used to test and evaluate the performance of the SDRE based formation flight controller. The results of the tests are given and discussed.

In chapter 4, a Lyapunov based formation flight controller is designed. The approach used in designing the formation flight controller is discussed. As in chapter 3, three formation flight scenarios are used to test and evaluate the performance of the Lyapunov based formation flight controller. The results of the tests are given and discussed.

In chapter 5, Performance comparisons between the Lyapunov based and the SDRE based formation control systems are made.

Finally, in chapter 6, conclusions are made from the performances of the two nonlinear controllers. Also, recommendations for future works are given.

CHAPTER 2

FORMULATION OF THE PROBLEM

2.1   Formation Kinematics

In this thesis, the Leader-follower approach is the information structure chosen to solve our formation problem. In the leader-follower approach, one aircraft in the formation is designated as leader and the rest of the aircrafts are treated as followers. The leaders maintain a prescribed trajectory while the followers track a fixed relative distance from the neighboring aircraft. The formation behavior is therefore prescribed by specifying the relative distances the followers must maintain. Thus, a kinematic relation of the relative distance between the Leader and follower UAV has to be derived.
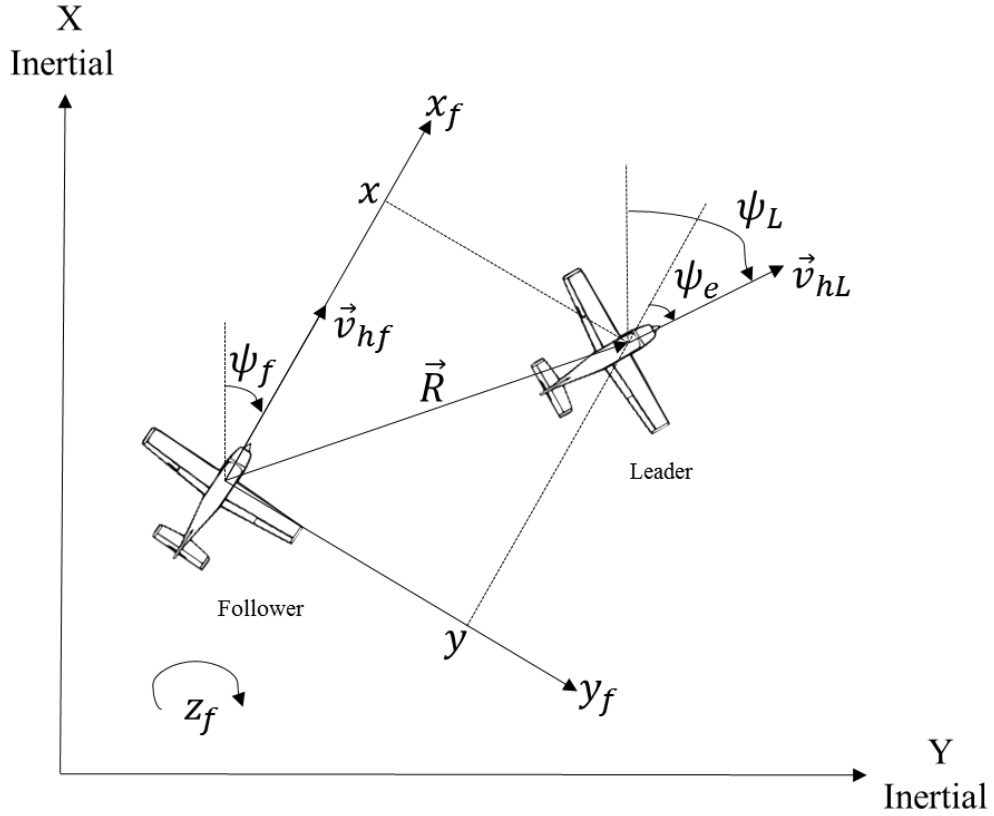
Figure 2.1: Formation Geometry

Using the above figure, a kinematic relation of the relative distance of the leader UAV with respect to the follower UAV is derived [19]. In the derivation process, two reference frames are used. An inertial horizontal reference frame and a rotating reference frame. The rotating reference frame is attached to the follower UAV. $\vec{v}_{hL}$ is the velocity vector of the leader UAV with respect to the inertial horizontal frame. Likewise, $\vec{v}_{hf}$ is the velocity vector of the

follower UAV with respect to the inertial horizontal frame. ψ_L, ψ_f respectively represent the heading of the leader and follower UAVs with respect to the inertial horizontal frame. $\psi_e = \psi_L - \psi_f$. $\vec{R}$ is the position vector of the leader UAV with respect to the follower UAV. x, y are the components of $\vec{R}$ in the follower UAV's rotating reference frame. The rotating reference frame of the follower UAV has its x axis, x_f, aligned with $\vec{v}_{hf}$; the y axis, y_f, along the follower UAV's starboard wing and the z axis, z_f, is in the down direction. $\vec{i}, \vec{j}, \vec{k}$ are the unit vectors of the follower UAV's rotating reference frame. The relative velocity of the two UAVs with respect to the inertial horizontal reference frame is then:

$$\frac{d\vec{R}}{dt} = \vec{v}_{hL} - \vec{v}_{hf} \tag{1}$$

Writing the parameters in equation (1) in the components of the follower UAV rotating reference frame, we have:

$$\vec{v}_{hL} = v_{hL} \cos\psi_e \vec{i} + v_{hL} \sin\psi_e \vec{j} \tag{2}$$

$$\vec{v}_{hf} = v_{hf} \vec{i} \tag{3}$$

$$\frac{d\vec{R}}{dt} = (\dot{x}\vec{i} + \dot{y}\vec{j}) + \dot{\psi}_f \vec{k} \times (xi + yj) \tag{4}$$

Combining equations (1), (2), (3) and (4), we have:

$$v_{hL} \cos\psi_e \vec{i} + v_{hL} \sin\psi_e \vec{j} - v_{hf}\vec{i} = (\dot{x}\vec{i} + \dot{y}\vec{j}) + \dot{\psi}_f \vec{k} \times (xi + yj) \tag{5}$$

From equation (5), we obtain:

$$\dot{x} = v_{hL} \cos\psi_e + \dot{\psi}_f y - v_{hf} \tag{6}$$

$$\dot{y} = v_{hL} \sin\psi_e - \dot{\psi}_f x \tag{7}$$

Equations (6) and (7) gives us a kinematic relation of the two UAVs' relative velocities. Integrating the two equations give us the relative position of the leader UAV with respect to the follower UAV in x and y components. For the z component of the relative position, we simply take the difference in altitude of the two. Thus,

$$\dot{z} = \dot{h}_f - \dot{h}_L \tag{8}$$

2.2   Formation Control

In the Leader-follower approach to formation flight, the leader maintains a prescribed trajectory while the followers track a fixed relative distance from the neighboring aircraft. Thus, the formation behavior is prescribed by specifying the relative distances that the followers must maintain. Then, the formation control problem simplifies to ensuring that the kinematic relations in equations (6) and (7) track our desired reference formation geometry. The formation geometry, which is the relative distance we want the leader UAV to maintain with respect to the follower UAV, is specified by choosing desired values for x, y and z. In other words, (x, y, z) represents the relative position of the leader UAV with respect to the follower UAV and a reference geometry is specified by choosing reference values for x, y and z.

The formation kinematic equations are nonlinear. Thus, two nonlinear controllers are examined for the formation-hold problem. The formation-hold problem is ensuring that (x, y, z) tracks $(x_{ref}, y_{ref}, z_{ref})$, where $(x_{ref}, y_{ref}, z_{ref})$ is the desired formation geometry. The two nonlinear control algorithms examined in this thesis for the formation-hold problem are state dependent Ricatti equation (SDRE) based control algorithm and a Lyapunov based control algorithm.

The overall control structure for the autonomous formation flight of the two UAVs in this thesis is a two-loop structure. The outer loop contains the formation-hold controller, or guidance loop. The formation-hold controller ensures that (x, y), which is the x and y component of the leader UAV's relative position to the follower UAV, track the desired (x_{ref}, y_{ref}). Using equations (6) and (7), the formation-hold controller is designed using both the SDRE based control algorithm and the Lyapunov based control algorithm. The formation-hold controller determines the necessary commands that the follower UAV must realize in order to maintain the x and y components of its relative position to the leader UAV. The commands from the formation-hold controller are sent into the inner loop of the overall control structure. In the inner loop, controllers are designed on the follower UAV to enable it track the command signals it receives from the formation-hold controller. To specify a formation geometry i.e. desired relative position, we need three components, $(x_{ref}, y_{ref}, z_{ref})$ but the formation-hold controller designed here only handles two components (x_{ref}, y_{ref}). However, as stated earlier, the z component of the relative position is simply the difference in altitude between the leader and the follower UAV. Thus, an altitude hold/acquire controller is designed in the inner loop to handle the z component of the formation geometry.

Simulations were done using MATLAB and SIMULINK to test the effectiveness of our control approach on a formation flight involving two UAVs. This approach was tested using a linear model of the SIG RASCAL 110 UAV for both the leader UAV and follower UAV. Two simulations were carried out to test our approach. The first simulation involved using the SDRE based controller in the outer loop and linear quadratic optimal tracking controller (LQT) in the inner loop of our control structure. The second simulation involved uses Lyapunov based controller in the outer loop and LQT controller as well in the inner loop.
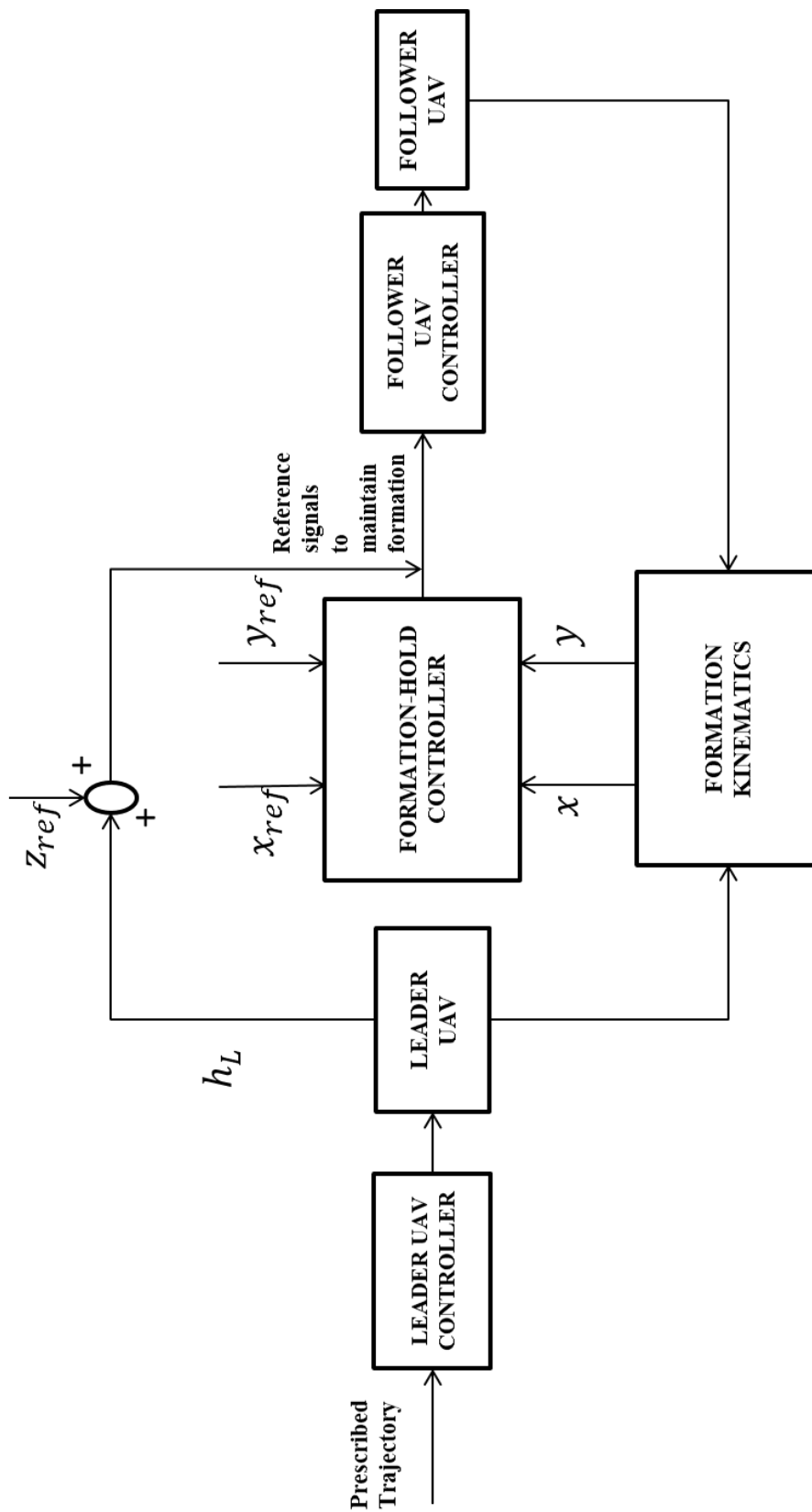
Figure 2.2: Model of the Control Approach

12

2.3   Design of the Inner Loop Controllers

As stated in section 2.2, the overall formation control system in this thesis is two-loop structured. The outer loop contains the formation-hold controller, it is the guidance loop. It determines the signals the follower UAV must track in order to maintain its relative position to the leader UAV. In the inner loop, attitude controllers are designed on the follower UAV. These controllers enable the follower UAV track the signals it receives from the guidance loop. The design of the formation-hold controller will be discussed in subsequent chapters, while the design of the inner loop controllers is discussed in this section. The inner loop controllers were designed using the linear quadratic optimal tracking control algorithm (LQT). The inner loop controllers designed are as follows: an Altitude/Velocity acquire controller and a roll/yaw rate acquire controller.

Given the following linear observable system [20],

$$\dot{x}(t) = A(t)\,x(t) + B(t)\,u(t) \tag{9}$$

$$y(t) = C(t)\,x(t) \tag{10}$$

the desired output $z(t)$, the error $e(t) = z(t) - y(t)$, and the performance index

$$J = \frac{1}{2}e^t(t_f)\,F(t_f)\,e(t_f) + \frac{1}{2}\int_{t_0}^{t_f}[e(t)^t\,Q(t)\,e(t) + u^t(t)\,R(t)\,u(t)]\,dt \tag{11}$$

where $F(t_f)$ and $Q(t)$ are mxm symmetric, positive semi definite matrices. $R(t)$ is a rxr symmetric positive definite matrix. $z(t)$ is the mth order desired output and $u(t)$ is the rth order control vector. It is desired that the output of the system, $y(t)$, tracks the reference signal $z(t)$ while minimizing the quadratic cost function in equation(11). The optimal control which is derived in reference [20] is given by:

$$\begin{aligned} u*(t) &= -R^{-1}(t)\,B^t(t)[P(t)\,x*(t) - g(t)] \\ &= -K(t)\,x*(t) + R^{-1}(t)\,B^t(t)\,g(t) \end{aligned} \tag{12}$$

where the nxn symmetric, positive definite matrix $P(t)$ is the solution of the nonlinear, matrix differential Riccati equation (DRE)

$$\dot{P}(t) = -P(t)\,A(t) - A^t(t)\,P(t) + P(t)\,E(t)\,P(t) - V(t) \tag{13}$$

with final condition

$$P(t_f) = C^t(t_f)\,F(t_f)\,C(t_f) \tag{14}$$

and the nth order $g(t)$ is the solution of the linear, nonhomogeneous vector differential equation

$$\dot{g}(t) = [P(t)\,E(t) - A^t(t)]\,g(t) - W(t)\,z(t) \tag{15}$$

with final condition

$$g(t_f) = C^t(t_f)F(t_f)z(t_f) \tag{16}$$

and

$$E(t) = B(t)R^{-1}(t)B^t(t) \tag{17}$$

$$V(t) = C^t(t)Q(t)c(t) \tag{18}$$

$$W(t) = C^t(t)Q(t) \tag{19}$$

The optimal state (trajectory) is the solution of the linear state equation

$$\dot{x}*(t) = [A(t) - E^t(t)P(t)]x*(t) + E(t)g(t) \tag{20}$$

And the optimal cost $J*$

$$J*(t_0) = \frac{1}{2}x^{*t}(t_0)P(t_0)x*(t_0) - x*(t_0)g(t_0) + h(t_0) \tag{21}$$

where $h(t)$ is the solution of

$$\dot{h}(t) = -\frac{1}{2}g^t(t)E(t)g(t) - \frac{1}{2}z^t(t)Q(t)z(t) \tag{22}$$

with final condition

$$h(t_f) = -z^t(t_f)P(t_f)z(t_f) \tag{23}$$

However, equations 9 to 23 are for a finite-time case problem. For the infinite-horizon problem, consider equations (9) and (10) but with time invariant system matrices, and the performance index chosen as

$$\lim_{t_f \to \infty} J = \lim_{t_f \to \infty} \frac{1}{2}\int_{t_0}^{t_f}[e^t(t)Q(t)e(t) + u^t(t)R(t)u(t)]dt \tag{24}$$

By using the results obtained in the finite-time case above and letting $t_f \to \infty$, we obtain the solutions for the infinite time case. As $t_f \to \infty$, the matrix function $P(t)$ in equation (13) tends to the steady-state value P as the solution of the following algebraic Riccati equation

$$-PA - A^tP + PBR^{-1}B^tP - C^tQC = 0 \tag{25}$$

Also, the vector function $g(t)$ in equation (15) tends to a finite function. For slowly varying input signals $z(t)$, $g(t)$ can be obtained by setting the derivative in equation (15) to zero and solving for $g(t)$. Thus,

$$g(t) = [PE - A^t]^{-1} Wz(t) \qquad (26)$$

where

$$E = BR^{-1}B^t \qquad (27)$$

$$W = C^t Q \qquad (28)$$

Then the optimal control becomes:

$$u(t) = -R^{-1} B^t [Px(t) - g(t)] \qquad (29)$$

Substituting equation (26) into equation (29) and factorizing:

$$u(t) = Kx(t) + K_Z\, z(t) \qquad (30)$$

where

$$\begin{aligned} K &= -R^{-1}B^t P \\ K_Z &= R^{-1}B[PE - A^t]^{-1} W \end{aligned} \qquad (31)$$

K and K_Z are the controller gains for a linear quadratic optimal tracking controller.

2.3.1 Altitude/Velocity Acquire Controller

As stated in section 2.3, an altitude/velocity acquire controller is one of the controllers designed in the inner loop of our formation-hold control system. The reason for this choice will be explained in chapter 3. This controller was designed using the algorithm for a linear quadratic optimal tracking controller detailed in section 2.3.

The Linear model of the SIG RASCAL 110 UAV is used in this thesis. The system matrices for this UAV are obtained from reference [21]. From reference [21], we have:

$$Along = \begin{bmatrix} -0.0893 & 0.1064 & 0.3701 & -9.8039 & -0.0001 \\ -1.1273 & -7.4207 & 17.7733 & 0.2041 & -0.0010 \\ 0.0406 & -0.3144 & -8.0281 & 0 & 0 \\ 0 & 0 & 1 & 0 & 0 \\ 0.0208 & 0.9988 & 0 & -20.0043 & 0 \end{bmatrix}$$

$$Blong = \begin{bmatrix} -0.5302 & 0.1135 \\ -9.8269 & -0.0001 \\ -33.0768 & -0.0003 \\ 0 & 0 \\ 0 & 0 \end{bmatrix} \qquad Xlong = \begin{bmatrix} u \\ w \\ q \\ \theta \\ h \end{bmatrix} \qquad ulong = \begin{bmatrix} \delta elev \\ \delta th \end{bmatrix}$$

where *Along* and *Blong* are the system matrices for the longitudinal dynamics of the SIG RASCAL 110 UAV. *Xlong* is the longitudinal state vector and *ulong* is the longitudinal control vector. $\delta elev$ is the elevator control and δth is the throttle control.
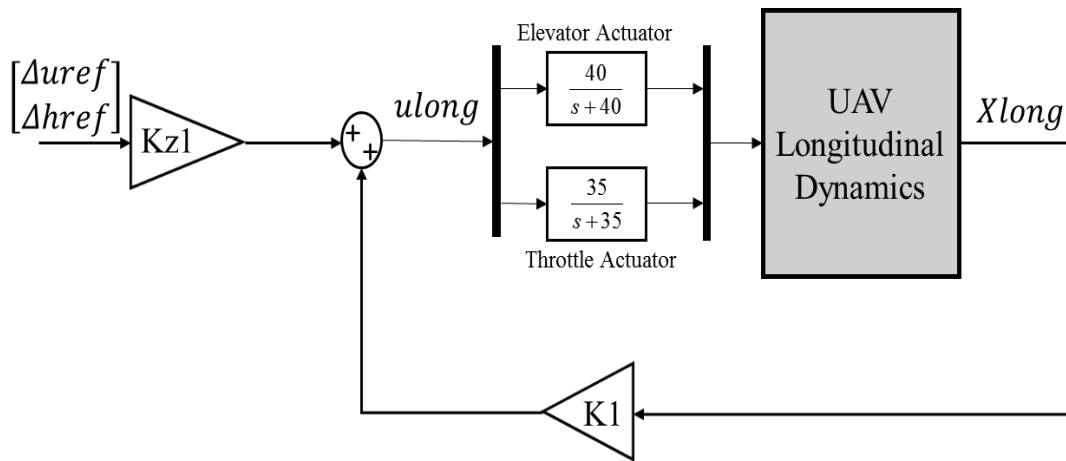
Figure 2.3: Block Diagram for the Altitude/Velocity Acquire Control System

The elevator and throttle actuator transfer functions are also obtained from reference [21]. The elevator control surface deflection is limited to $\pm$ 20 degrees. The SIG RASCAL model was linearized at 1000m altitude and 20m/s velocity [21].

Using the algorithm detailed in section 2.3, gains K1 and Kz1 are obtained.

Table 2.1: LQT Gains for the Altitude/Velocity Acquire Controller

K1					**Kz1**	
$\begin{bmatrix} -0.0031 & -0.0050 & 0.0573 & 0.6028 & -0.0211 \\ -3.2969 & 0.0897 & 0.2481 & 2.6776 & 1.0388 \end{bmatrix}$					$\begin{bmatrix} 0.0089 & 0.0211 \\ 3.6248 & -1.0384 \end{bmatrix}$	

Table 2.2: Eigenvalues of the Altitude/Velocity Acquire Control System

Eigenvalues	Mode
$-7.7296 \pm 2.3558i$	Short Period
$-0.9606 \pm 1.0124i$	Phugoid
-0.3776	

From table 2.2, the real part of all the eigenvalues are negative. Thus, we have an asymptotically stable system. To test the performance of the altitude/velocity acquire control system, reference signals for the velocity and altitude are sent into the control system. The outputs and the control surface deflections are then examined to see if the reference signals are closely tracked without saturations in the deflections of the control surfaces. We say there is a saturation in the deflection of a control surface when that control surface deflects to its maximum allowable limits. In the case of the elevator of our SIG RASCAL 110 UAV, the deflection limits are ± 20 degrees. Thus in tracking the reference signals, we avoid a deflection of ± 20 degrees in the elevator as saturations in control surface deflections tend to cause instability in the control system. The results of our test are presented below. It should be noted that all the results presented below are variational parameters, i.e. they are all deflections from trim conditions. $\Delta uref$ and $\Delta href$ are respectively the velocity and altitude commands to the controller. Δu and Δh are respectively the velocity and altitude outputs of the plant.
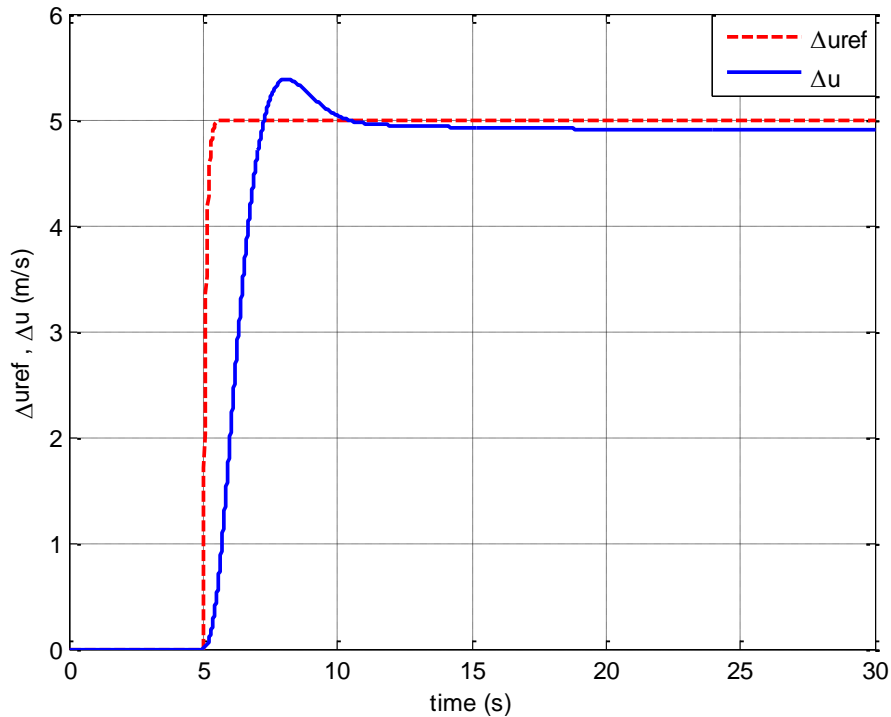
Figure 2.4: Time history of the desired velocity command and velocity output of the altitude/velocity acquire control system

17
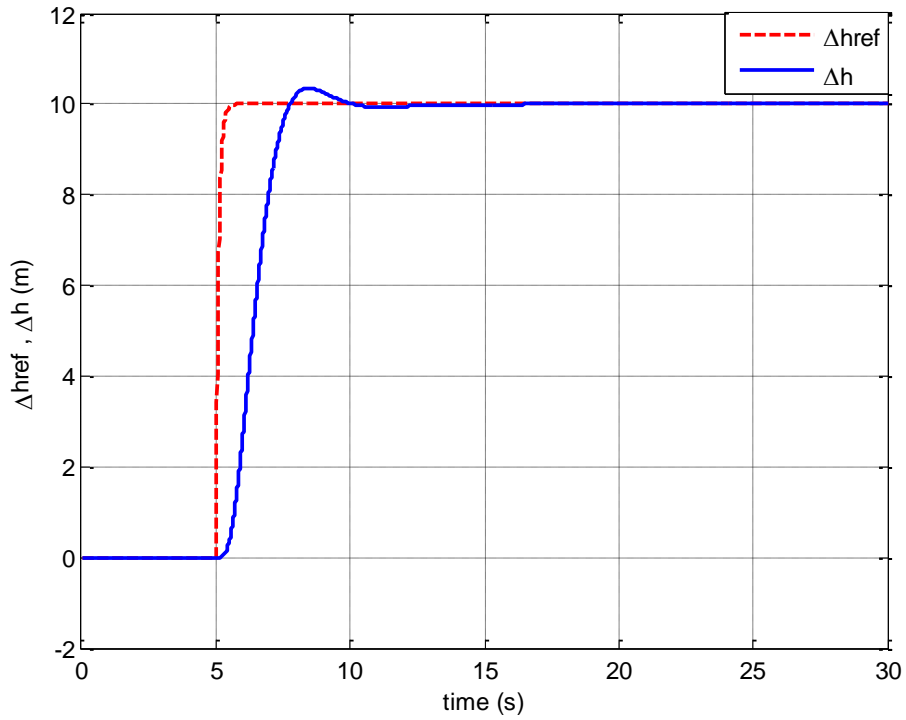
Figure 2.5: Time history of the desired altitude command and altitude output of the altitude/velocity acquire control system
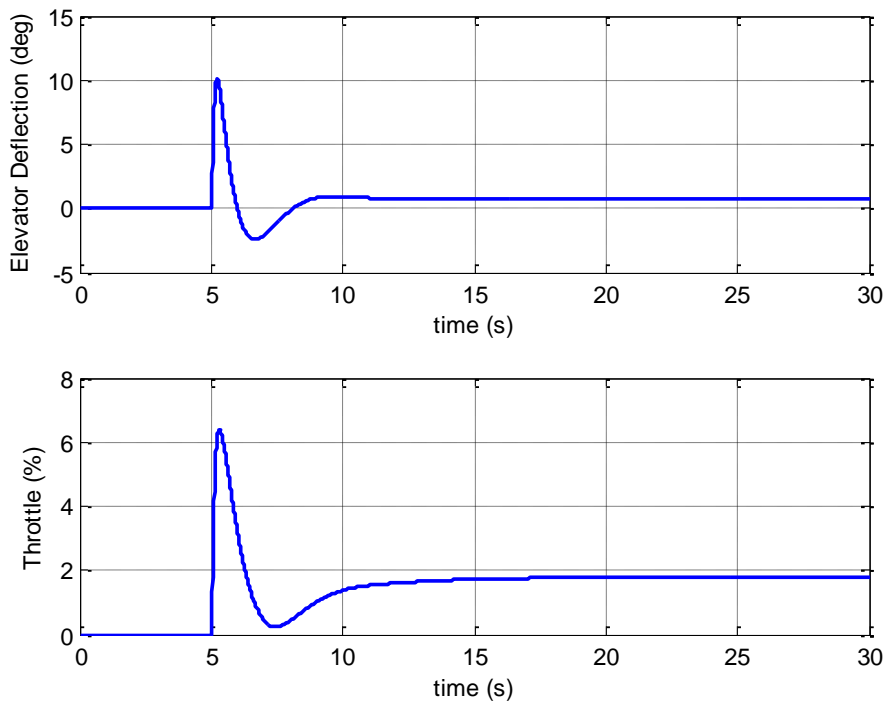
Figure 2.6: Time history of the elevator deflection and throttle of the altitude/velocity acquire control system

18

Once again, it should be noted that the results presented from figures 2.4 to 2.6 are all deflections from the trim values. From figures 2.4 to 2.6, we see that our control system tracks the reference signals without saturating the control surfaces. From figure 2.4, the controller is able to closely follow the reference velocity signal albeit a negligible steady state error of 0.09m/s. In figure 2.5, the reference altitude signal is also closely followed without a steady state error. Also, looking at the elevator deflection in figure 2.6, we observe no saturation. Thus, we can conclude that the designed altitude/velocity acquire controller has an admirable performance.

2.3.2   Roll/Yaw rate Acquire Controller

The roll/yaw rate acquire controller is one of the controllers designed in the inner loop of our formation-hold control system. The reason for this choice will also be explained in chapter 3. This controller was designed using the algorithm for a linear quadratic optimal tracking controller detailed in section 2.3. The system matrices for the SIG RASCAL 110 UAV are also obtained from reference [21]. From reference [21], we have:

$$Alate = \begin{bmatrix} -0.4807 & -0.6362 & -20 & -9.8039 \\ -0.9700 & -8.2639 & 0.1482 & 0 \\ 0.2808 & -0.3477 & -0.5848 & 0 \\ 0 & 1 & -0.0208 & 0 \end{bmatrix}$$

$$Blate = \begin{bmatrix} 0 & 2.3139 \\ 55.7042 & 1.0549 \\ -3.5463 & -7.8857 \\ 0 & 0 \end{bmatrix} \quad Xlate = \begin{bmatrix} v \\ p \\ r \\ \phi \end{bmatrix} \quad ulate = \begin{bmatrix} \delta ail \\ \delta rud \end{bmatrix}$$

where *Alate* and *Blate* are the system matrices for the lateral dynamics of the SIG RASCAL 110 UAV. *Xlate* is the lateral state vector and *ulate* is the control vector. δail is the aileron control and δrud is the rudder control. The aileron and rudder actuator transfer functions are obtained from reference [21] as well. The aileron control surface deflection is limited to ± 20 degrees while the rudder control surface deflection is limited to ± 15 degrees. The controller gains K2 and Kz2 in figure 2.7 are obtained using the algorithm detailed in section 2.3. $\Delta \phi ref$ and $\Delta rref$ in figure 2.7 are respectively the roll and yaw rate commands to the controller. $\Delta \phi$ and Δr are respectively the roll and yaw rate outputs of the plant.
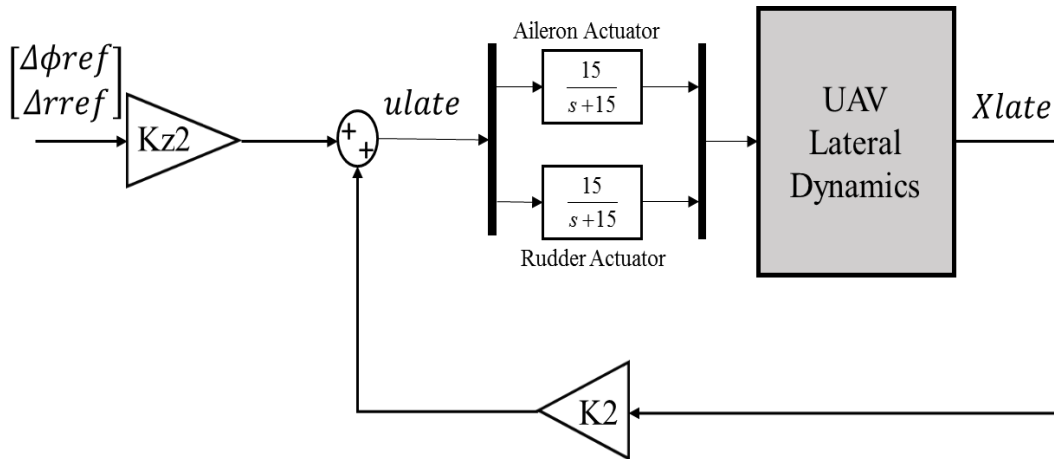
Figure 2.7: Block Diagram for the roll/yaw rate Acquire Control System

Table 2.3: LQT Gains for the Roll/Yaw rate Acquire Controller

K2	Kz2
$\begin{bmatrix} 0.0010 & -0.1238 & 0.7936 & -1.3549 \\ 0.0173 & 0.0182 & 1.1866 & 0.3872 \end{bmatrix}$	$\begin{bmatrix} -0.1639 & 1.0817 \\ -1.0504 & -0.4742 \end{bmatrix}$

Table 2.4: Eigenvalues of the roll/yaw rate Acquire Control System

Eigenvalues	Mode
$-10.1209 \pm 3.6526i$	Dutch roll
-7.4011	Roll
-0.6964	Spiral

The real part of all the eigenvalues in table 2.4 are negative. Thus, we have an asymptotically stable system. The same approach used in section 2.3.1 is again employed here to test the performance of the roll/yaw rate acquire control system. Reference signals for the roll and yaw rate are sent into the control system. The outputs and the control surface deflections are then examined to see if the reference signals are closely tracked without saturations in the deflections of the control surfaces. The results of our test are presented below. It should be noted again that all the results presented below are variational parameters, i.e. they are all deflections from trim conditions.
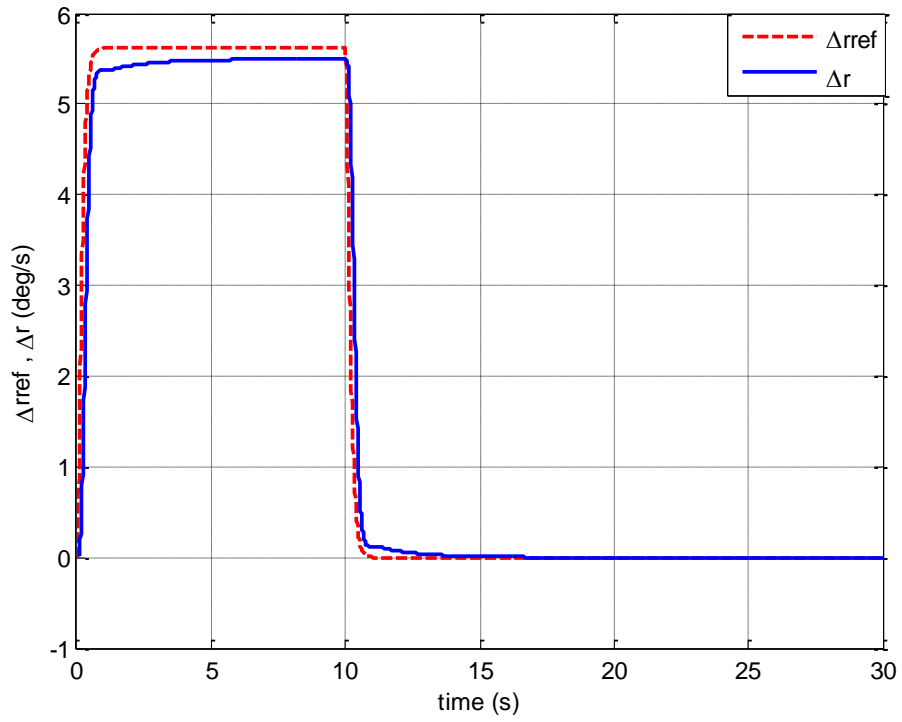
Figure 2.8: Time history of the desired yaw rate command and yaw rate output of the roll/yaw rate acquire control system
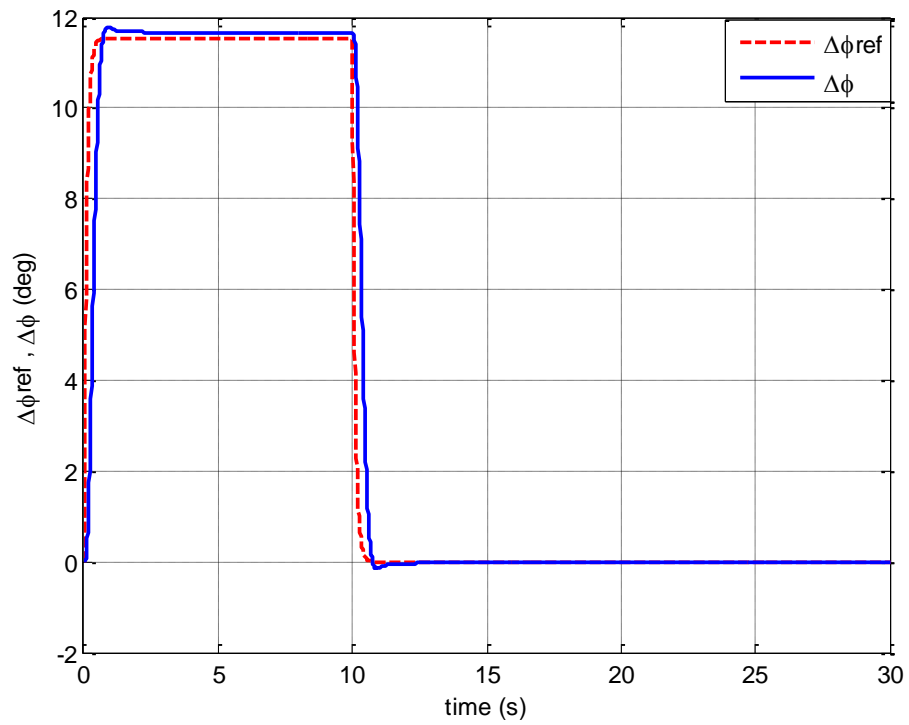
Figure 2.9: Time history of the desired roll command and roll output of the roll/yaw rate acquire control system

21
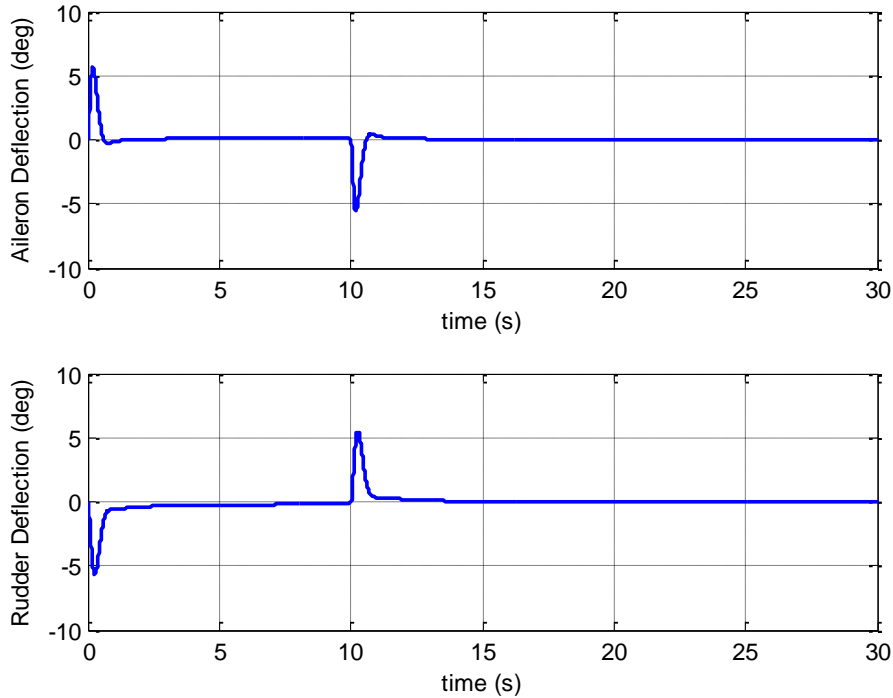
Figure 2.10: Time history of the Aileron and Rudder deflections of the altitude/velocity acquire control system

From figures 2.8 to 2.10, we see that our control system tracks the reference signals without saturating the control surfaces. In figure 2.8, the controller is able to closely follow the reference yaw rate signal. In the first 10 seconds, we see a steady state error of 0.12 deg/s which is negligible. After 10 seconds, the steady state error goes to zero. In figure 2.9, the reference roll signal is closely followed without a steady state error. We observe no saturation in the aileron deflection in figure 2.10. The limits for aileron deflection is ± 20 degrees. The deflections observed for the aileron deflection are well under ± 20 degrees. Also, there are no saturations in the rudder deflections as seen in figure 2.10. The limits for the rudder deflection are ± 15 degrees. Thus, we can conclude that the designed roll/yaw rate acquire controller has an admirable performance.

2.4   Leader UAV Controllers

As stated in chapter 1, this thesis uses the leader-follower approach to formation flight. In the leader-follower approach, the leader flies at a prescribed trajectory while the follower maintains its relative position to the leader. Thus, in order to prescribe the trajectory of the leader, we implemented a velocity/altitude acquire controller and a heading acquire controller on the leader UAV. Since the dynamics of the SIG RASCAL 110 UAV are used for both the leader and follower UAVs, the velocity/altitude acquire controller designed in section 2.3.1 is also implemented on the leader UAV.

2.4.1   Heading Acquire Controller

This controller was designed using the algorithm for a linear quadratic optimal tracking controller. From reference [21], the system matrices are:

$$Alate = \begin{bmatrix} -0.4807 & -0.6362 & -20 & -9.8039 & 0 \\ -0.9700 & -8.2639 & 0.1482 & 0 & 0 \\ 0.2808 & -0.3477 & -0.5848 & 0 & 0 \\ 0 & 1 & -0.0208 & 0 & 0 \\ 0 & 0 & 1.0002 & 0 & 0 \end{bmatrix}$$

$$Blate = \begin{bmatrix} 0 & 2.3139 \\ 55.7042 & 1.0549 \\ -3.5463 & -7.8857 \\ 0 & 0 \\ 0 & 0 \end{bmatrix} \qquad Xlate = \begin{bmatrix} v \\ p \\ r \\ \phi \\ \psi \end{bmatrix} \qquad ulate = \begin{bmatrix} \delta ail \\ \delta rud \end{bmatrix}$$

where *Alate* and *Blate* are the system matrices for the lateral dynamics of the SIG RASCAL 110 UAV. *Xlate* is the lateral state vector and *ulate* is the control vector. δail is the aileron control and δrud is the rudder control. The aileron and rudder actuator transfer functions are obtained from reference [21] as well. The aileron control surface deflection is limited to ± 20 degrees while the rudder control surface deflection is limited to ± 15 degrees. A constraint is placed on the leader UAV side slip velocity, v. It is desired that it remains zero while the leader UAV tracks the desired heading command.
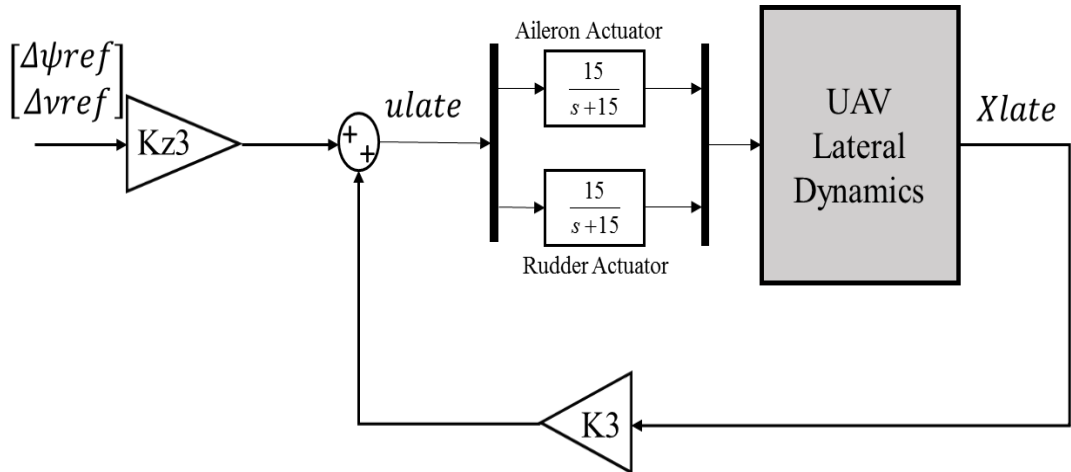
Figure 2.11: Block Diagram for the heading Acquire Control System

The controller gains K3 and Kz3 in figure 2.11 are obtained using the algorithm detailed in section 2.3. $\Delta \psi ref$ and $\Delta vref$ in figure 2.11 are respectively the heading and side slip velocity commands to the controller. $\Delta \psi$ and Δv are respectively the heading and side slip velocity outputs of the plant.

Table 2.5: LQT Gains for the Roll/Yaw rate Acquire Controller

K3	Kz3
$\begin{bmatrix} -0.2554 & -0.0785 & 0.5205 & -0.9733 & -1.5340 \\ -0.4440 & -0.0052 & 1.2654 & -0.3262 & 0.9901 \end{bmatrix}$	$\begin{bmatrix} 0.3126 & 1.5340 \\ 0.4843 & -0.9901 \end{bmatrix}$

Table 2.6: Eigenvalues of the roll/yaw rate Acquire Control System

Eigenvalues	Mode
$-6.7398 \pm 8.2475i$	Dutch roll
$-1.4020 \pm 1.3791i$	
-10.2773	Roll

The real part of all the eigenvalues in table 2.6 are negative. Thus, we have an asymptotically stable system. The same approach used in section 2.3.1 is again employed here to test the performance of the heading acquire control system. Reference signals for heading and side slip velocity $(v = 0)$ are sent into the control system. The outputs and the control surface deflections are then examined to see if the reference signals are closely tracked without saturations in the deflections of the control surfaces. The results of our test are presented below. It should be noted again that all the results presented below are variational parameters, i.e. they are all deflections from trim conditions.
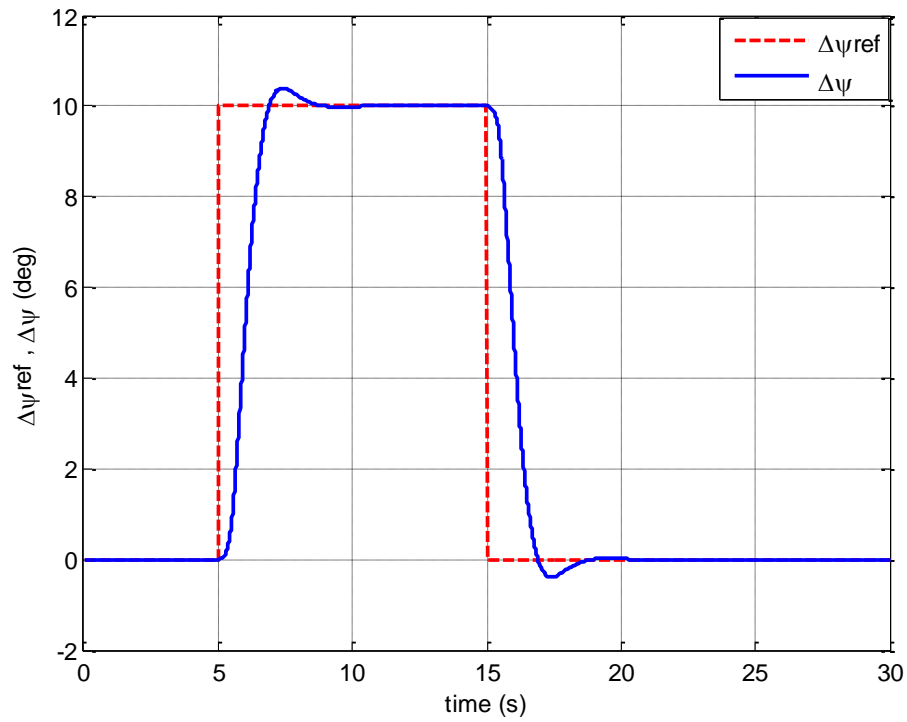
Figure 2.12: Time history of the desired heading command and heading output of the heading acquire control system
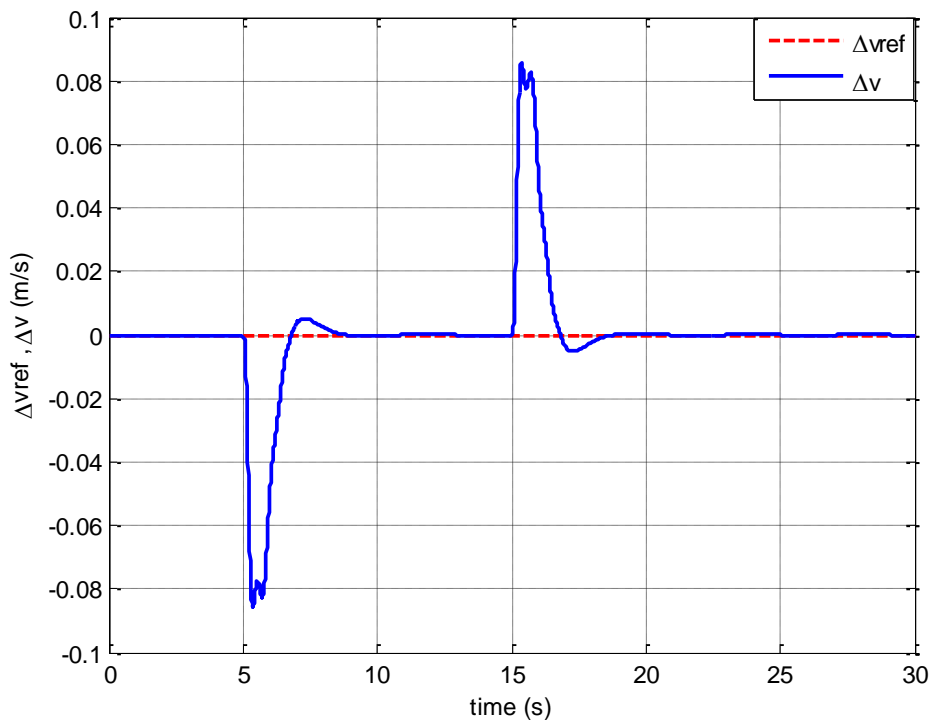
Figure 2.13: Time history of the desired side slip velocity command and side slip velocity output of the heading acquire control system

25
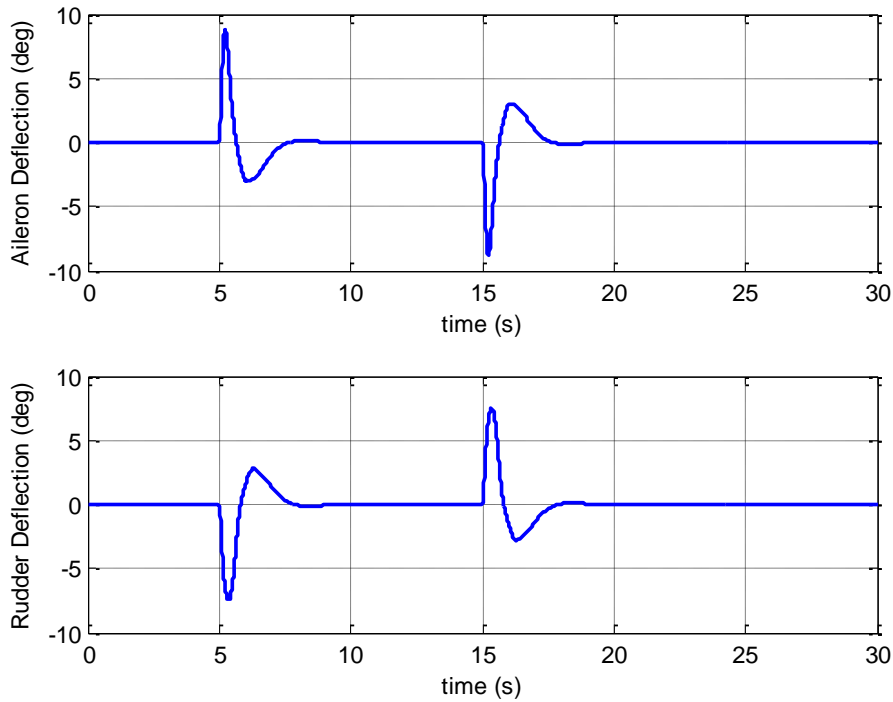
Figure 2.14: Time history of the Aileron and Rudder deflections of the altitude/velocity acquire control system

From figures 2.12 to 2.14, we see that our control system tracks the reference signals without saturating the control surfaces. In figure 2.12, the controller is able to closely follow the reference heading signal without a steady state error. There is also an acceptable overshoot of about 0.4 degrees which is quite. In figure 2.13, the side slip velocity is desired to be kept at zero as the UAV tracks the heading command, our controller does just that albeit overshoots of about 0.08 m/s which is approximately zero. In figure 2.14, we observe no saturations in the deflections of the control surfaces as the UAV performs the desired maneuver. The limits for aileron deflection is ± 20 degrees. The deflections observed for the aileron deflection are well under ± 20 degrees. Also, there are no saturations in the rudder deflections as seen in figure 2.14. The limits for the rudder deflection are ± 15 degrees. Thus, we can conclude that the designed heading acquire controller has an admirable performance.

CHAPTER 3

SDRE BASED CONTROL OF UNMANNED AIRCRAFT FORMATIONS

3.1   State Dependent Ricatti Equation (SDRE)

The state dependent ricatti equation control method has become quite popular over the last decade. It is a nonlinear control technique for synthesizing nonlinear feedback controls by allowing nonlinearities in the system states while also offering great design flexibility through state-dependent weighting matrices [15]. This method has been extensively studied by pearson [16], Wernli and Cook [17], and Mracek and Cloutier [18]. The SDRE algorithm captures the nonlinearities of a system by converting the nonlinear system to a linear-like structure using state-dependent coefficient (SDC) matrices. In this way, the controller gains are frequently computed ensuring the stability and performance of the nonlinear system. Thus, an Algebraic Riccati equation, (ARE) with SDC matrices is then solved on-line to obtain the control gains. Consequently, algebraic Riccati equation becomes state-dependent Riccati equation, or SDRE.

The non-uniqueness of the parameterization creates additional degrees of freedom, which can be used to enhance controller performance.

3.2   SDRE Control Approach

The State Dependent Riccati Equation (SDRE) control methodology uses extended linearization as the key concept in formulating the nonlinear optimal control problem [22]. At each time instant, the method treats the state-dependent coefficient matrices as being constant, and computes a control action by solving a Linear Quadratic optimal control problem. Similar to the linear counterpart the system has to be full-state observable, controllable. It should also be affine in input. The weighing matrices of the quadratic cost function may be state dependent. Consider a system of the following form [22]:

$$\dot{x}(t) = Ax + Bu + f \tag{32}$$

where $x \in \Re^n$ is the state vector, $u \in \Re^m$ is the input vector and $t \in [0, \infty]$, with functions $A : \Re^n \to \Re^n$, $B : \Re^m \to \Re^{n \times m}$ and $f \in \Re^n$. The minimization of the following performance index is considered.

$$J = \frac{1}{2} \int_0^T [(Cx - d)^t Q (Cx - d) + u^t Ru] dt \tag{33}$$

where $d \in \Re^m$ is the reference input, and as defined by the control objectives, $C : \Re^n \to \Re^m$. Q must be at least positive semi definite, and R must be positive definite at all times. In other to obtain the control law, the Hamiltonian and its derivatives with respect to the control input u, states x and co-state variables λ are needed [22].

$$H = \frac{1}{2}(Cx-d)^t Q(Cx-d) + \frac{1}{2}u^t Ru + \lambda^t (Ax+Bu+f) \qquad (34)$$

$$\dot{u} = \frac{\partial H}{\partial u} = Ru + B^t\lambda = 0 \rightarrow u = -R^{-1}B^t\lambda \qquad (35)$$

$$\dot{x} = \frac{\partial H}{\partial \lambda} = Ax + f - E\lambda \qquad (36)$$

$$\dot{\lambda} = \frac{\partial H}{\partial x} = -(A^t\lambda + C^tQ(Cx-d)) \qquad (37)$$

Combing equations (32), (33) and (34), we have:

$$H = (Cx-d)^t Q(Cx-d) + \lambda^t(Ax+f) - \frac{1}{2}\lambda^t E\lambda \qquad (38)$$

where $E = BR^{-1}B^t$. Define the function λ including a bias term due to the tracking problem. Let the solution be:

$$\lambda = Px - g \qquad (39)$$

If we take the derivative of λ and use equations (33) and (34), we have:

$$-A^t(Px-g) - C^tQ(Cx-d) = P(Ax+f-E(Px-g)) - \dot{g} + \dot{P}x \qquad (40)$$

Collecting the terms with state variables and equating them to zero, we have:

$$\dot{P} + PA - PEP + A^tP + C^tQC = 0 \qquad (41)$$

which is the differential state dependent Riccati equation. The remaining terms become:

$$\dot{g} - Pf + PEg + A^tg + C^tQd = 0 \qquad (42)$$

If we search for steady state solutions, assuming that f and d are constants, equation (41) becomes algebraic Riccati equation with well-known solution methods.

$$PA - PEP + A^tP + C^tQC = 0 \qquad (43)$$

Then the solution of the auxiliary equation and the control law becomes:

$$g = -(PE - A^t)^{-1}(Pf - C^tQd) \qquad (44)$$

$$u = -R^{-1}B^t(Px - g) \qquad (45)$$

Using equations (6) and (7), a formation-hold controller may be designed. To do this, equations (6) and (7) are written in the state-dependent coefficient form.

$$\begin{Bmatrix} \dot{x} \\ \dot{y} \end{Bmatrix} = \begin{bmatrix} y & -1 \\ -x & 0 \end{bmatrix} \begin{Bmatrix} \dot{\psi}_f \\ v_{hf} \end{Bmatrix} + \begin{Bmatrix} v_{hL}\cos\psi_e \\ v_{hL}\sin\psi_e \end{Bmatrix} \qquad (46)$$

Comparing equation (46) with equation (32), it may be observed that in this factorization, the system matrix, A, is zero. For a given reference formation, $d = \{x_{ref}, y_{ref}\}$, the SDRE formation-hold controller may be designed to generate the necessary control commands $u = \{\dot{\psi}_f, v_{hf}\}$ to realize the desired formation in a stable manner. Thus, the proposed formation control is a guidance methodology used to generate the necessary heading rate and velocity commands to the follower.

A singularity problem exists in obtaining the control law for the state dependent coefficient matrix in equation (46) when $x = 0$. To obtain the control law for our SDC, we need to calculate g. From equation (44), $g = -(PE - A^t)^{-1}(Pf - C^t Qd)$ where $E = BR^{-1}B^t$. When $x = 0$, $B = \begin{bmatrix} y & -1 \\ 0 & 0 \end{bmatrix}$. For $R^{-1} = \begin{bmatrix} a & 0 \\ 0 & b \end{bmatrix}$, we have:

$$E = \begin{bmatrix} y & -1 \\ 0 & 0 \end{bmatrix} \begin{bmatrix} a & 0 \\ 0 & b \end{bmatrix} \begin{bmatrix} y & 0 \\ -1 & 0 \end{bmatrix} = \begin{bmatrix} ay^2 + b & 0 \\ 0 & 0 \end{bmatrix} \tag{47}$$

For our SDC in equation (46), the A matrix is zero. Thus, for $P = \begin{bmatrix} p_{11} & p_{12} \\ p_{12} & p_{22} \end{bmatrix}$, $(PE - A^t)^{-1}$ in g becomes:

$$(PE - A^t)^{-1} = \left(\begin{bmatrix} p_{11} & p_{12} \\ p_{12} & p_{22} \end{bmatrix} \begin{bmatrix} ay^2 + b & 0 \\ 0 & 0 \end{bmatrix} \right)^{-1} = \begin{bmatrix} p_{11}(ay^2 + b) & 0 \\ p_{12}(ay^2 + b) & 0 \end{bmatrix}^{-1} \tag{48}$$

Thus, when $x = 0$, the inverse in equation (48) does not exist. Consequently, g in equation (44) cannot be computed and hence, the control law u in equation (45) cannot be computed.

For cases where the x-separation between the leader UAV and the follower UAV is desired to be zero, a workaround is developed. Whenever we have $-0.5 \leq x \leq 0.5$ signal going into our SDRE formation-hold controller, the value for x is set to 0.5 in the B matrix of the formation-hold controller. By doing this, we make sure x never goes to zero in the B matrix thereby avoiding the singularity problem discussed above. We did consider other ranges besides ± 0.5, however, we got the best performance with this range. The approach just explained seemed to work best among the number of approaches we considered to solve the singularity problem. For example, we stopped updating the SDRE feedback gain whenever x goes close to zero, however this approach was unsuccessful.

3.3 SDRE Tuning Technique

The State Dependent Riccati Equation (SDRE) control methodology uses extended linearization as the key concept in formulating the nonlinear optimal control problem [22]. At each time instant, the method treats the state-dependent coefficient matrices as being constant, and computes a control action by solving a Linear Quadratic optimal control problem. Thus, tuning the SDRE formation-hold controller implies choosing the proper weighting matrices Q and R required to solve the resulting linear quadratic control problem at each respective time instant considered. The Q matrix penalizes the states and the R matrix penalizes the control commands.

To tune the SDRE formation-hold controller, a varying Q matrix and constant R matrix is employed. The weights on Q vary with respect to the difference between the desired relative

distance between the UAVs i.e. desired reference geometry and the actual relative distance between the UAVs.

$$Q = \begin{bmatrix} \dfrac{1}{x_{ref} - x} & 0 \\ 0 & \dfrac{1}{y_{ref} - y} \end{bmatrix} \tag{49}$$

From the choice above, when the error is large, penalty on the states is low so as to prevent saturation of the control surfaces, since the SDRE controller tries to immediately track the reference formation. As error reduces, penalty gets higher, thereby cancelling out the steady-state error. Obviously, when position error approaches to zero, the diagonal terms of the Q matrix becomes very large. To prevent this undesirable situation, as error gets small, a fixed Q is selected and no further changes are made to the Q matrix. However, if for some reason, the error stops being zero, the Q matrix is again tweaked with respect to the error until small enough error is again achieved.

The R matrix on the other hand, remains constant throughout the solution process. However, its initial weight varies directly proportionally with the desired reference geometry. In other words, the higher the reference value, the higher the initial weight on the control commands. This is done, because initially, when the error is large, penalty on the states are low. Thus, a larger R is required to compensate for the low penalty on Q.

At every time instant considered, a new feedback gain is computed using Q and R. Thus, for an effective controller, a good feedback gain update rate has to be chosen.

3.4 Formation Control Implementation

As stated earlier, this thesis uses a leader-follower approach for the formation control problem. In the Leader-follower approach to formation flight, the leader maintains a prescribed trajectory while the followers track a fixed relative distance from the neighboring aircraft. We only have two UAVs in our case with one of them designated as the leader while the other is designated as the follower. The follower UAV must always maintain the desired relative distance from the leader UAV in spite of maneuvers carried out by the leader UAV.

To enable the leader UAV carry out desired flight maneuvers (prescribing desired trajectory), as stated in section 2.4, two LQT controllers are implemented on the leader UAV. These controllers are the velocity/altitude acquire controller and the heading-acquire controller. To maintain the desired formation geometry, i.e. the desired relative position of the follower UAV from the leader UAV, the formation-hold controller computes the desired heading rate and velocity the follower UAV must track in order to keep up with the leader UAV. Thus, controllers must be implemented on the follower UAV as well to enable it track the commands from the formation-hold controller. Considering the turn geometry, where the

lateral acceleration is zero, the following relation between the roll angle and heading rate may be written [23]:

$$\phi_{fc} = \arctan\left(\frac{v_{hf} \cdot \dot{\psi}_f}{g}\right) \tag{50}$$

The body fixed yaw rate to be realized by the follower then may be calculated from:

$$r_{fc} = \dot{\psi}_f \cdot \cos(\theta_f) \cdot \cos(\phi_{fc}) \tag{51}$$

$\dot{\psi}_f, v_{hf}$ are the outputs from the formation-hold controller. They are the guidance commands the follower UAV must track in order for it to maintain the desired relative separation from the leader UAV. Thus, v_{hf} is then sent into the inner loop of our formation-hold control system, however, $\dot{\psi}_f$ is not directly sent into the inner loop. $\dot{\psi}_f$ is first converted to ϕ_{fc} and r_{fc} using equations (50) and (51) and then sent into the inner loop. As stated before in section 2.2, the formation-hold controller provides reference signals to the follower UAV to enable it track (x_{ref}, y_{ref}), which is the x and y components of the desired relative position of the follower UAV with respect to the leader UAV. To enable the follower track z_{ref}, an altitude controller is also implemented on the follower UAV as well. Input to this altitude controller is the leader UAV's altitude plus the desired offset, z_{ref}. Thus, the guidance signals going into the inner loop from the formation-hold controller are v_{hf}, ϕ_{fc}, r_{fc} and h_{fc}. To enable the follower UAV track these guidance signals, an altitude/velocity acquire controller and a roll/yaw rate acquire controller are implemented on the follower UAV. The design details of these controllers can be found in section 2.3. The inner loop controllers, i.e. the controllers implemented on the follower UAV always track the guidance signals received from the formation-hold controller, thus, in order to prevent saturations in the deflections of the control surfaces of the inner loop controllers, $\dot{\psi}_f$ is limited to $\pm$ 10 deg/s. ϕ_{fc} and r_{fc} are dependent on $\dot{\psi}_f$ as shown in equations (50) and (51). Thus, by limiting $\dot{\psi}_f$, we also limit ϕ_{fc} and r_{fc}. Limiting the signals going into the inner loop ensures that overly large signals are not sent into the inner loop thereby reducing the chances of saturating the control surfaces.
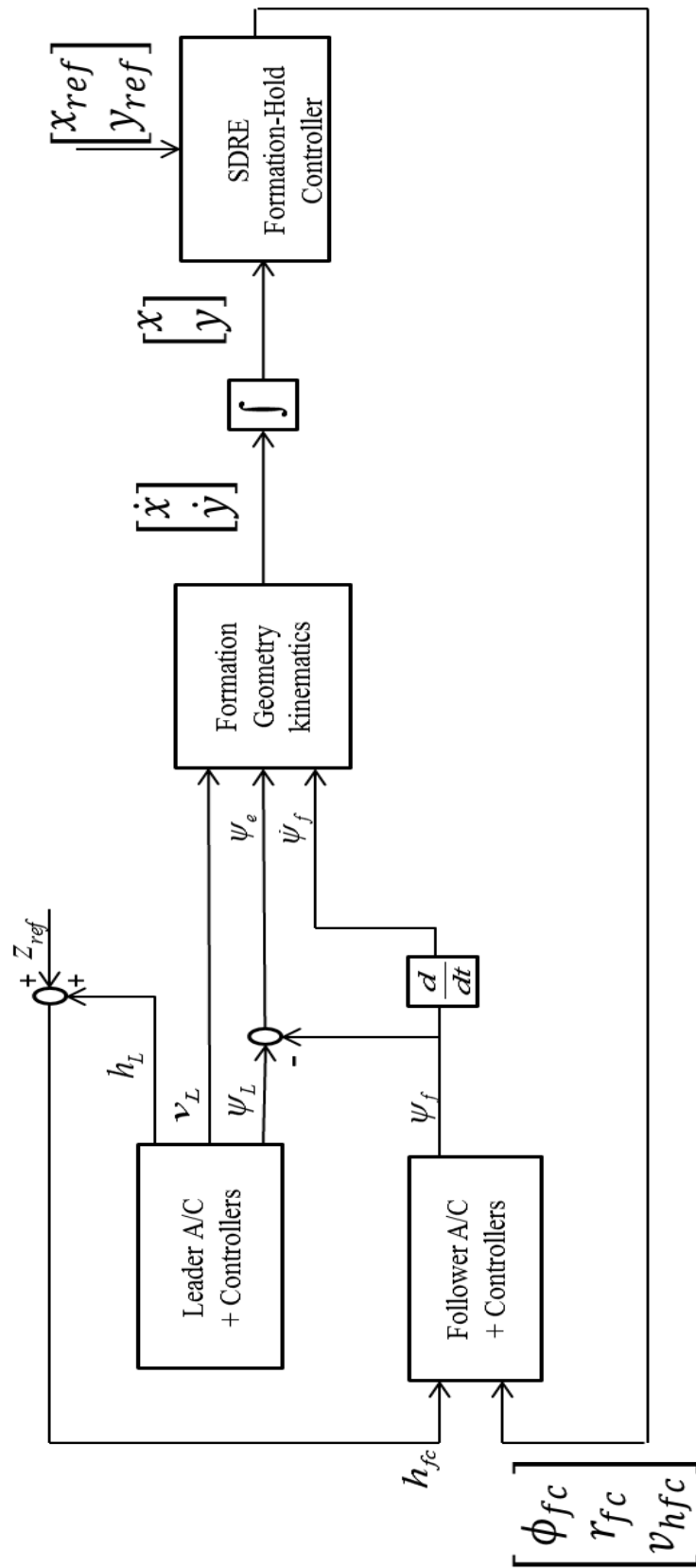
Figure 3.1: Block Diagram of the SDRE Formation Control System

3.5   Results and Discussion

The formation control system is tested using the linearized model of the SIG RASCAL 110 model aircraft for both the leader and follower UAVs. For this purpose, simulation code is written in MATLAB/SIMULINK. The block diagram for the simulation code is given in Figure 2.2. To examine the effectiveness of the SDRE approach in realizing the desired formation geometry in spite of maneuvers carried out by the leader aircraft, three cases are considered. In each case, SDRE feedback gain update rate was set to 1 Hz, i.e. every 1second. In addition, the control surface deflections for the follower UAV as in section 2.3 are limited to ± 20 degrees for both the elevator and aileron and ± 15 degrees for the rudder. The throttle maximum value is also constrained. The SIG RASCAL model was linearized at 1000m altitude and 20m/s velocity, and it is given in the Appendix.

Case 1: In the leader follower approach, the leader flies at a prescribed trajectory while the follower maintains the desired relation distance from the leader. In this thesis, we give altitude, velocity and heading commands to the leader UAV to prescribe its trajectory. In this flight scenario, case 1, the leader UAV flies at the velocity, altitude and heading depicted in figure 3.3, 3.4 and 3.5 respectively. The leader and follower UAVs are initially flying at separation distances of $(x_{ini}, y_{ini}, z_{ini}) = (9, 8, 0)$ m. It is desired that the follower's relative position be brought to $(x_{ref}, y_{ref}, z_{ref}) = (6, 4, 5)$ m. Our aim is to see if the follower UAV can track and maintain the desired formation geometry in spite of the maneuvers carried out by the leader UAV. The terms relative position, separation distance and formation geometry are all equivalent.
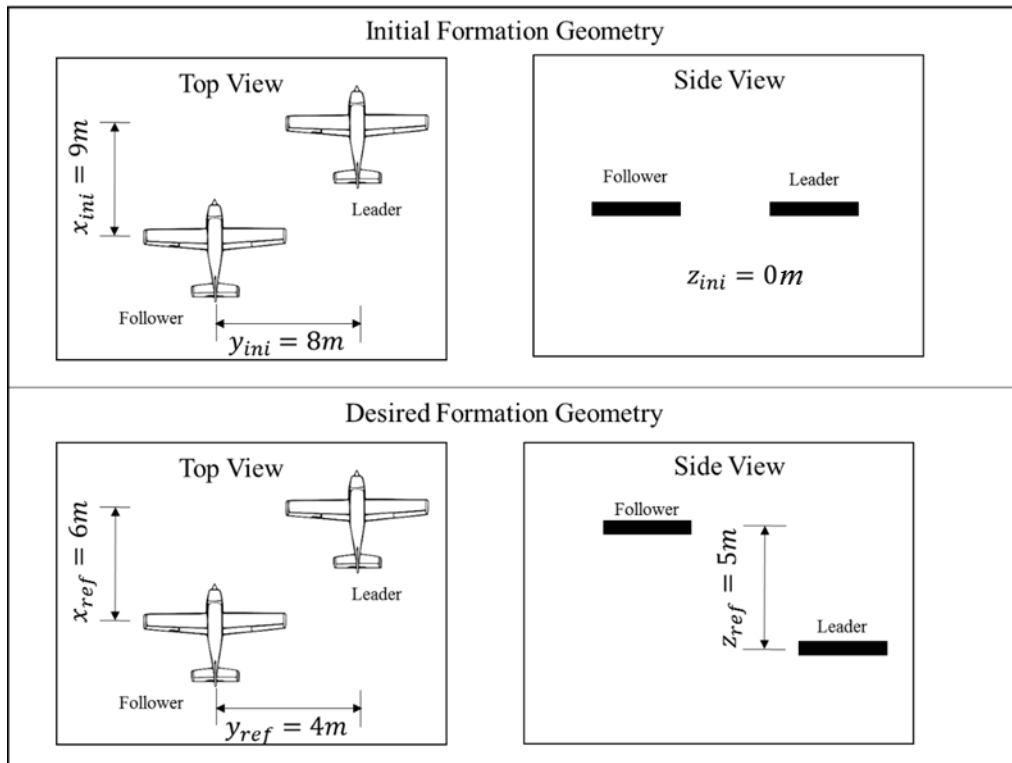

Figure 3.2: Initial and Desired Formation Geometries, Case 1, SDRE
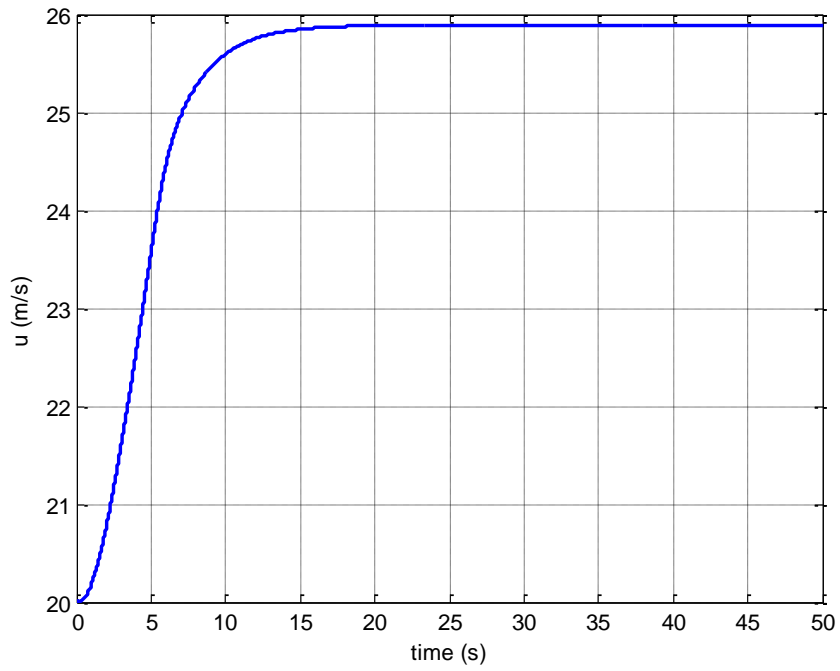
Figure 3.3: Time history of the leader UAV's velocity, Case 1, SDRE
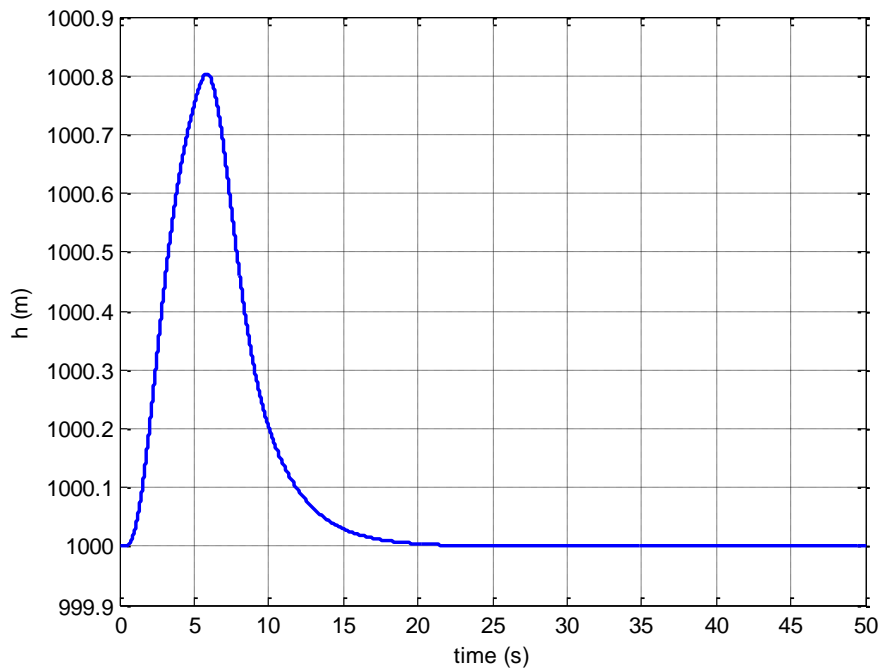
Figure 3.4: Time history of the leader UAV's altitude, case 1, SDRE

34
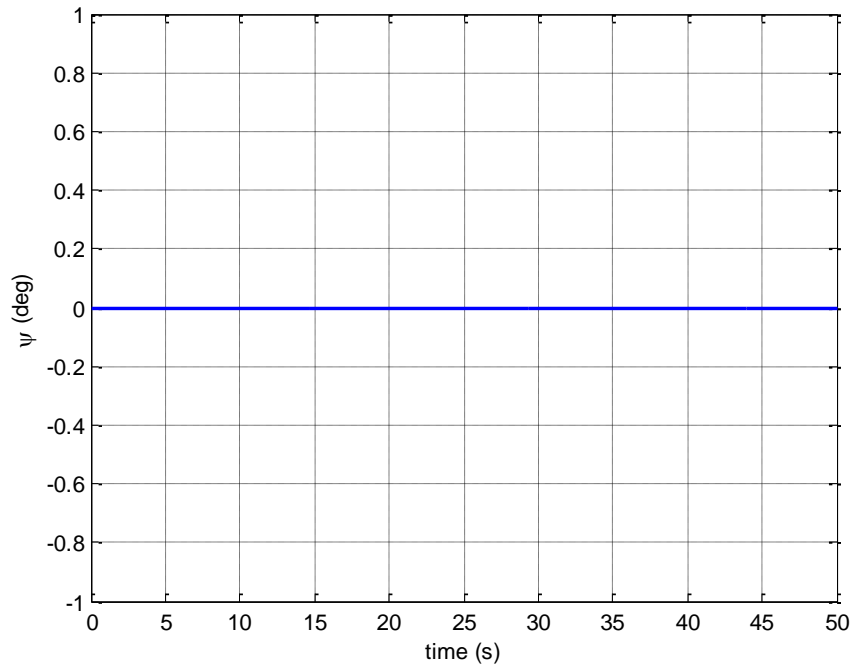
Figure 3.5: Time history of the leader UAV's heading, Case 1, SDRE
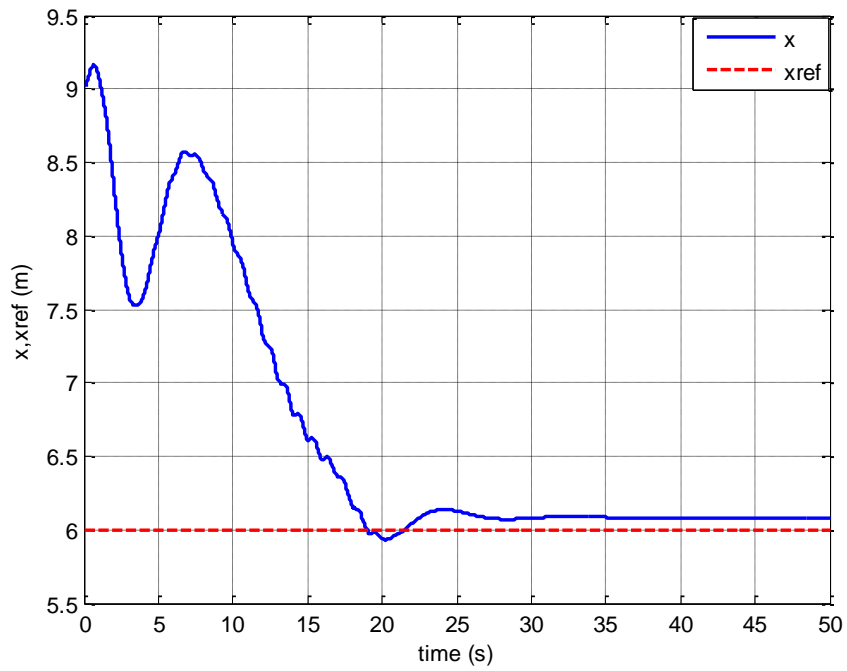
Figure 3.6: Time history of the follower UAV's relative position, x-component, Case 1, SDRE

35
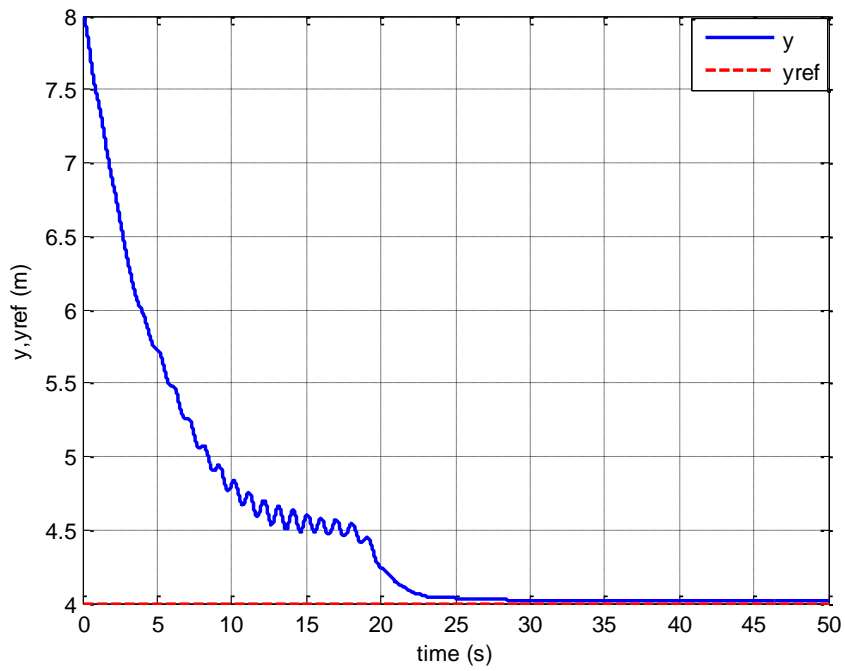
Figure 3.7: Time history of the follower UAV's relative position, y-component, Case 1, SDRE
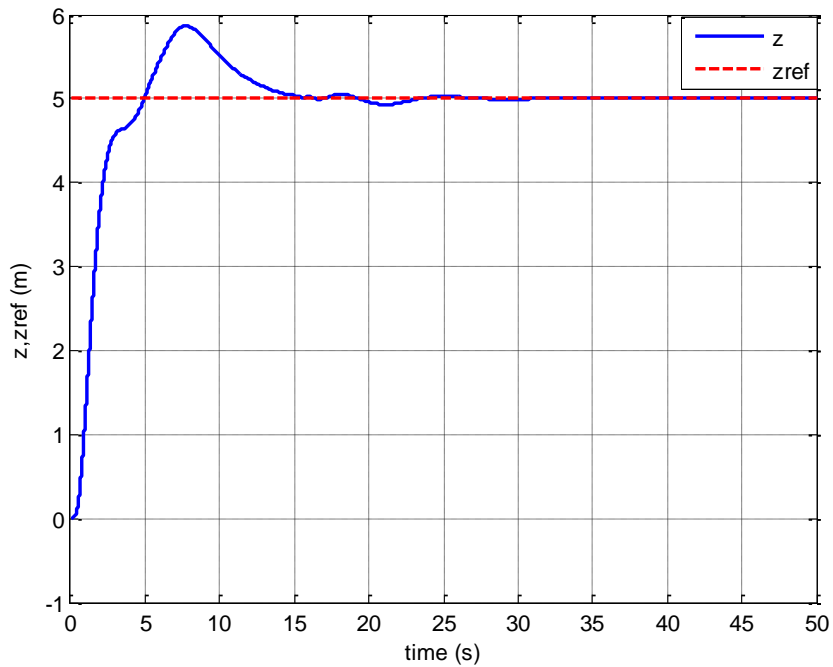
Figure 3.8: Time history of the follower UAV's relative position, z-component, Case 1, SDRE

36
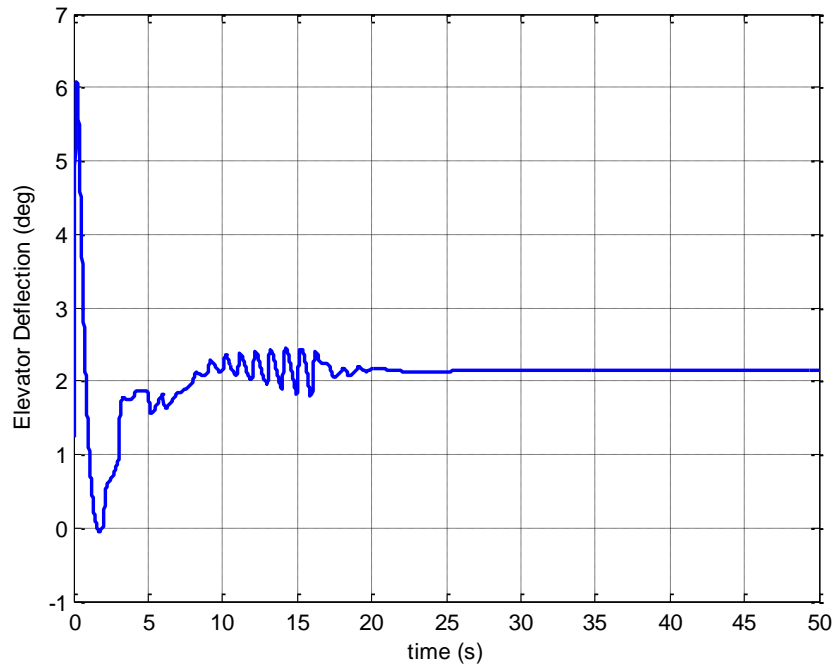
Figure 3.9a: Time history of the elevator deflection, Case 1, SDRE, 50 seconds time scale
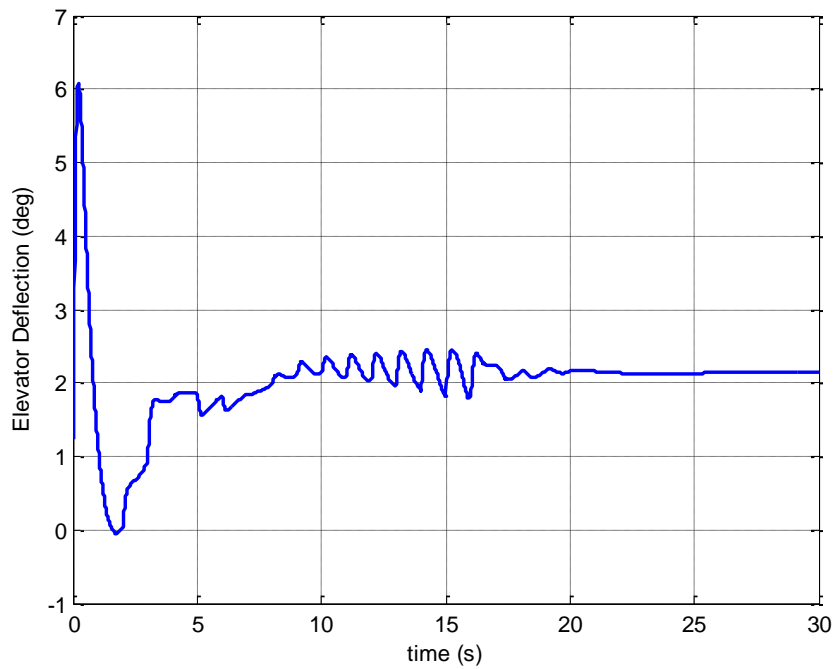
Figure 3.9b: Time history of the elevator deflection, Case 1, SDRE, 30 seconds time scale
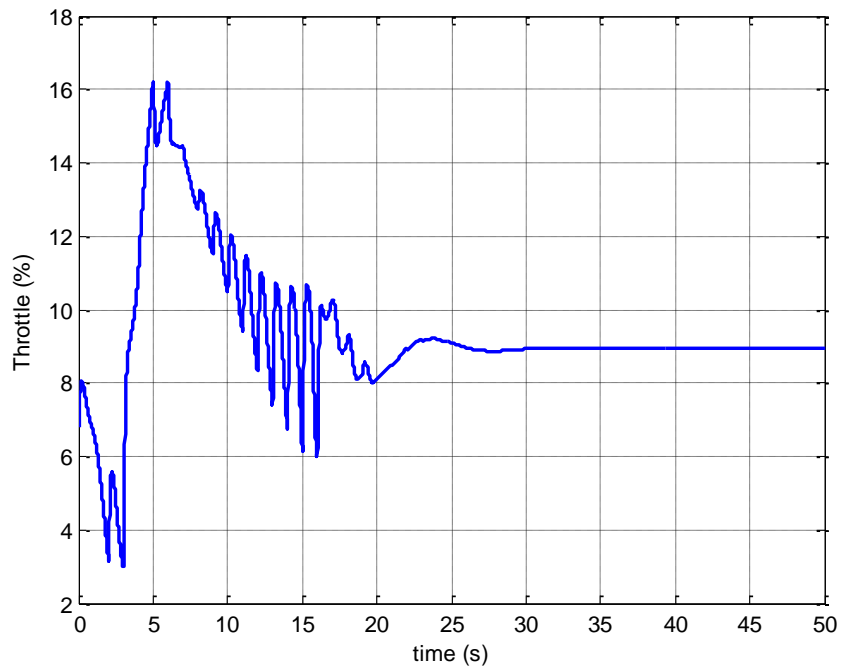
Figure 3.10a: Time history of the throttle, Case 1, SDRE, 50 seconds time scale
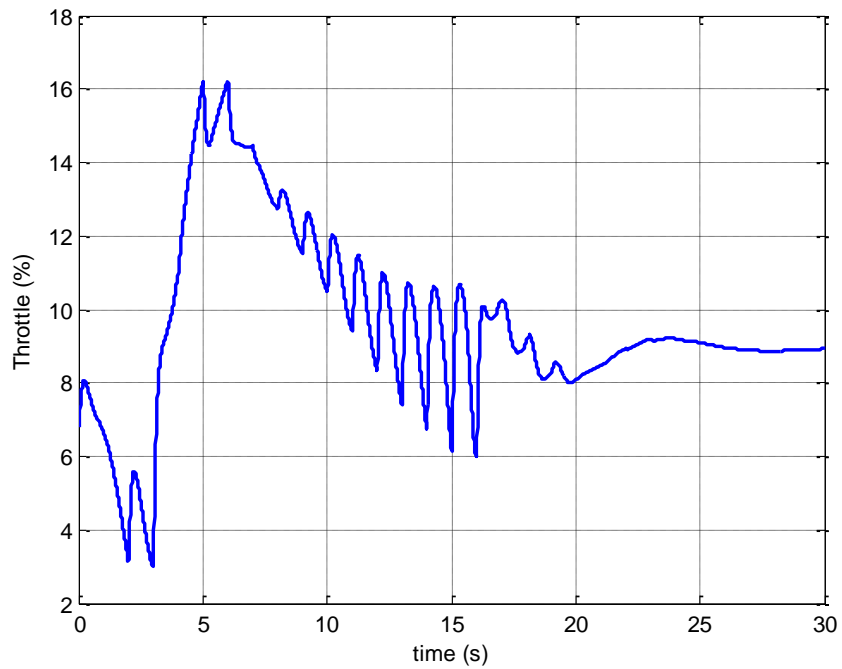
Figure 3.10b: Time history of the throttle, Case 1, SDRE, 30 seconds time scale

38
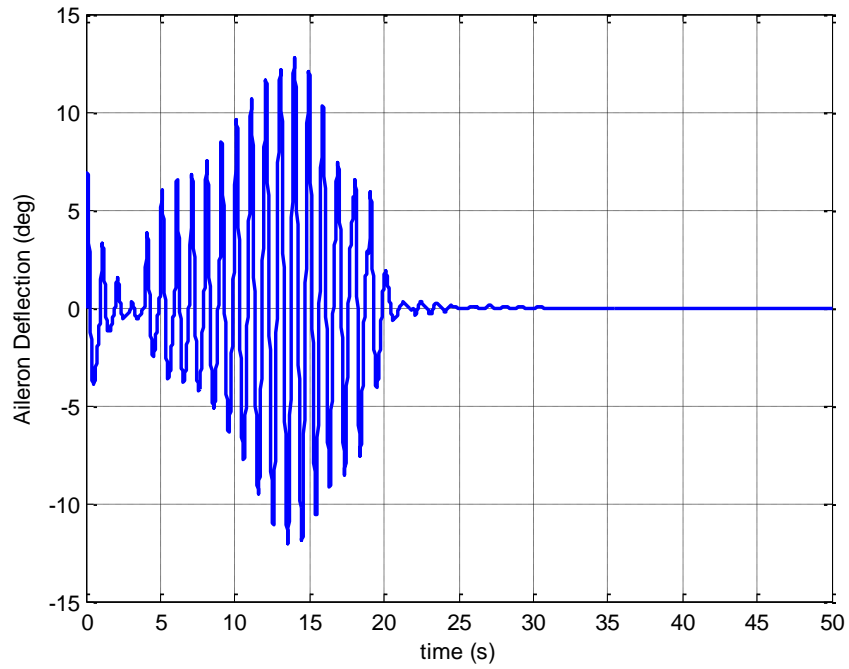
Figure 3.11a: Time history of the aileron deflection, Case 1, SDRE, 50 seconds time scale
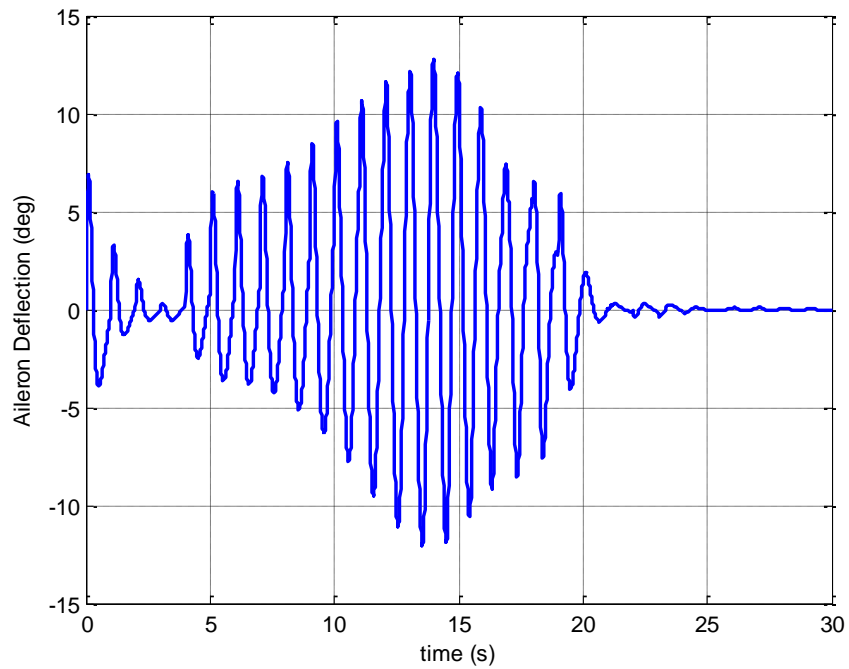
Figure 3.11b: Time history of the aileron deflection, Case 1, SDRE, 30 seconds time scale
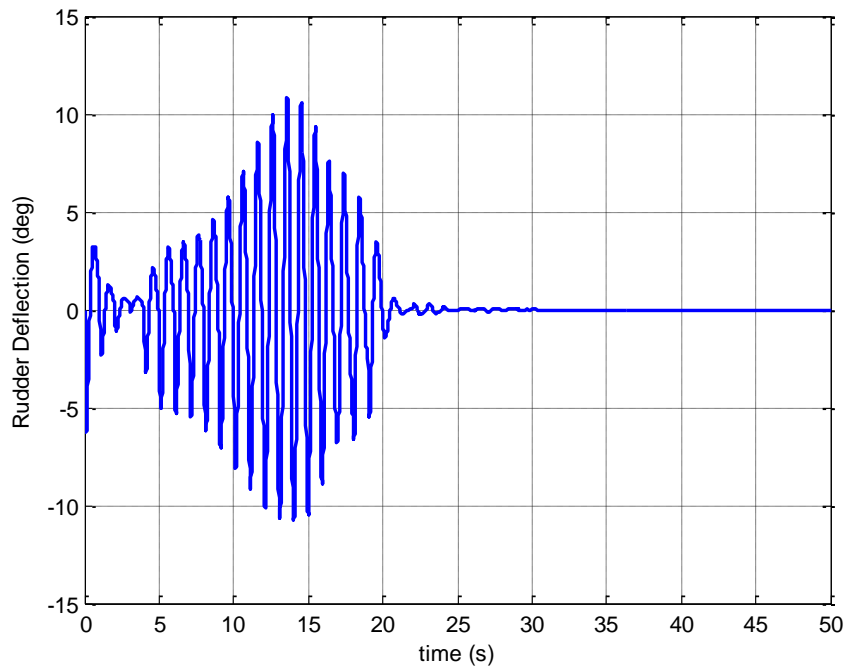
Figure 3.12a: Time history of the rudder deflection, Case 1, SDRE, 50 seconds time scale
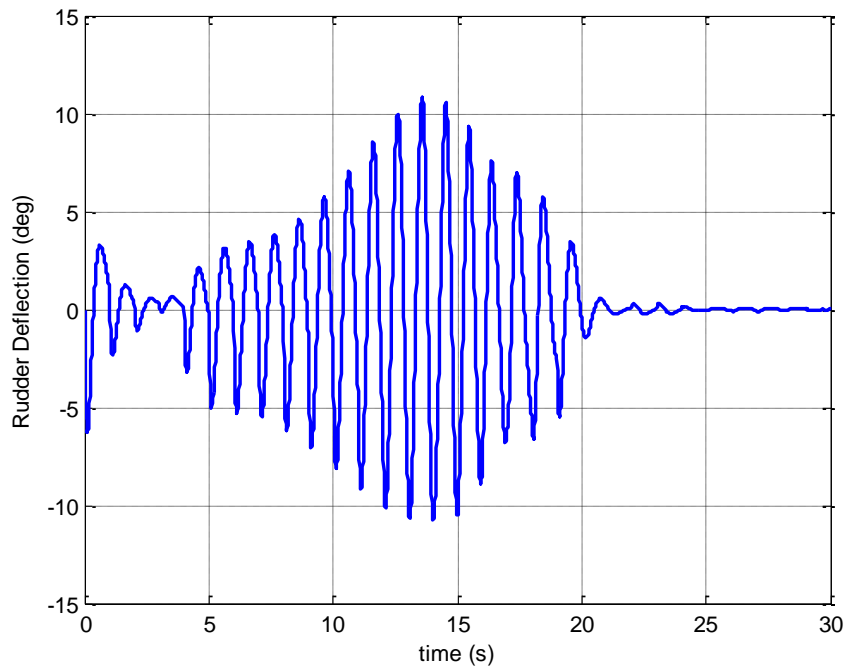
Figure 3.12b: Time history of the rudder deflection, Case 1, SDRE, 30 seconds time scale
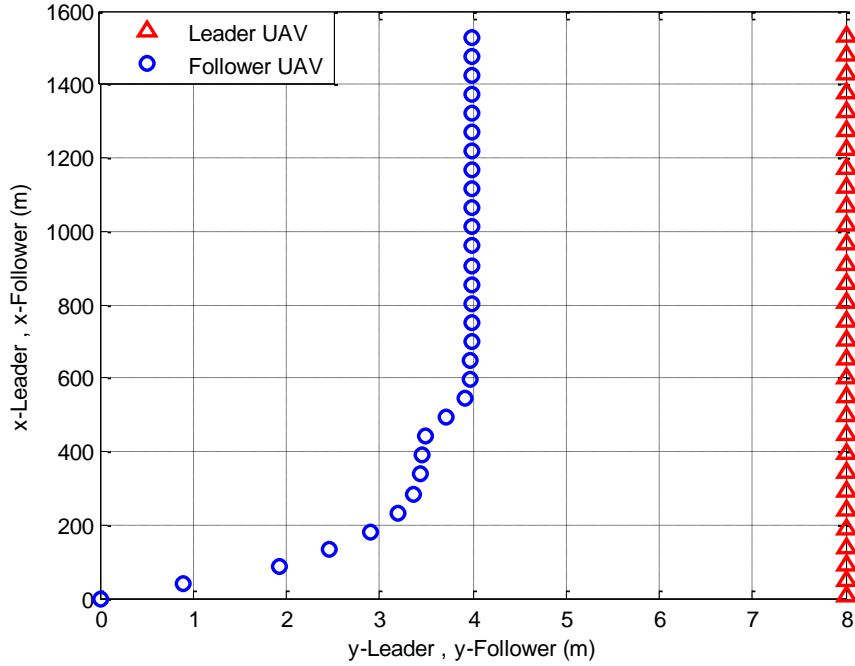
Figure 3.13: Leader UAV position vs Follower UAV position, Case 1, SDRE

Figure 3.3 shows the leader UAV's velocity. The velocity is increased from 20 m/s to 26 m/s albeit a steady state error of 0.09m/s due to the controller implemented on the leader. As seen in figure 3.4, the leader UAV's altitude momentarily rises to about 1000.8m and then settles at 1000m. This is as a result of the leader UAV's increase in velocity. However, a rise of 0.8m is negligible, thus in this flight scenario, we can say that the altitude is kept constant at 1000m. Figure 3.5 shows the time history of the leader UAV's heading which is kept constant at 0 degrees. We desire to see if the follower UAV can track and maintain the reference formation geometry in spite of the increase in velocity of the leader UAV. In figure 3.6, we see that the follower UAV is able to track the desired x-separation between it and the leader UAV. The initial x-separation between the leader and follower UAV is 9m and it is desired that an x-separation of 6m be maintained. In other words, we would like to reduce the x-separation between the leader and follower UAV in spite of an increase in the velocity of the leader UAV. The follower UAV is able to track the desired x-separation in about 23 seconds. A steady state error of 0.08m can be seen. This is probably as a result of the steady state error present in the design of the follower UAV controllers i.e., the inner loop controllers of our formation control system. In figure 3.7, we see that the follower UAV is also able to track the desired y-separation between it and the leader UAV. The initial y-separation between the two UAVs is 8m and a 4m separation is desired. It takes about 23 seconds for the follower UAV to track the desired y-separation. A steady state error of 0.01m can be seen and this also as a result of the inner loop controllers. In figure 3.8, the follower UAV is also able to track the desired z-separation of 5m. It takes about 15 seconds for the follower UAV to track the desired z-separation. No steady state error can be seen. We can conclude then that the follower UAV is able to track the desired formation geometry since all the desired x, y and z separation distances are tracked. It took 23 seconds for the follower UAV to go from the initial formation geometry to the desired formation geometry. Figures

41

3.9a to 3.12b shows us the time histories of the deflections of the follower UAV control surfaces as the follower UAV tracks the desired formation geometry. We see no saturations in the deflection of the control surfaces. Figure 3.9a shows the deflection of the follower UAV's elevator. The highest deflection angle was about 9 degrees and the lowest was about 0 degrees. These values are way below the maximum limit of ± 20 degrees set for the elevator. Figure 3.10a is the plot of the percentage increase of the follower UAV throttle. The throttle was initially at 6.7%, it then increases to 16% before dropping back to about 9%. The increase in throttle is expected because in order for the follower UAV to reduce its x-separation from the leader in spite of the acceleration of the leader, it has to momentarily move faster than the leader. After achieving the required separation, it then has to slow down to match the leader UAV's velocity. Figure 3.11a shows the deflection of the follower UAV's aileron. It deflected within the range of ± 12 degrees. This is also under the maximum set range limit of ± 20 degrees. Figure 3.12a shows the deflection of the follower UAV's rudder. There is no saturation in its deflection since it deflected within the range of ± 11 degrees which is below the maximum set range limit of ± 15 degrees. Looking at figures 3.9b, 3.10b, 3.11b and 3.12b, we see that there are oscillations in the deflections of the control surfaces. Looking closely at these figures, we see that there are 5 peaks within every 5 second interval, i.e. 1 peak per second. This is as a result of the SDRE formation-hold controller's update rate. For this simulation, an update rate of 1 second was chosen. This implies that at every second, new gains are computed and new signals are sent to the inner loop controllers. Thus, the control surfaces deflect at every second to track the new signals received. Figure 3.13 shows us the positions of both the leader UAV and the follower UAV. From the figure, we see how the follower UAV changes its relative y separation from the leader UAV from 8m to 4m as desired. We can also see that the desired formation geometry is maintained. For a clearer picture of the relative x-separation between the leader and follower UAV, refer to figure 3.6.

Case 2: In this flight scenario, case 2, the leader UAV flies at the velocity, altitude and heading depicted in figure 3.15, 3.16 and 3.17 respectively. The leader and follower UAVs are initially flying at separation distances of $(x_{ini}, y_{ini}, z_{ini}) = (4, 0, 0)$ m. It is desired that the follower's relative position be maintained in spite of the change in heading of the leader UAV, i.e. $(x_{ref}, y_{ref}, z_{ref}) = (4, 0, 0)$ m. In other words, we would like to see if the follower UAV can maintain a trail formation geometry in spite of a change in heading of the leader UAV.
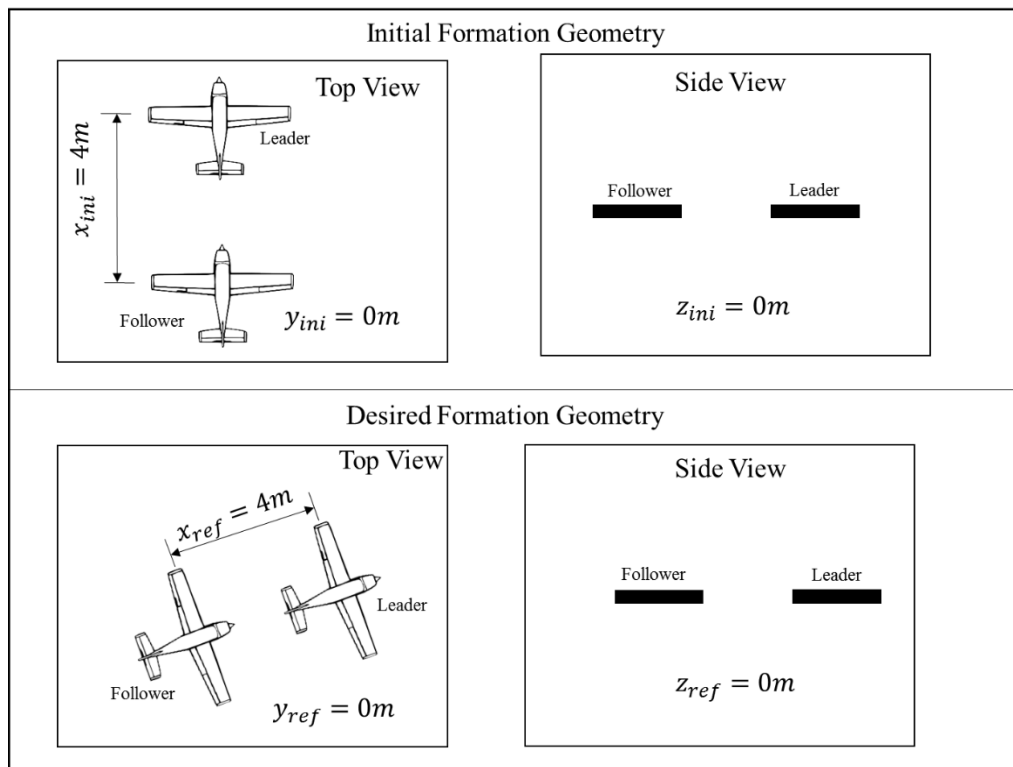
Figure 3.14: Initial and Desired Formation Geometries, Case 2, SDRE
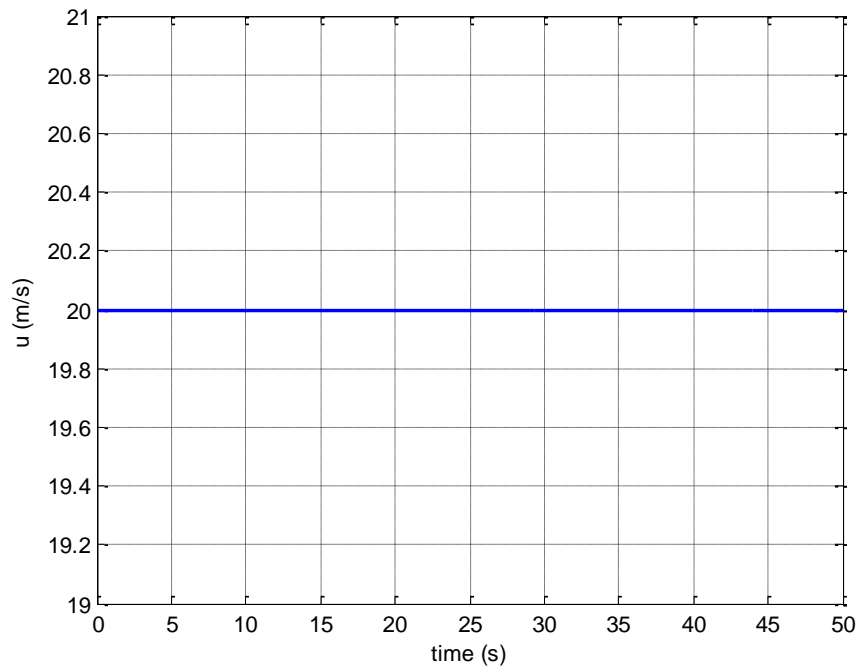
Figure 3.15: Time history of leader UAV's velocity, Case 2, SDRE
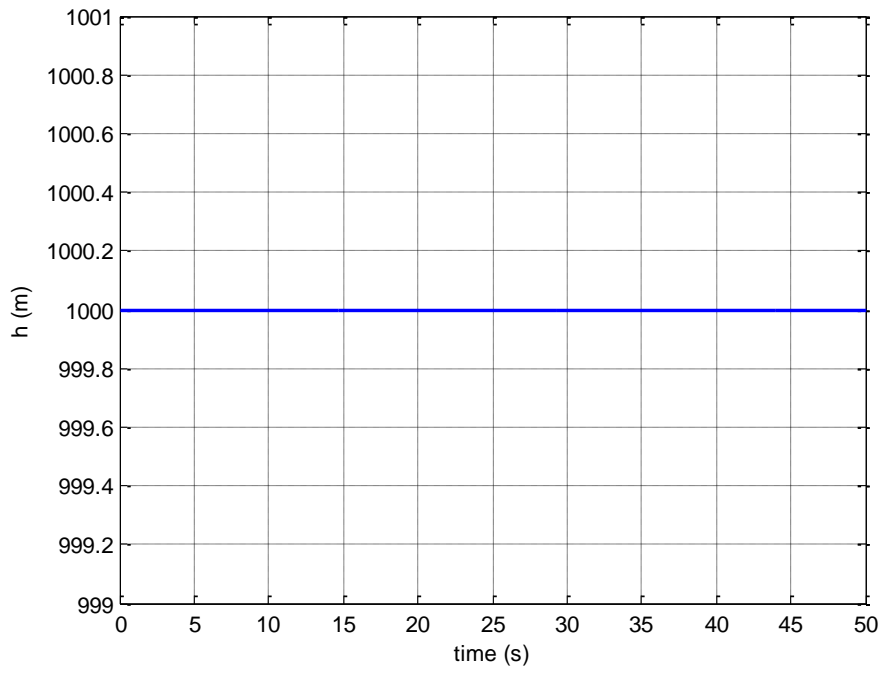
Figure 3.16: Time history of leader UAV's altitude, Case 2, SDRE
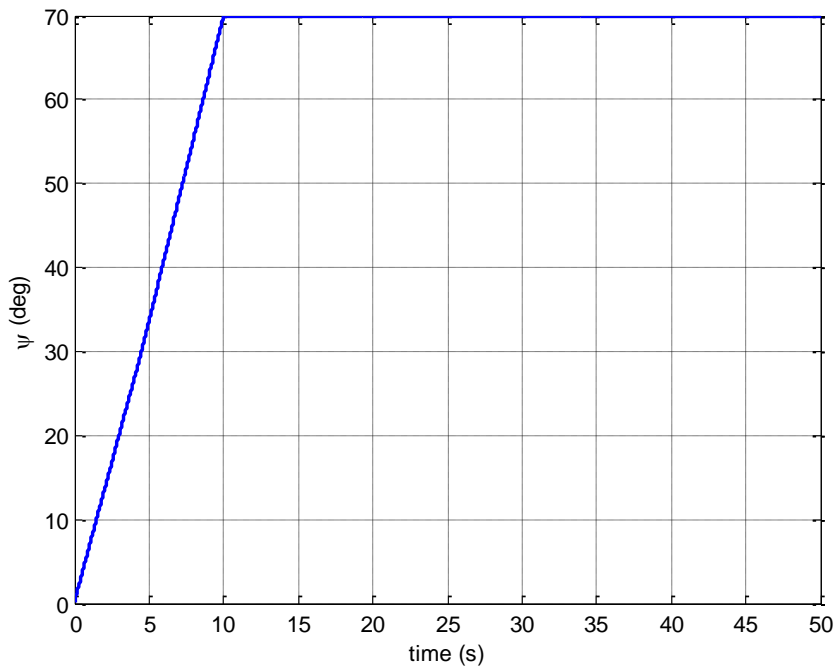
Figure 3.17: Time history of leader UAV's heading, Case 2, SDRE

44
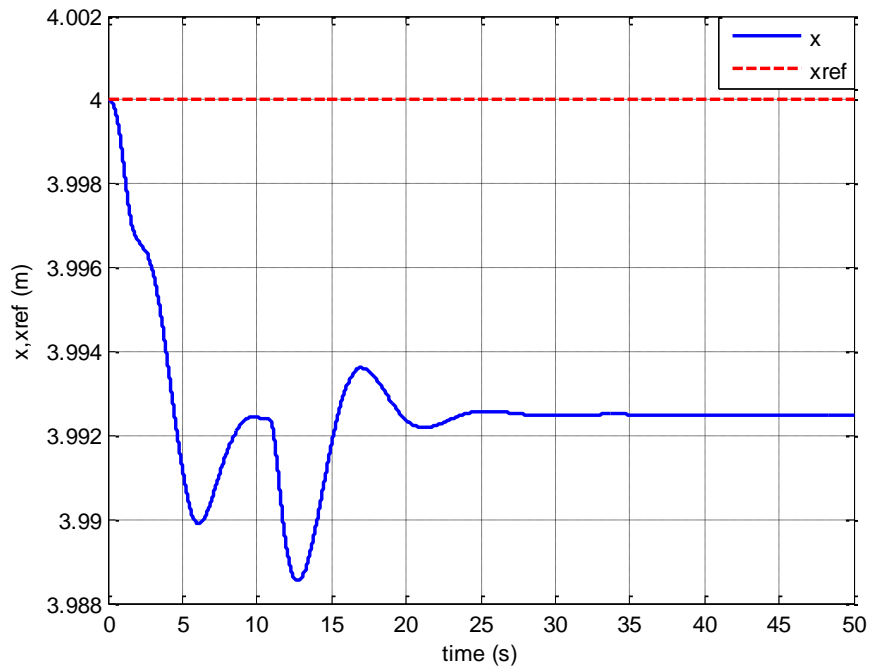
Figure 3.18: Time history of the follower UAV's relative position, x-component, Case 2, SDRE
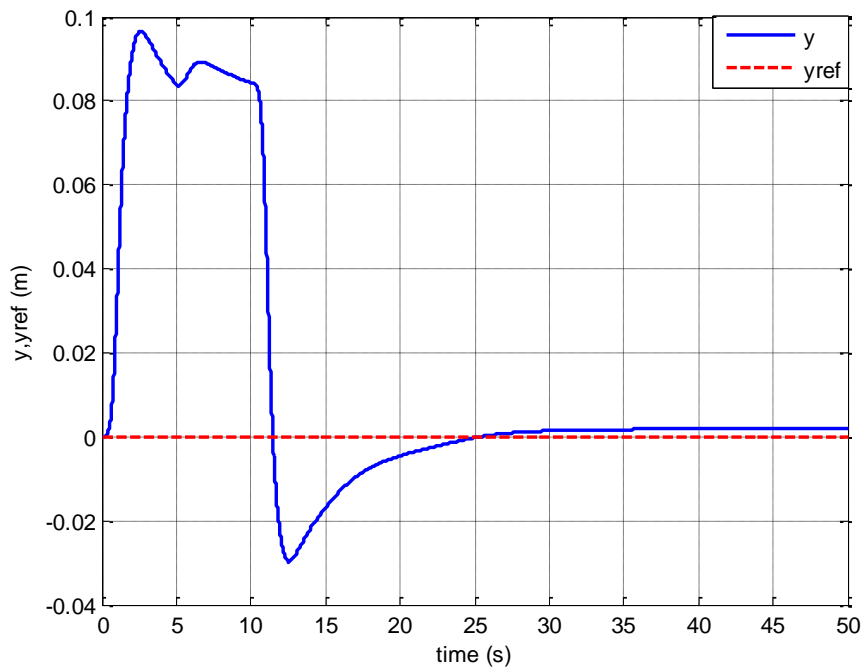
Figure 3.19: Time history of the follower UAV's relative position, y-component, Case 2, SDRE
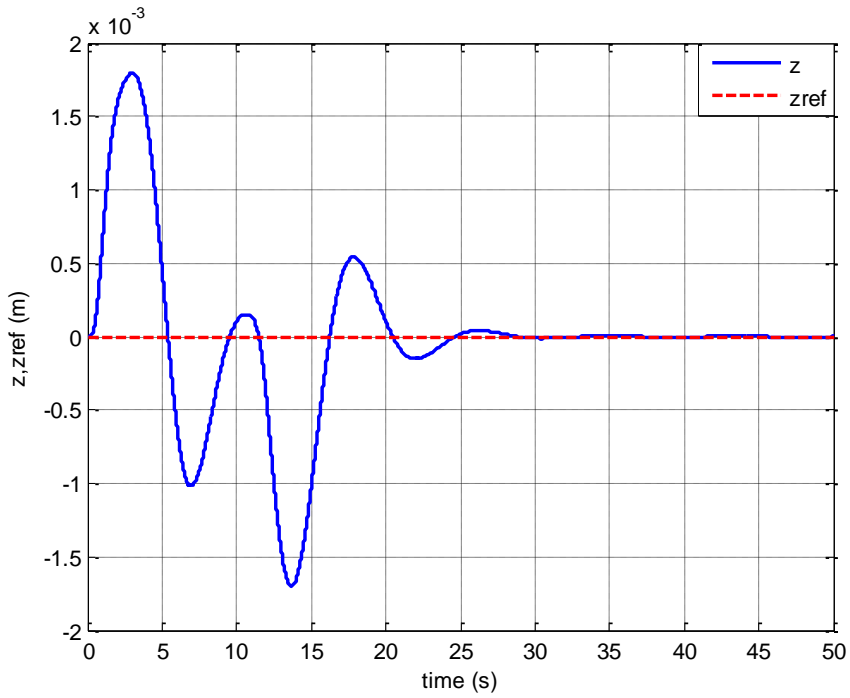
Figure 3.20: Time history of the follower UAV's relative position, z-component, Case 2, SDRE
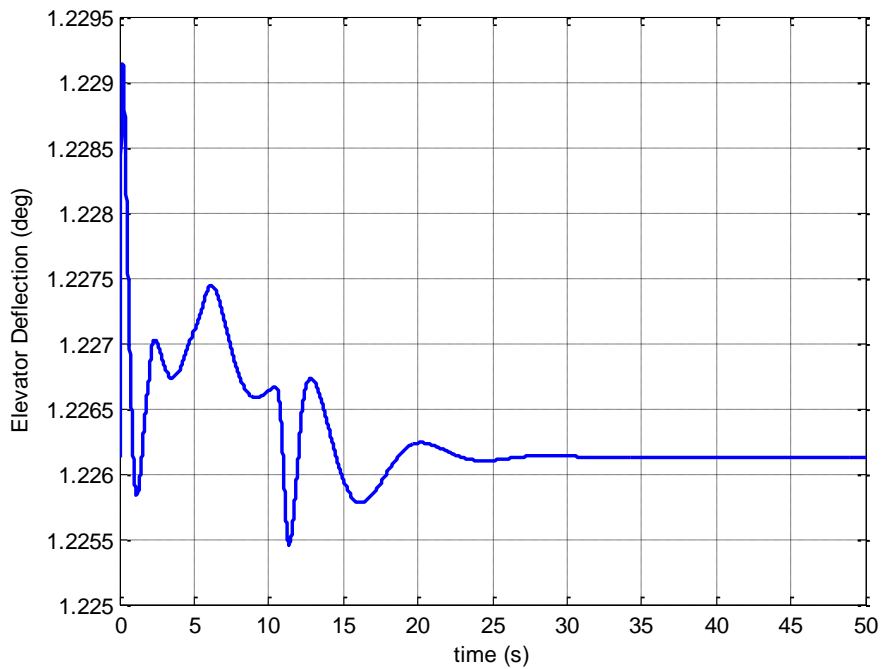
Figure 3.21: Time history of the elevator deflection, Case 2, SDRE
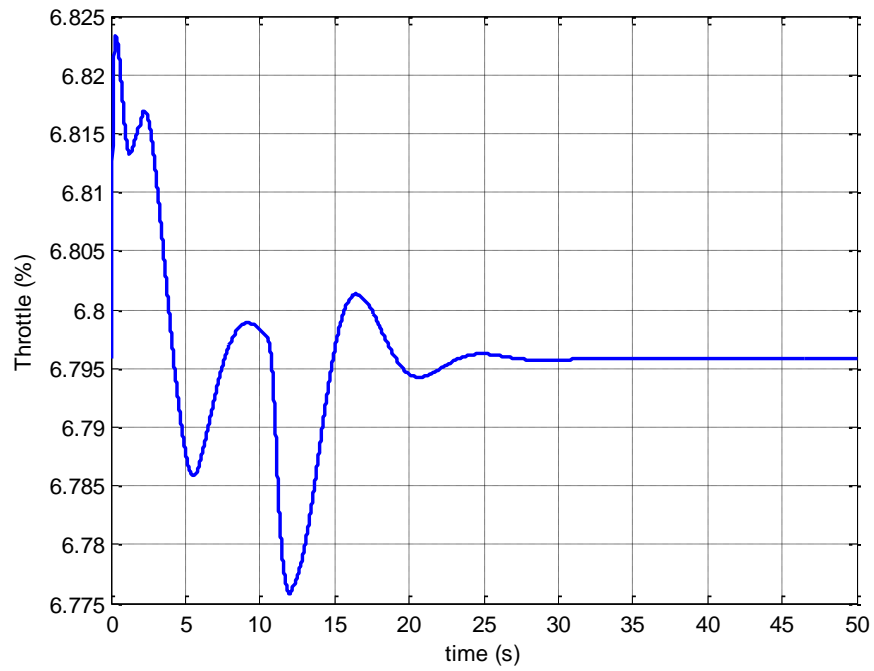
Figure 3.22: Time history of the throttle, Case 2, SDRE
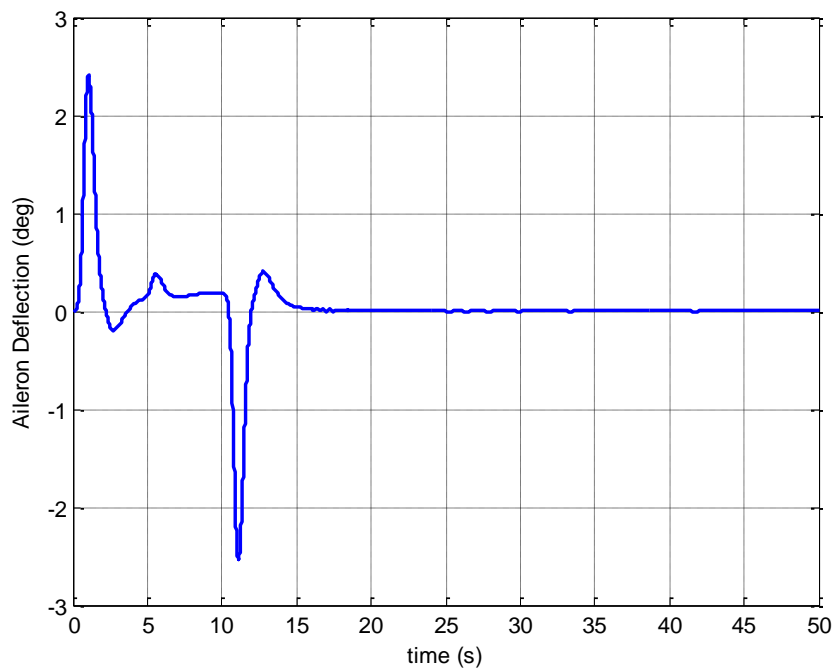
Figure 3.23: Time history of the aileron deflection, Case 2, SDRE

47
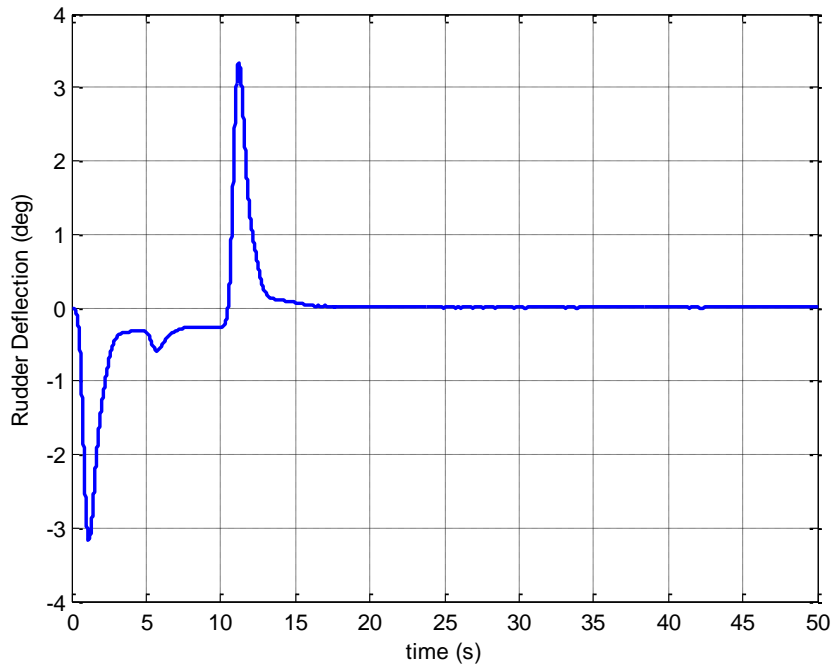
Figure 3.24: Time history of the rudder deflection, Case 2, SDRE
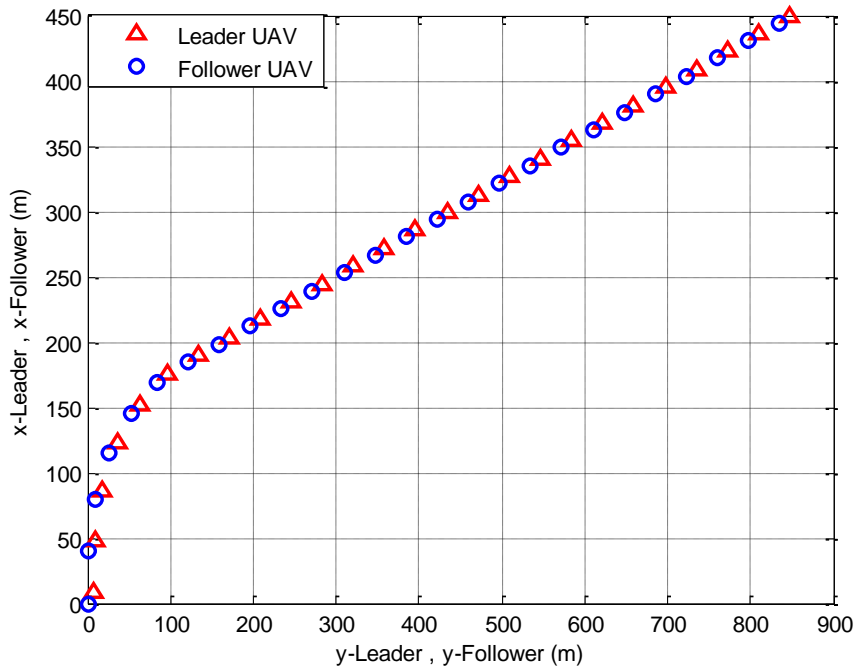
Figure 3.25: Leader UAV position vs Follower UAV position, Case 2, SDRE

For this formation flight scenario, the leader UAV velocity is kept constant at 20m/s, figure 3.15. The altitude is also kept constant at 1000m, figure 3.16. However, the leader UAV's heading is varied from 0 degrees to 70 degrees at a rate of 7 degrees per second, figure 3.17. It is desired that we maintain a trail formation in spite of this varying heading, figure 3.14. Figure 3.18 shows the time history of the relative x-separation between the leader and follower UAV. It is desired that this x-separation be kept constant at 4m while the leader UAV changes its heading. We see from the figure that our follower UAV was able to track the desired x-separation with a negligible error of about 8mm. We also desire that the y-separation be maintained at 0m i.e. we want the follower to fly directly behind the leader UAV as the leader UAV changes its heading. Figure 3.19, shows the time history of the relative y-separation between the leader and follower UAVs. We see from figure 3.19, that in the first 10 seconds, the follower UAV is to the left of the leader UAV by only about 9cm as the leader UAV changed its heading from 0 degrees to 70 degrees (figure 3.16). As the leader starts flying at the new heading, i.e. after 10 seconds, the follower UAV corrects its y-separation as to 0m as desired. The follower UAV veers off the desired 0m separation by an acceptable 9cm in the first ten seconds and then by about an acceptable 3 cm in the next ten seconds before settling at the desired 0m. We also desired the throughout this formation flight scenario, the leader and follower UAVs fly level with each other i.e. a z-separation of 0m be maintained. From figure 3.20, we see that our follower UAV maintains the desired z-separation. Figures 3.21 to 3.24 shows the time histories of the deflections of the control surfaces. We see no saturations in the deflections of any of the control surfaces. Figure 3.21 shows the follower UAV's elevator deflection, we see that it deflects well under the maximum set range limit of ± 20 degrees. Figure 3.22 shows the percentage change in throttle of the follower UAV. Figure 3.23 shows the time history of the follower UAV's aileron deflection as the follower UAV maintains its separation distance from the leader UAV. We see a deflection range of about ± 3 degrees which is well under the set limit of ± 20 degrees. Figure 3.24 shows the rudder deflection of the follower UAV, the rudder also deflects well under its maximum range of ± 15 degrees. From figure 3.25, we can easily see that the follower maintains the desired trail formation i.e. flies directly behind the leader UAV even as the leader UAV changes its heading.

Case 3: In this flight scenario, case 3, the leader UAV flies at the velocity, altitude and heading depicted in figure 3.27, 3.28 and 3.29 respectively. The leader and follower UAVs are initially flying at separation distances of $(x_{ini}, y_{ini}, z_{ini}) = (8, 8, 0)$ m. It is desired that these separation distances be brought to $(x_{ref}, y_{ref}, z_{ref}) = (0, 3, 0)$ m. In other words, it is desired that the leader and follower UAVs fly side by side each other while maintaining a 3m relative y-separation distance between them. An x-separation distance of 0m is desired in this flight scenario. As discussed in section 3.2, this creates a singularity problem in obtaining the control law for the SDRE formation-hold controller. This flight scenario was specifically tested to see if the workaround designed in section 3.2 works.
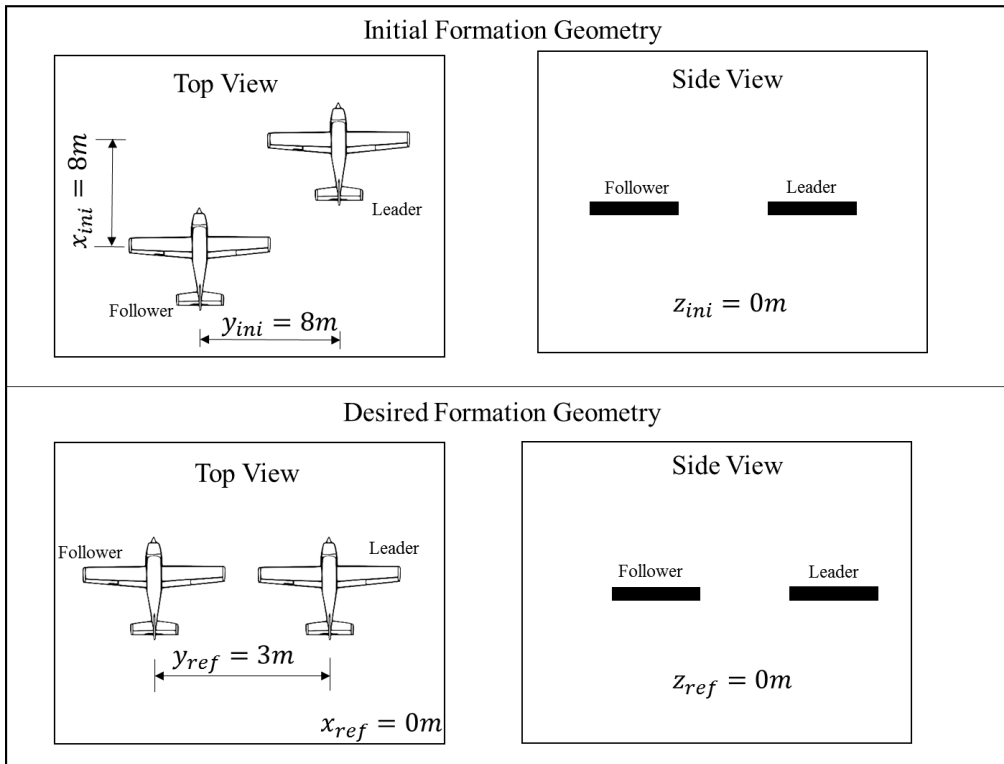
Figure 3.26: Initial and Desired Formation Geometries, Case 3, SDRE
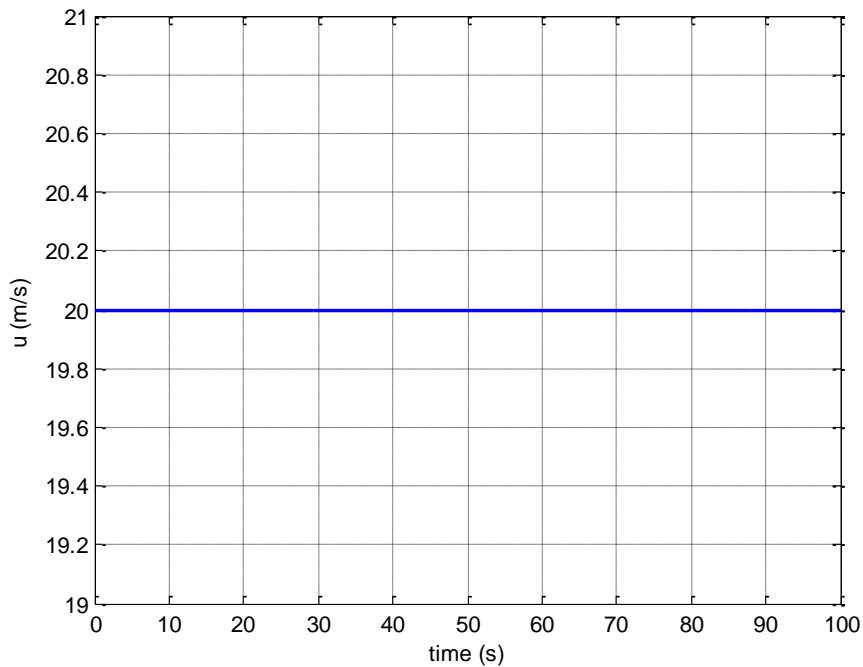
Figure 3.27: Time history of leader UAV's velocity, Case 3, SDRE
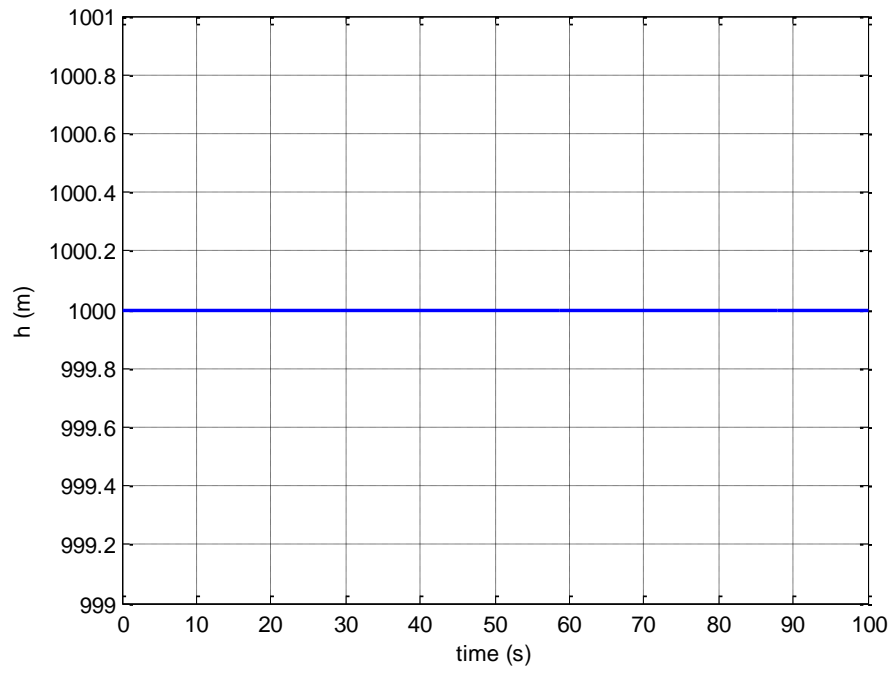
Figure 3.28: Time history of leader UAV's altitude, case 3, SDRE
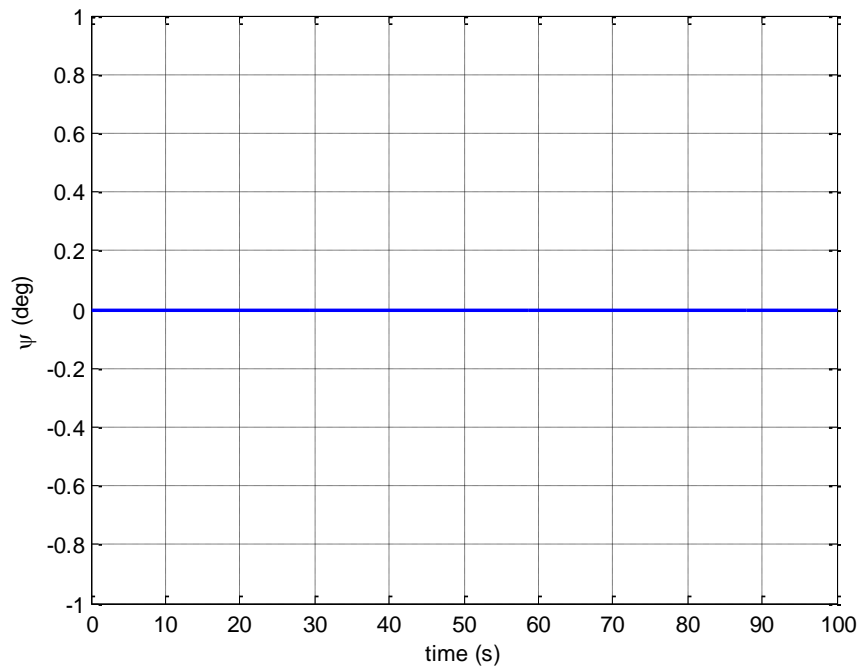
Figure 3.29: Time history of leader UAV's heading, Case 3, SDRE
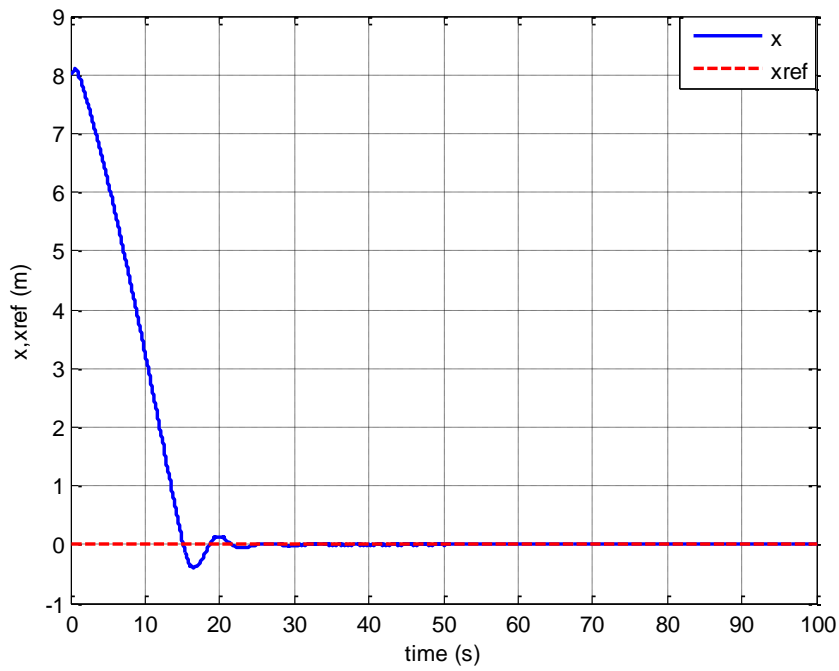
Figure 3.30: Time history of the follower UAV's relative position, x-component, Case 3, SDRE
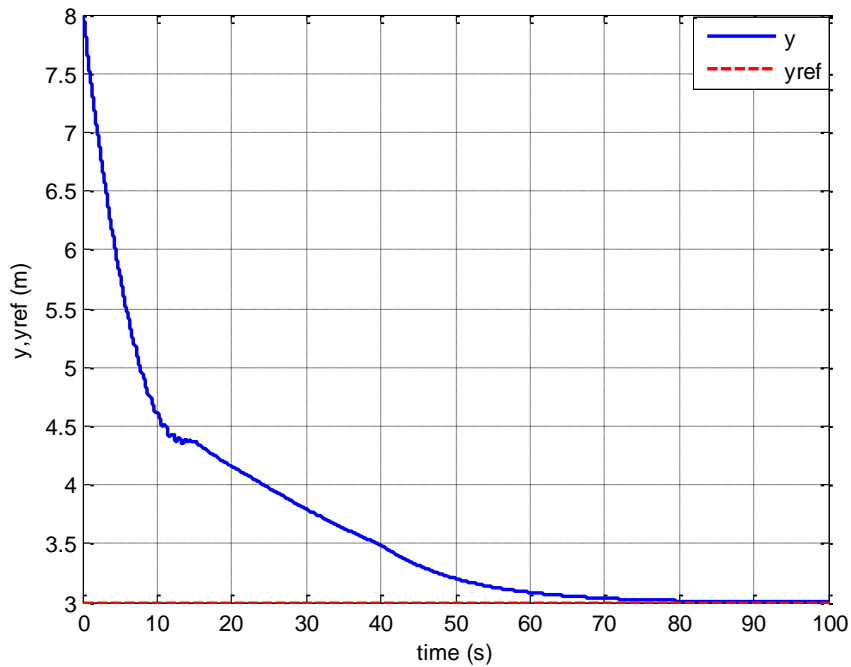
Figure 3.31: Time history of the follower UAV's relative position, y-component, Case 3, SDRE
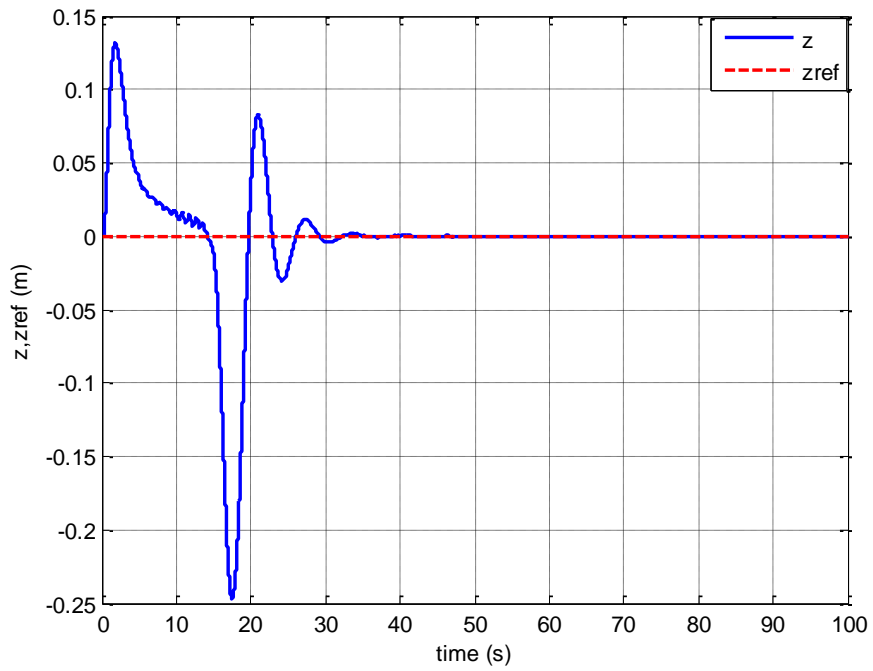
Figure 3.32: Time history of the follower UAV's relative position, z-component, Case 3, SDRE
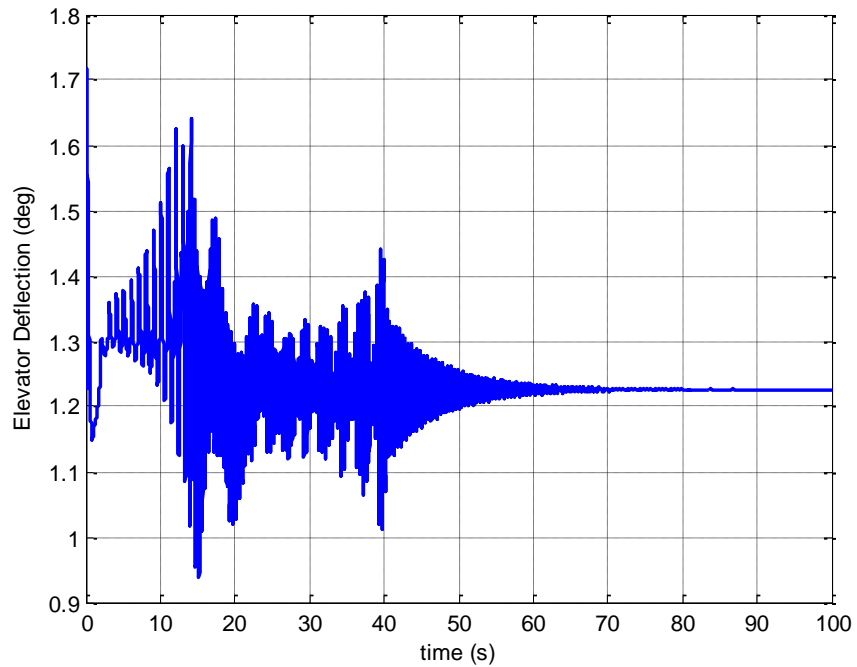
Figure 3.33a: Time history of the elevator deflection, Case 3, SDRE, 100 seconds time scale
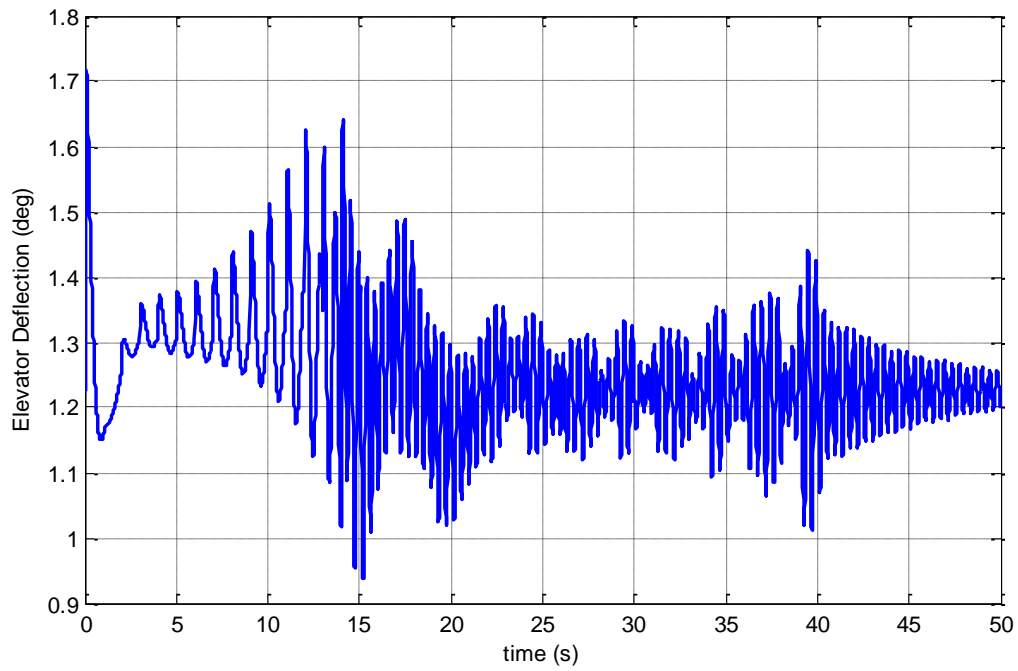
Figure 3.33b: Time history of the elevator deflection, Case 3, SDRE, 50 seconds time scale
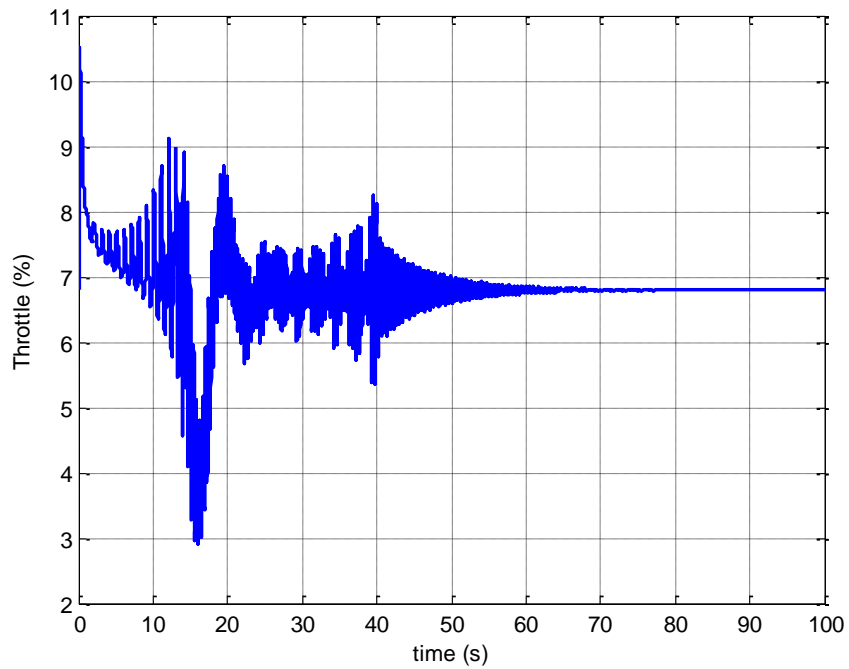
Figure 3.34a: Time history of the throttle, Case 3, SDRE, 100 seconds time scale
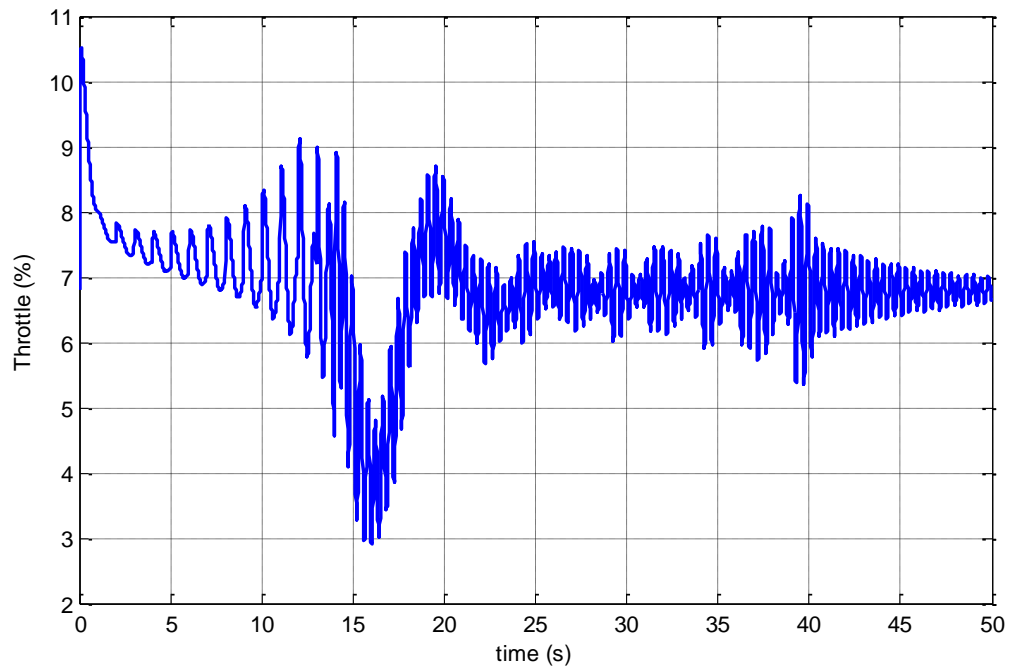
Figure 3.34b: Time history of the throttle, Case 3, SDRE, 50 seconds time scale
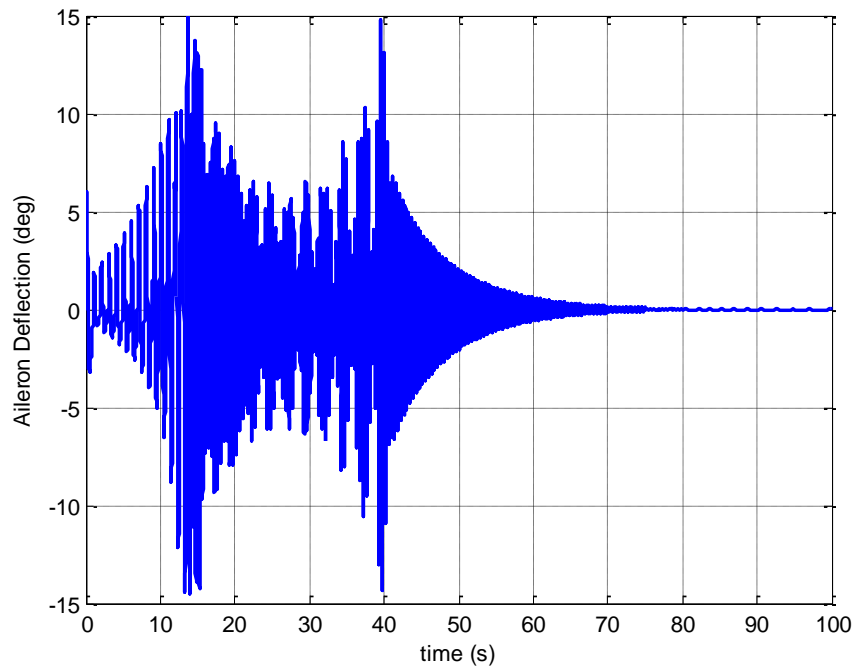
Figure 3.35a: Time history of the aileron deflection, Case 3, SDRE, 100 seconds time scale
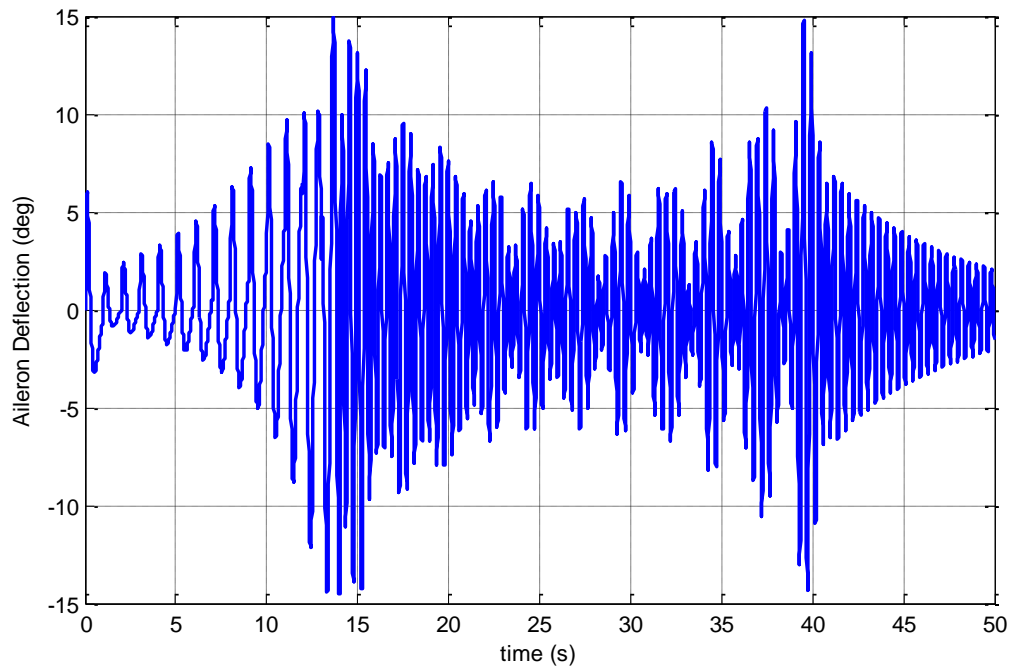
Figure 3.35b: Time history of the aileron deflection, Case 3, SDRE, 50 seconds time scale
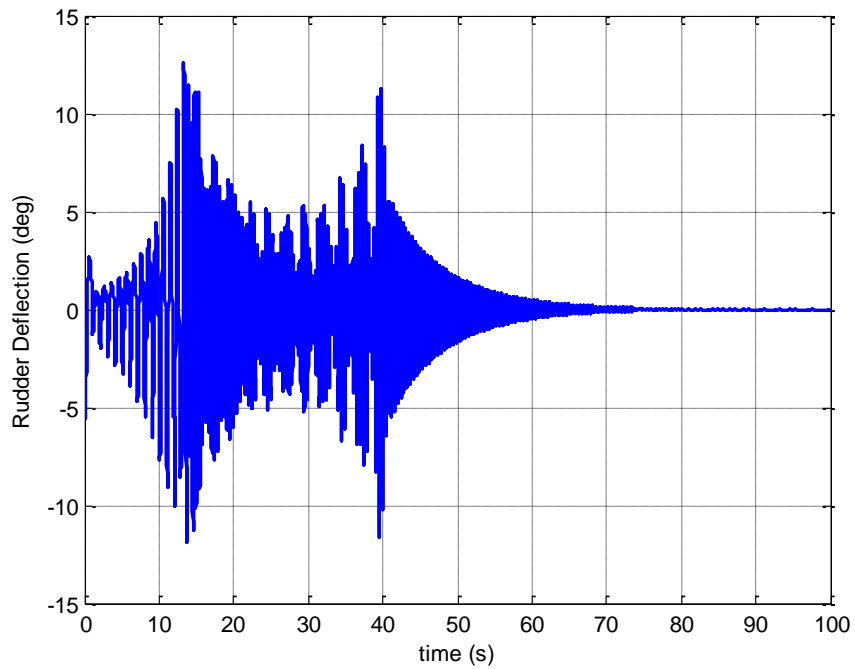
Figure 3.36a: Time history of the rudder deflection, Case 3, SDRE, 100 seconds time scale
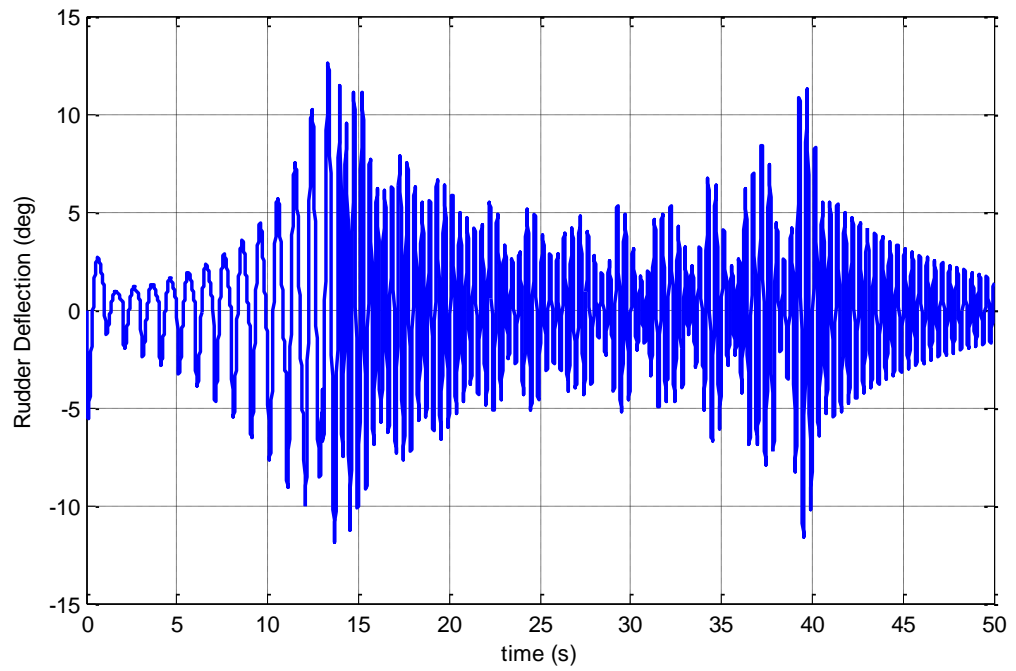
Figure 3.36b: Time history of the rudder deflection, Case 3, SDRE, 50 seconds time scale
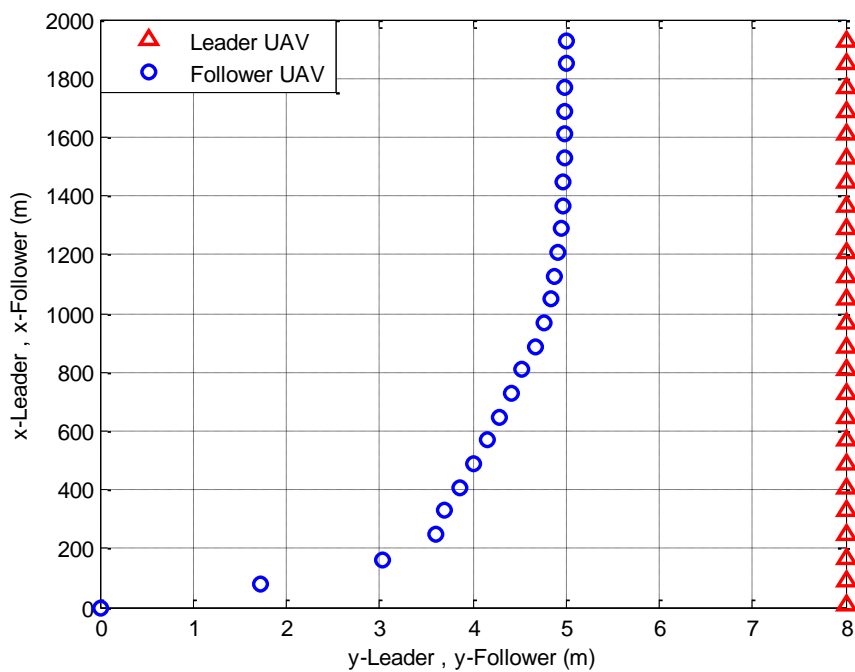
Figure 3.37: Leader UAV position vs Follower UAV position, Case 3, SDRE

For this formation flight scenario, the leader UAV flies at a constant velocity of 20 m/s as seen in figure 3.27. Its altitude is kept constant at a 1000m, figure 3.28 and it flies at a constant heading of 0 degrees, figure 3.29. The initial x-separation between the leader UAV and follower UAV is 8m. It is desired that this separation be brought to 0m. Figure 3.30 shows us the time history of the relative x-separation between the leader and follower UAV. From the figure, we see that the follower is able to track the desired x-separation in about 20 seconds without a steady state error. For a desired x-separation of 0m, we normally would have a singularity problem as shown in equation (48), but by using the workaround developed in section 3.2 whereby the x value in the B matrix of the formation-hold controller is set to 0.5 for cases where $-0.5 \leq x \leq 0.5$, we avoid this problem. The result obtained in figure 3.30 validates the efficacy of the workaround developed. Figure 3.31 shows the relative y-separation between the leader and the follower UAV, the two UAVs are initially at a y-separation of 8m. It is desired that this separation be brought to 3m. We see from the figure that the follower UAV is able to track the desired y-separation of 3m. From the figure, we have a settling time of about 60 seconds and no steady state error is seen. It is also desired that the leader and follower UAV fly level with one another i.e. they maintain a z-separation of 0m. From figure 3.32, we see that the relative z-separation between the two UAVs is practically kept at 0m. In the first 15 seconds, the follower UAV is about 15cm above the leader UAV, and in the next 5 seconds, its 25cm below the leader UAV and then it finally settles to 0m in the next 10 seconds. This deviations from 0m by a few centimeters is acceptable. Figures 3.33a to 3.36b show the time histories of the deflections of the control surfaces of the follower UAV as it tracks the desired formation geometry. We see no saturations in any of the deflections of the control surfaces as none of them deflect to their maximum angle limit. The deflection limit for the aileron and elevator is $\pm$ 20 degrees, and for the rudder, its $\pm$ 15 degrees. In figure 3.33a, we see that the elevator deflects between 1 degree and 1.7 degrees. This little deflection angle is expected because the follower and leader UAV are initially flying level with each other and it is desired that they both keep flying level. Thus, a climb or descent of the follower UAV is not necessary, hence not much deflection is needed in the follower UAVs elevator. Figure 3.33b zooms in on the first 50 seconds of figure 3.33a for a better picture of figure 3.33a. Figure 3.34a shows the percentage change in throttle. An initial rise in throttle can be seen, this is because the follower UAV needs to increase its velocity to cut its x-separation from the leader UAV from 8m to 0m. A drop in throttle is then seen since as soon as the leader approaches 0m, it needs to slow down to match the leader UAV's velocity. We also see an oscillation around 7 percent for the throttle after the follower UAV has tracked the desired x-separation of 0m. This is probably as a result of the workaround developed to avoid the singularity problem in the SDRE formation-hold controller. This is probably due to the fact that when $x = 0$ is fed back into our SDRE formation-hold controller, the value for x is set to 0.5 in the B matrix of the controller. The controller then in turn tries to reduce the "apparent" steady-state error and this translates into oscillations in the throttle and elevator as well. Figure 3.34b zooms in on the first 50 seconds of figure 3.34a for a better picture of figure 3.34a. Figure 3.35b shows aileron deflection. From the figure, we see a maximum deflection of $\pm$ 15 degrees which is below the maximum deflection limit for the aileron. Figure 3.36a shows the rudder deflection, we see a maximum deflection of about $\pm$ 12 degrees which is also below the maximum deflection limit for the rudder. . Figure 3.37 shows us the positions of both the leader UAV and the follower UAV. From the figure, we see how the follower UAV changes

58

its relative y separation from the leader UAV from 8m to 3m as desired. We can also see that the two UAVs fly side by side each other.

From the above simulations provided in case 1, 2, and 3, we can conclude that our SDRE formation control system is very effective in enabling the follower UAV track a formation geometry while the leader UAV flies at a prescribed trajectory.

3.5.1   SDRE Feedback Gain Update Rate

As stated earlier in section 3.1 and 3.2, the SDRE algorithm captures the nonlinearities of a system by converting a nonlinear system to a linear-like structure using state-dependent coefficient (SDC) matrices. At each time instant, the method treats the state-dependent coefficient matrices as being constant, and computes a control action by solving a Linear Quadratic optimal control problem. In other words, at every time instant, a new feedback gain is calculated by solving the Linear Quadratic optimal control problem. The question "how often should we calculate a new feedback gain?" thus arises. The results presented and discussed in section 3.5 were obtained using a 1 second gain update rate for the formation-hold controller. In this section, gain feedback update rates of 0.5, 1 and 5 seconds will be compared.

To test the performance of the formation-hold controller while using the new feedback update rates, the formation flight scenario of case 1 in section 3.5 will be employed. The result for the z-component is not presented here because as explained earlier, the formation-hold controller only handles the x and y component of the relative position. For the z-component, an altitude controller is implemented on the follower UAV. Input to this altitude controller is the leader UAV's altitude plus the desired offset, z_{ref} .

As in case 1 of section 3.5, the leader and follower UAVs are initially flying at separation distances of $(x_{ini}, y_{ini}, z_{ini}) = (9, 8, 0)$ m. It is desired that the follower's relative position be brought to $(x_{ref}, y_{ref}, z_{ref}) = (6, 4, 5)$ m. Our aim is to see if the follower UAV can track and maintain the desired formation geometry in spite of the maneuvers carried out by the leader UAV. Refer to figures 3.3, 3.4 and 3.5 respectively for the time histories of the leader UAV's velocity, altitude and heading.
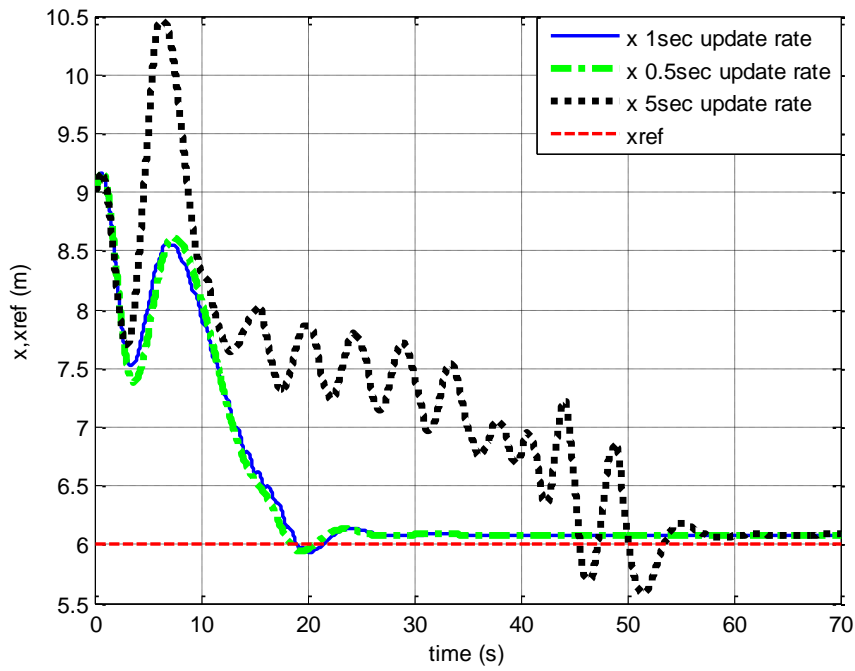
Figure 3.38: Time history of the x-component of the follower UAV's relative position with different SDRE update rates
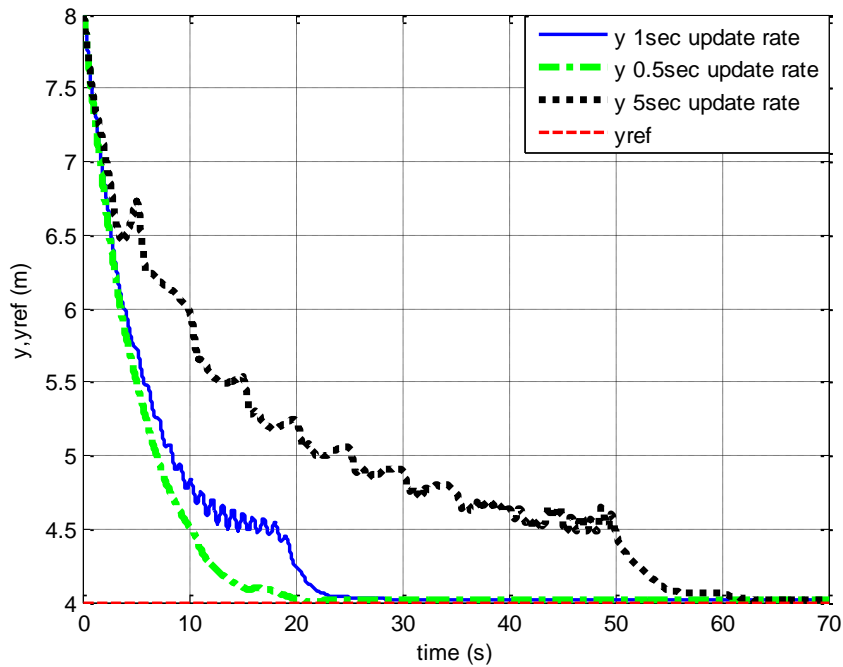
Figure 3.39: Time history of the y-component of the follower UAV's relative position with different SDRE update rates
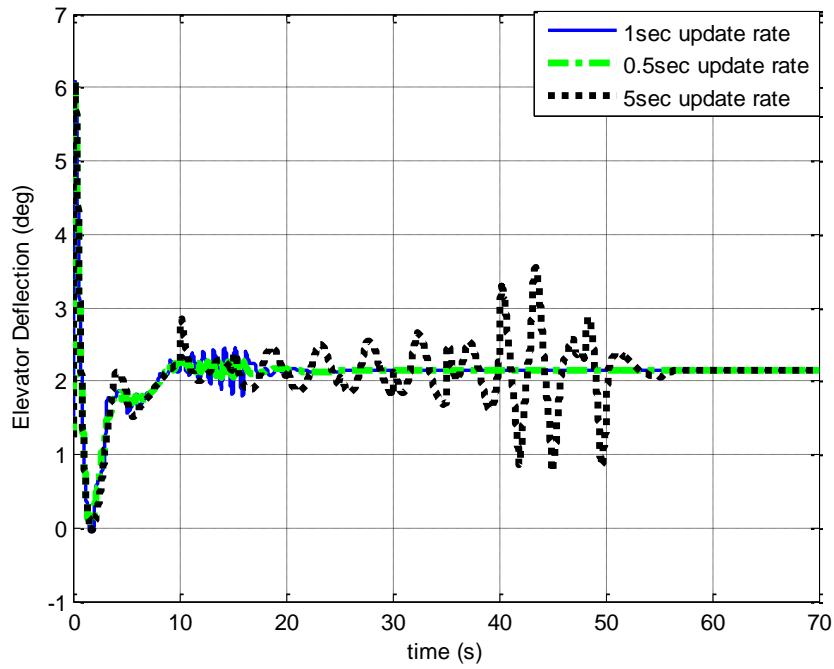
Figure 3.40a: Time history of the elevator deflection with different SDRE update rates, 70 seconds time scale
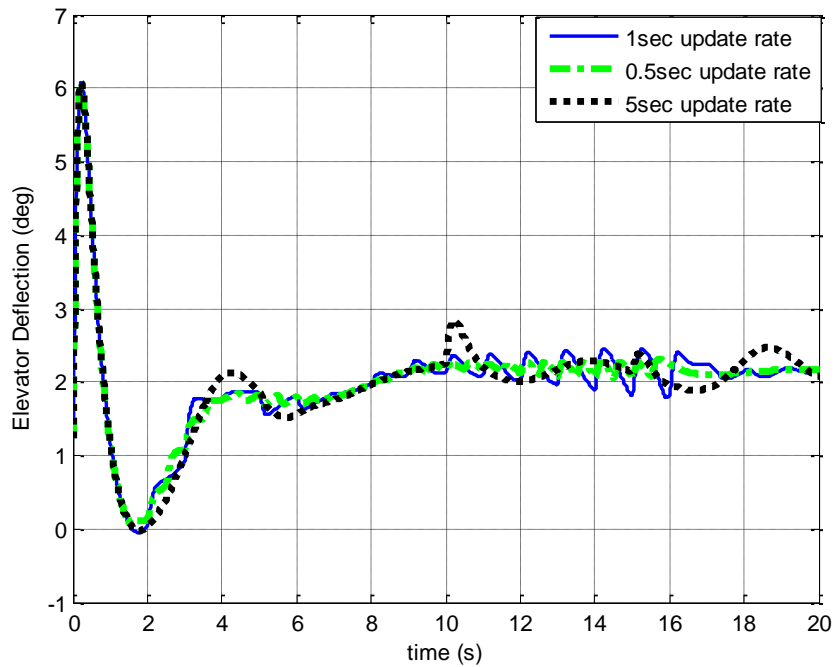
Figure 3.40b: Time history of the elevator deflection with different SDRE update rates, 20 seconds time scale

61
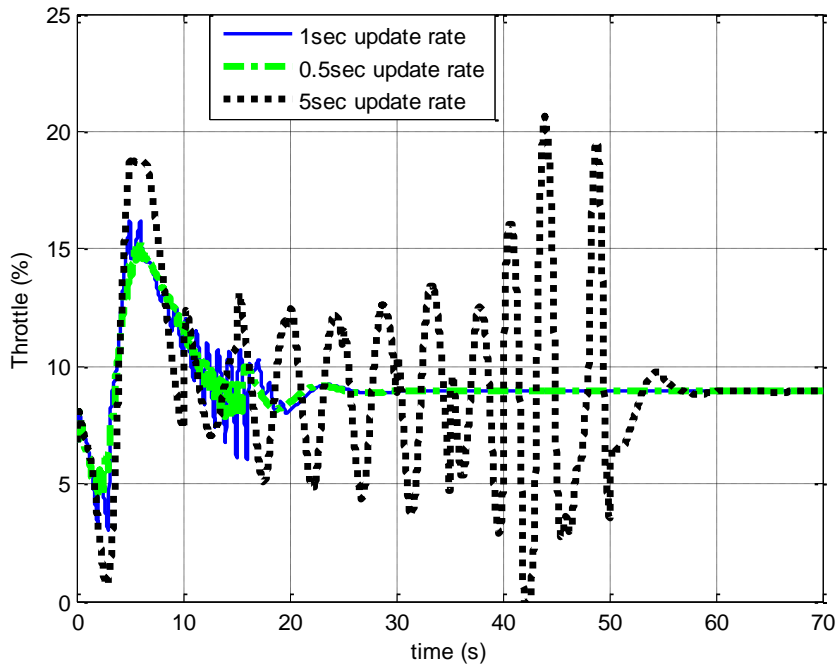
Figure 3.41a: Time history of the throttle with different SDRE update rates, 70 seconds time scale
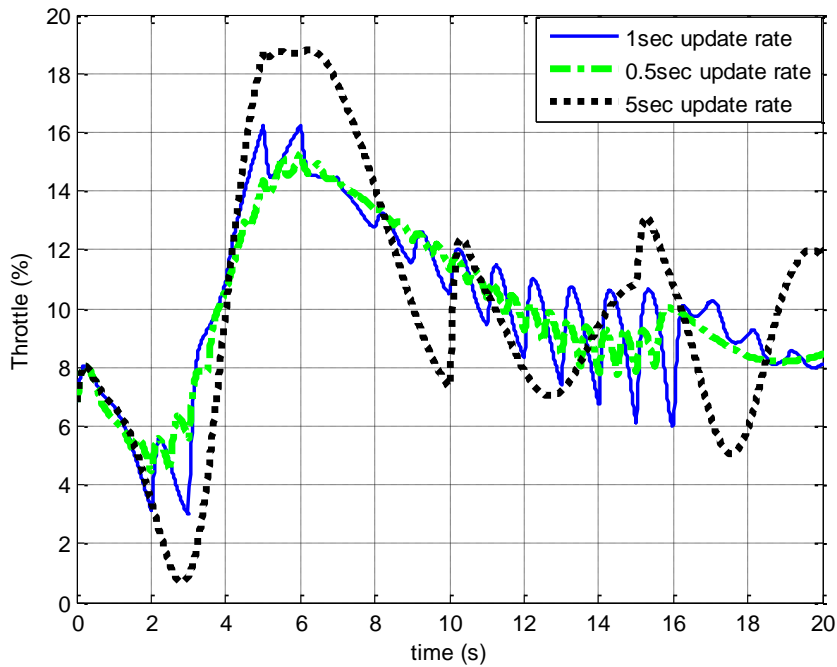
Figure 3.41b: Time history of the throttle with different SDRE update rates, 20 seconds time scale
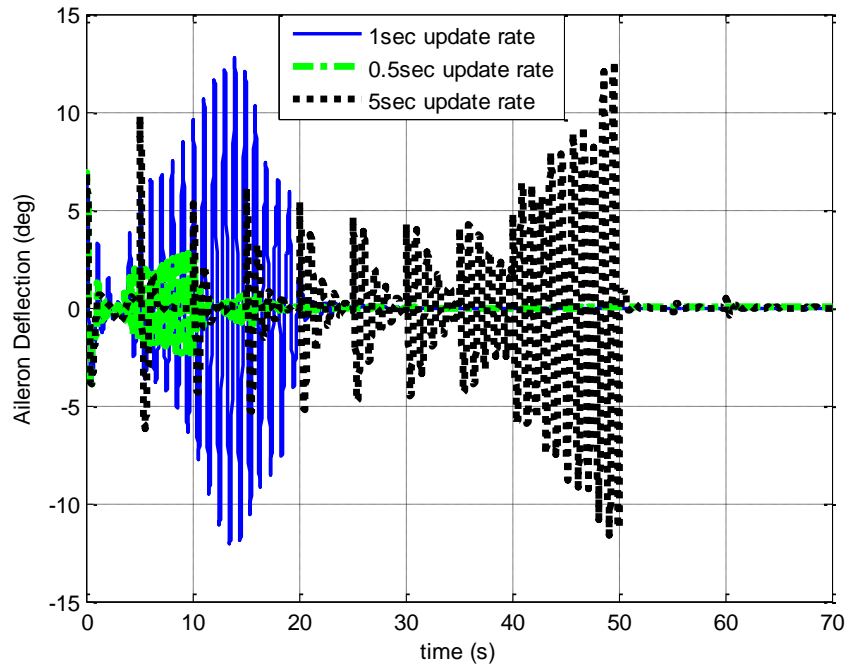
Figure 3.42a: Time history of the aileron deflection with different SDRE update rates, 70 seconds time scale
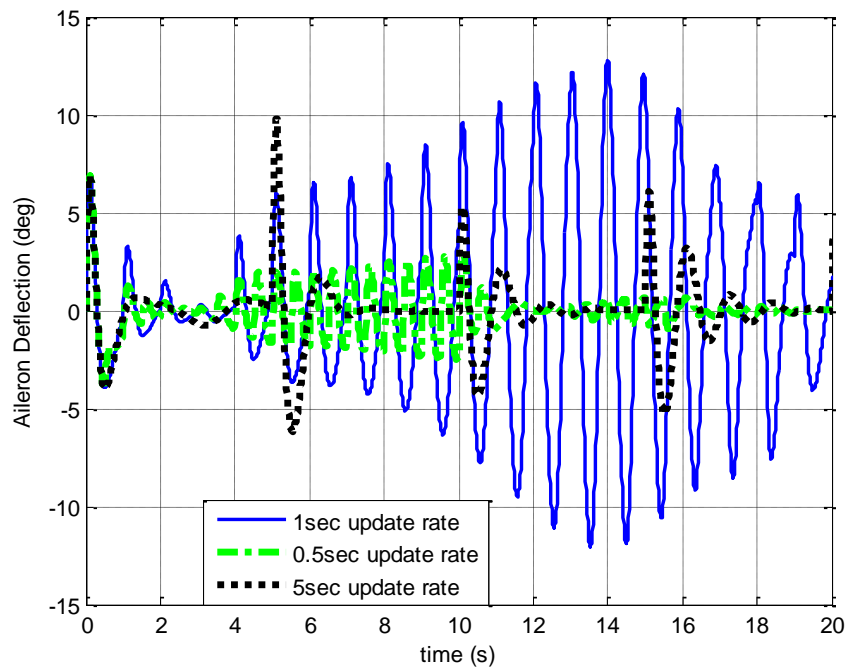
Figure 3.42b: Time history of the aileron deflection with different SDRE update rates, 20 seconds time scale
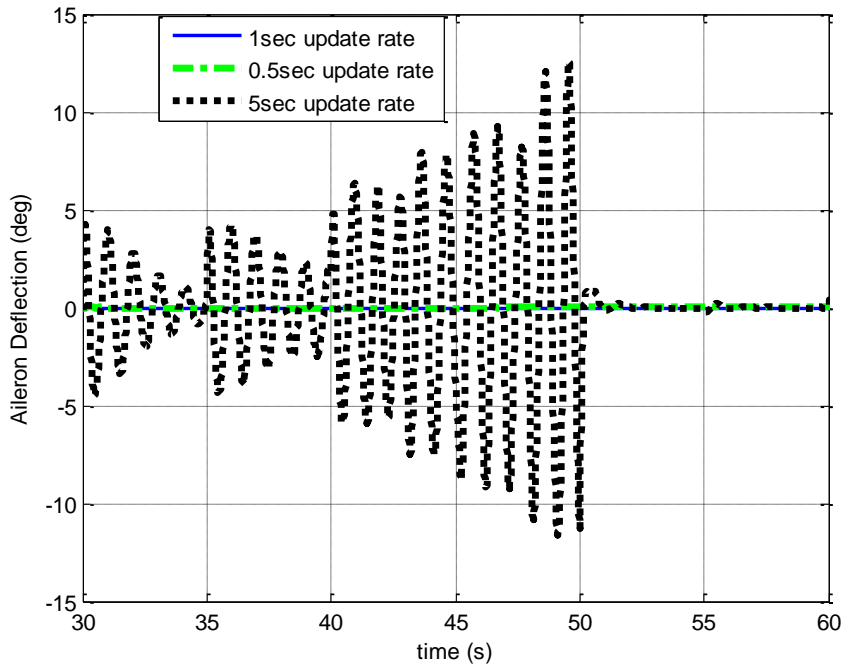
Figure 3.42c: Time history of the aileron deflection with different SDRE update rates, 30-60 seconds time scale
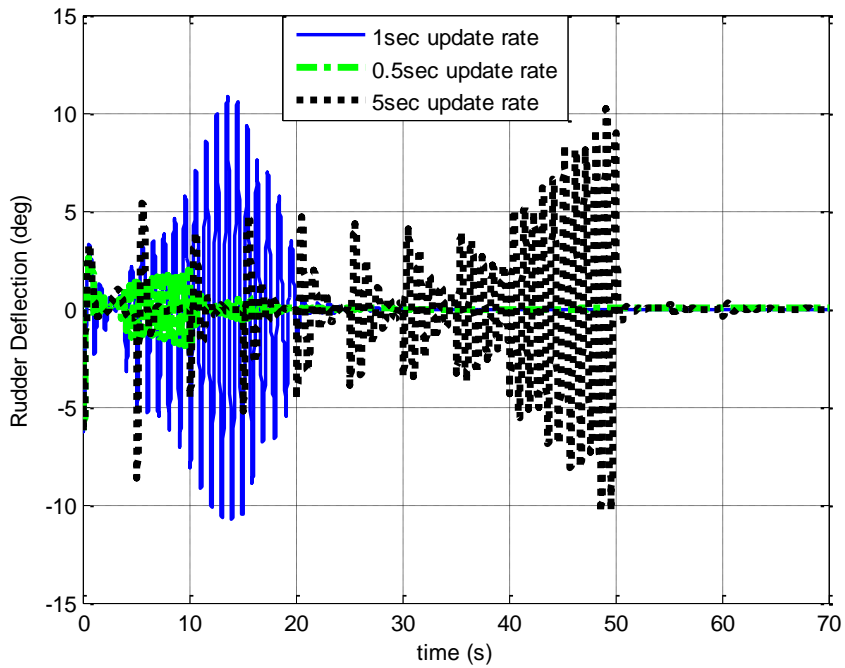
Figure 3.43a: Time history of the rudder deflection with different SDRE update rates, 70 seconds time scale
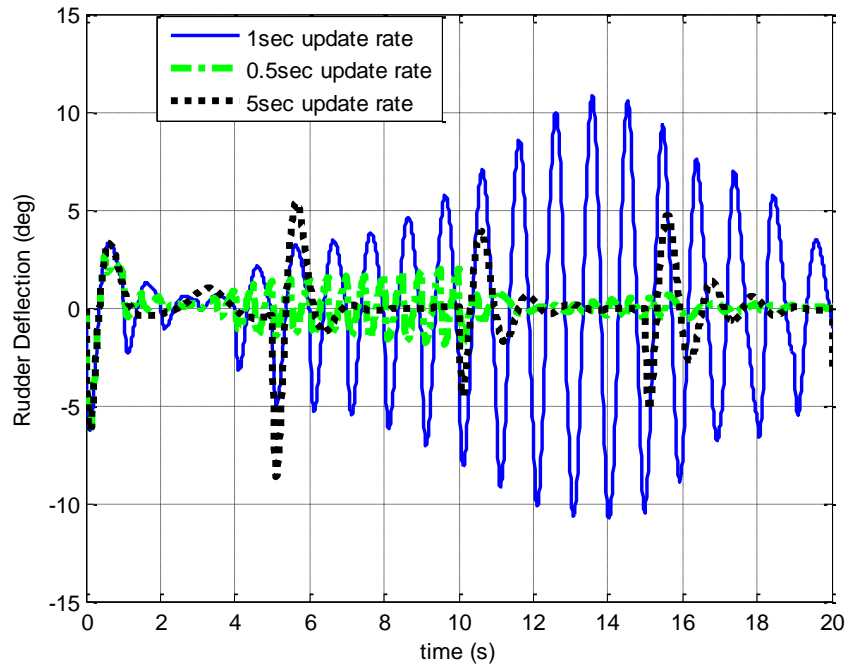
Figure 3.43b: Time history of the rudder deflection with different SDRE update rates, 20 seconds time scale
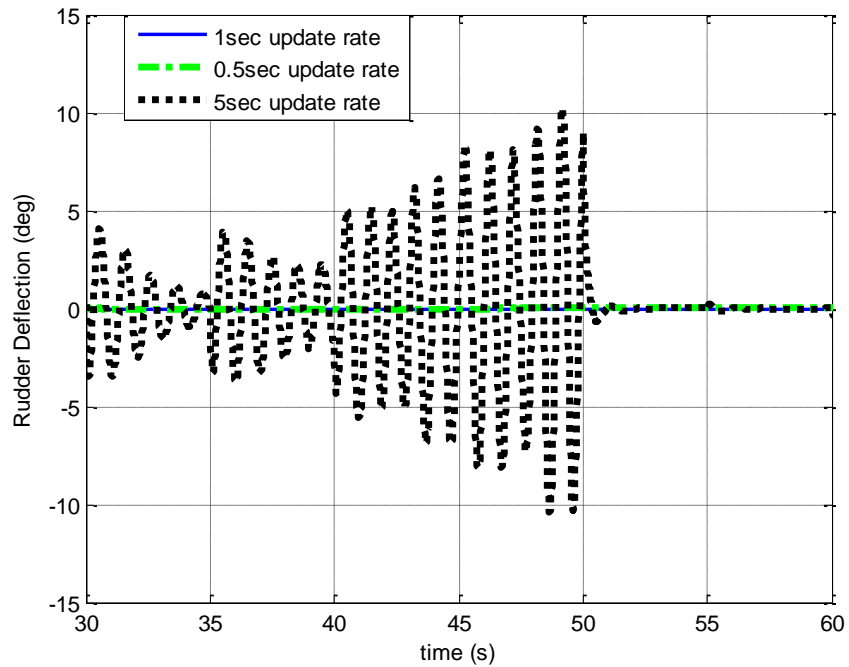
Figure 3.43c: Time history of the rudder deflection with different SDRE update rates, 30-60 seconds time scale

65

Figure 3.38 shows the time history of the follower UAV's relative x-separation with the leader UAV under three different update rates. The follower UAV was able to track to the desired x-separation of 6m under these update rates. The responses for the 0.5 and 1 second SDRE update rate are quite similar. They both settle to 6m in about 20 seconds. However, the response for the 5 seconds update rate is not as smooth as its counterparts. It settles to 6m in about 55 seconds and it's a lot more oscillatory than the other two update rates. Figure 3.39 shows the time history of the y-separation of the follower UAV's relative position under the update rates being considered i.e. 0.5sec, 1 sec and 5 sec. The 0.5 second update rate has the best performance. Its response is much smoother than the other update rates. It also settles to the desired y separation of 4m in about 18 seconds which is faster than the other two update rates. The response for the 1 second update rate is a bit oscillatory but settles slightly slower than its 0.5 second counterpart. The 5 seconds update rate response is a lot more oscillatory than the other two and it settles to the desired 4m much later then the other two at 55seconds. Figures 3.40a to 3.43c are the plots of the corresponding time histories of the deflections of the follower UAV's control surfaces under the three update rates. Figure 3.40a is shows the deflection of the elevator under the three update rates. We see that the elevator deflection for the 5 seconds update rate deflects with less oscillations than its counterparts. In other words, it deflects at a lower rate. The 0.5 second update rate has the highest rate of deflection as compared with the other two update rates. This is expected because for an SDRE algorithm, new gains and therefore new signals to track are generated every time we update the SDRE. Thus, the elevator will have to deflect at a faster rate for a 0.5 second update rate as opposed to a 5 second update rate since the elevator will get 10 times more reference signals to track. Figure 3.40b zooms in on the first 20 seconds of figure 3.40a. Figure 3.41a shows the time history of the percentage change in throttle. As with the case of the elevator deflection, the 0.5 second update rate also has the highest deflection rate. Figure 3.41b also zooms in on the first 20 seconds of figure 3.41a. For the aileron deflection in figure 3.42a and rudder deflection in figure 3.43a, the 0.5second update rate again has the highest deflection rate as compared with the 1 second update rate. The 5 seconds update rate performs much worse than the other two update rates in these two figures.

We can conclude that for a smoother tracking while using SDRE, a high update rate is needed but at the cost a higher deflection rate of the control surfaces which might not always be feasible. A lower gain update rate reduces the control surfaces deflection rate but at the sacrifice of tracking performance. Depending on the mission profile, a trade off would have to be made between tracking performance and the load on the control surfaces. For this thesis, we stuck with a 1 second update rate because we had an acceptable tracking performance and control surface deflection rate under a 1 second update rate. It is also worth mentioning that when we ran the above simulation for update rates higher than 5 seconds, our formation control system was unable to track the desired formation geometry. For an update rate of 20 seconds, we had an unstable system. This is the case because, SDRE algorithm tries to estimate the behavior of the nonlinear system by updating a SDC matrix at predetermined time intervals. Thus, a much shorter time interval leads to a better approximation, and a longer time interval reduces the accuracy of the approximation. This is why we got a smoother response while using a 0.5 second update rate and an unstable system with a 20 seconds update rate.

3.5.2 Inner Loop Eigenvalues vs Outer Loop Eigenvalues

As stated in earlier in section 2.2, the formation control system in this system has a two loop structure. The outer loop contains the formation-hold controller and the inner loop contains the controllers implemented on the follower UAV. The outer loop is the guidance loop, it determines the necessary signals the follower UAV must track in order for it to maintain the desired relative position from the leader UAV. The outer loop in this section uses the SDRE control algorithm and the inner loop uses LQT control algorithm. Thus, there are two sets of eigenvalues i.e. the inner loop eigenvalues and the outer loop eigenvalues. The relationship between these sets of eigenvalues will be examined in this section. The formation flight scenario given in case 2 of section 3.5 will be used for this analysis. The inner loop has two sets of controllers, an altitude/velocity acquire controller and a roll/yaw rate acquire controller. The details of their design is given in section 2.3. To do this analysis, the SDRE formation controller used in case 2 of section 3.5 is retuned to make sure it is more sluggish than the inner loop controllers. The performance of this retuned SDRE formation-hold controller is then compared with the previous one given in case 2 of section 3.5. For the SDRE formation-hold controller, we know that at every update rate, new gains are calculated and thus resulting in new eigenvalues. For a 50 seconds simulation and a 1 second feedback gain update rate, we would have at least 50 sets of eigenvalues to work with. For this analysis, only the fastest and the slowest eigenvalues are presented in the table below. All the other eigenvalues of the SDRE formation-hold controller will fall within the range of these two eigenvalues.

Table 3.1: Inner Loop and Outer Loop Eigenvalues

Inner Loop Eigenvalue mode	Inner Loop Eigenvalues	SDRE Eigenvalues Case 2	Retuned SDRE Eigenvalues
	-0.3776		
Phugoid	$-0.9606 \pm 1.0124i$	-1.1547	-0.0894
Short Period	$-7.7296 \pm 2.3558i$		
Spiral	-0.6964		
Roll	-7.4011	-0.3568	-0.2066
Dutch roll	$-10.1209 \pm 3.6526i$		

From the above table, we see that for the SDRE formation-hold controller in case2 of section 3.5, the eigenvalue -1.1547 is faster than three of the inner loop eigenvalues i.e. the phugoid mode, the spiral mode and -0.3776. From the above table, we also see that the eigenvalues for the retuned SDRE are slower than all the modes of the inner loop controllers. The performance of these two SDRE controllers are presented below using the formation flight scenario given in case 2 of section 3.5. In that flight scenario, the leader and follower UAVs are initially flying at separation distances of $(x_{ini}, y_{ini}, z_{ini}) = (4, 0, 0)$ m. It is desired that the follower's relative position be maintained in spite of the change in heading of the leader UAV, i.e. $(x_{ref}, y_{ref}, z_{ref}) = (4, 0, 0)$ m. The leader UAV's heading is

changed from 0 degrees to 70 degrees, while the leader UAV's velocity and altitude is maintained at 20m/s and 1000m respectively.
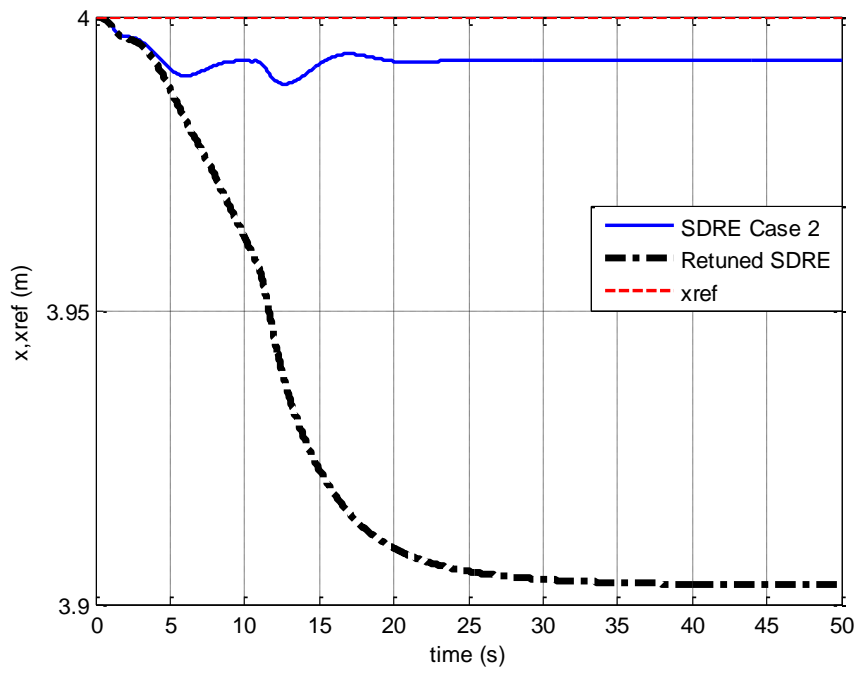
Figure 3.44: Time history of the follower UAV's relative position, x-component, SDRE Case 2 vs Retuned SDRE
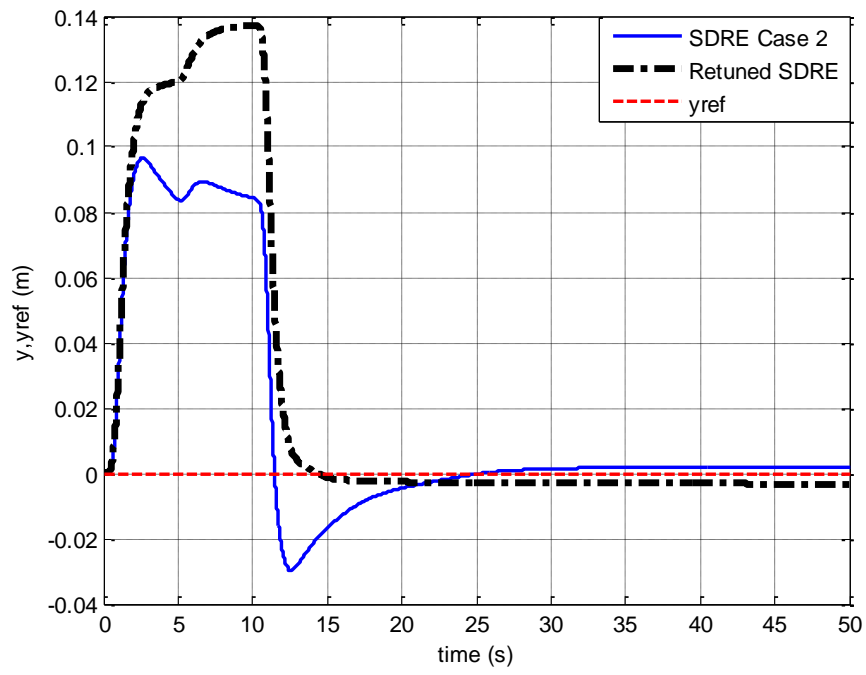
Figure 3.45: Time history of the follower UAV's relative position, y-component, SDRE Case 2 vs Retuned SDRE
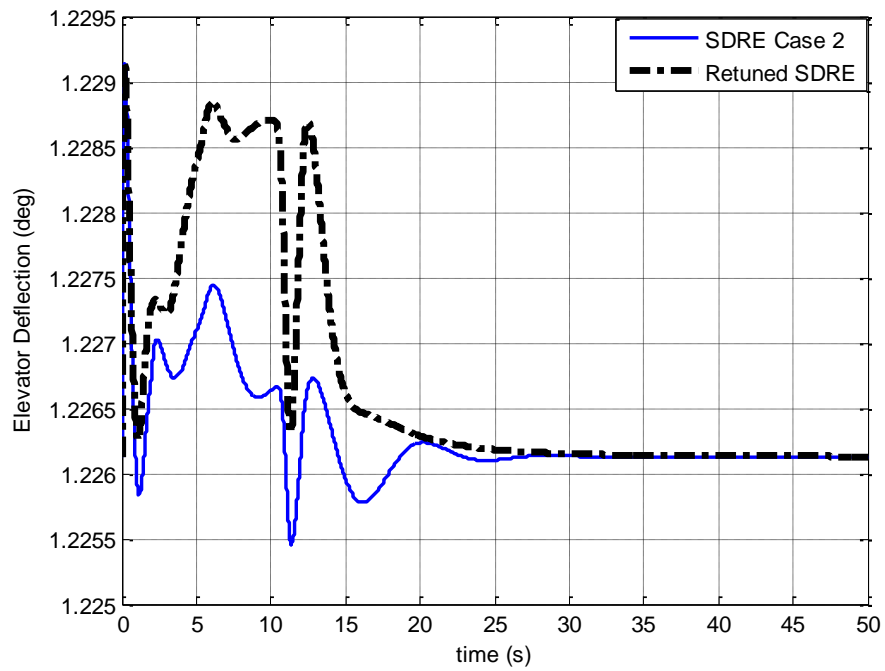
Figure 3.46: Time history of the elevator deflection, SDRE Case 2 vs Retuned SDRE
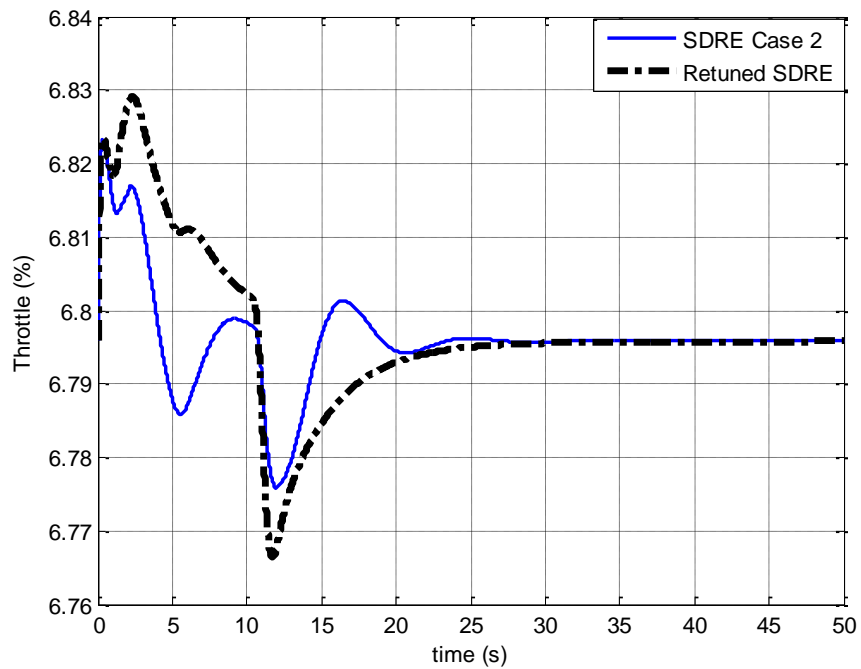

Figure 3.47: Time history of the throttle, SDRE Case 2 vs Retuned SDRE
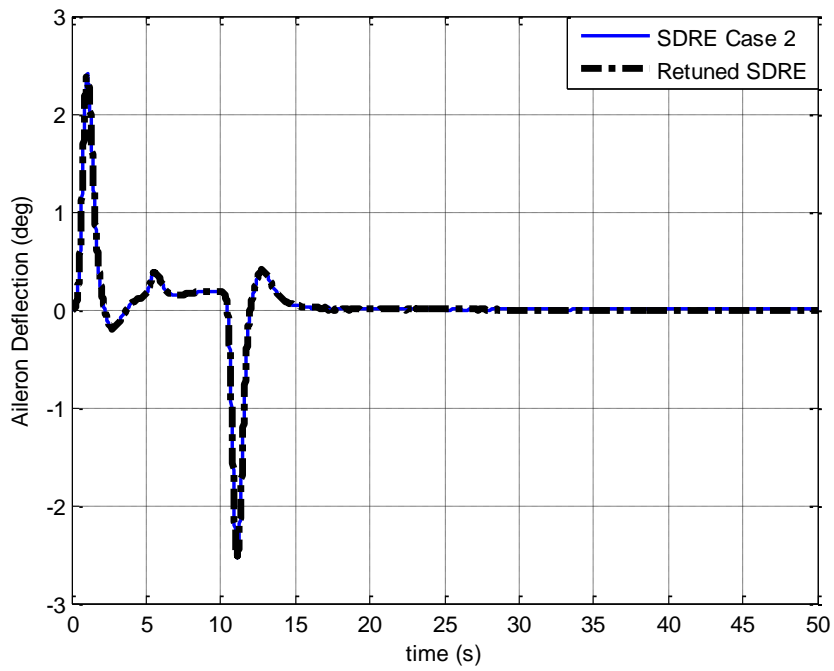
Figure 3.48: Time history of the aileron deflection, SDRE Case 2 vs Retuned SDRE
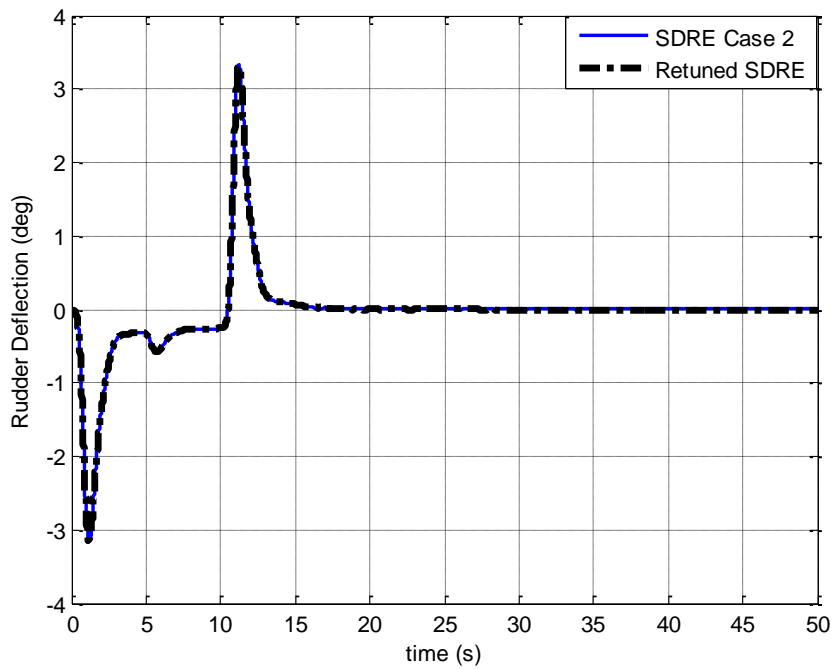
Figure 3.49: Time history of the rudder deflection, SDRE Case 2 vs Retuned SDRE

From figures 3.44 to 3.49, we can conclude that the two SDRE formation-hold controllers i.e. the SDRE formation-hold controller used in case 2 of section 3.5 and the retuned SDRE formation-hold controller used in this section have very similar performances. The deflections in the control surfaces for both cases are practically the same. The tracking performance of the two controllers are really close too. The only noticeable difference in performance of the two controllers can be seen in figure 3.44 where the steady state error for tracking the x-component of the relative position of the follower UAV to the leader UAV increased from about 8mm in the SDRE formation-hold controller in Case2 of section 3.5 to about 9cm in the retuned SDRE formation-hold controller which is actually a slight drop in performance. We can draw out from these results that ensuring that the outer loop is slower than the inner loop does not really provide much of a performance boost. As long as the inner loop controllers are fast enough, a good tracking performance can be achieved. In other words, it is ok for the outer loop eigenvalues to be faster than a few of the eigenvalue modes in the inner loop.

Due to the nature of the SDRE algorithm, it is actually quite difficult to select a set of weighting matrices Q and R that ensures that the SDRE formation-hold controller in the outer loop is slower than the inner loop controllers. This is because the SDRE algorithm uses state dependent coefficient matrices (SDC) to "linearize" the nonlinear model. This means that different formation flight scenarios means new entirely different SDC matrices. Thus, the pair Q and R for one case that ensure a slower formation-hold controller might not ensure a slower formation-hold controller for another case. Since it is impractical to use a different set of Q and R weighting matrices for every formation flight scenario, it is more practical to focus on the inner loop controllers instead by making them quite fast.

CHAPTER 4

LYAPUNOV BASED CONTROL OF UNMANNED AIRCRAFT FORMATIONS

4.1 Lyapunov Stability Theorem

Let $x = 0$ be an equilibrium point of a nonlinear system $\dot{x} = f(x)$. Let $V : D \rightarrow R$ be a continuously differentiable function on a neighborhood D of $x = 0$, such that $V(0) = 0$ and $V(x) > 0$ in $D - \{0\}$. If $\dot{V}(x) \le 0$, then $x = 0$ is stable. Moreover, if $\dot{V}(x) < 0$ in $D - \{0\}$, then $x = 0$ is asymptotically stable [24].

4.2 Lyapunov Control Approach

The Lyapunov stability theorem approach may be used to design stabilizing controllers for nonlinear systems [24].

Consider the following Lyapunov function:

$$V(\Delta x, \Delta y) = \frac{1}{2}(\Delta x)^2 + \frac{1}{2}(\Delta y)^2 \tag{52}$$

Where $\Delta x = x - x_{ref}$ and $\Delta y = y - y_{ref}$. Taking the derivative of equation 22, we have

$$\dot{V}(\Delta x, \Delta y) = \Delta x \Delta \dot{x} + \Delta y \Delta \dot{y} = \begin{bmatrix} \Delta x & \Delta y \end{bmatrix} \begin{Bmatrix} \Delta \dot{x} \\ \Delta \dot{y} \end{Bmatrix} \tag{53}$$

To ensure that equation (23) is negative definite, we make

$$\begin{bmatrix} \Delta x & \Delta y \end{bmatrix} \begin{Bmatrix} \dot{x} \\ \dot{y} \end{Bmatrix} = -\begin{bmatrix} \Delta x & \Delta y \end{bmatrix} Q \begin{bmatrix} \Delta x \\ \Delta x \end{bmatrix} \tag{54}$$

where Q is a positive definite matrix. Simplifying equation (24), we have

$$\begin{Bmatrix} \dot{x} \\ \dot{y} \end{Bmatrix} = -Q \begin{bmatrix} x - x_{ref} \\ y - y_{ref} \end{bmatrix} \tag{55}$$

Substituting equation (46) into equation (55) and solving for $\begin{Bmatrix} \dot{\psi}_f \\ v_f \end{Bmatrix}$, we have

$$\left\{ \begin{array}{c} \dot{\psi}_f \\ v_{hf} \end{array} \right\} = - \begin{bmatrix} y & -1 \\ -x & 0 \end{bmatrix}^{-1} Q \left\{ \begin{array}{c} x - x_{ref} \\ y - y_{ref} \end{array} \right\} - \begin{bmatrix} y & -1 \\ -x & 0 \end{bmatrix}^{-1} \left\{ \begin{array}{c} v_{hL} \cos \psi_e \\ v_{hL} \sin \psi_e \end{array} \right\} \tag{56}$$

$\left\{ \begin{array}{c} \dot{\psi}_f \\ v_{hf} \end{array} \right\}$ is the desired control law to bring the follower aircraft to the desired formation in a stable manner. Thus, the proposed formation control is a guidance methodology used to generate the necessary heading rate and velocity commands to the follower.

On closer inspection of equation (56), we see that there is a singularity problem when $x = 0$. The singularity occurs for $x = 0$ because:

$$\begin{bmatrix} y & -1 \\ -x & 0 \end{bmatrix}^{-1} = \frac{1}{x} \begin{bmatrix} 0 & 1 \\ x & y \end{bmatrix} \tag{57}$$

From equation (57), we see that the inverse always exists except when $x = 0$. Thus for cases where the x-separation between the leader UAV and the follower UAV is desired to be zero, a singularity problem will be encountered in obtaining the control law and hence, a workaround is developed. To solve this problem, whenever we have $-0.5 \leq x \leq 0.5$ signal going into our Lyapunov formation-hold controller, the value for x is set to 0.5 in the $\begin{bmatrix} y & -1 \\ -x & 0 \end{bmatrix}^{-1}$ matrix of the formation-hold controller. By doing this, we make sure that the inverse always exists and thereby avoiding the singularity problem.

4.3   Formation Control Implementation

The change in heading rate, and desired velocity for the follower UAV are computed form the Lyapunov based guidance technique described above. The flight control of the follower UAV may be easily implemented as before. Refer to section 3.4 for details.
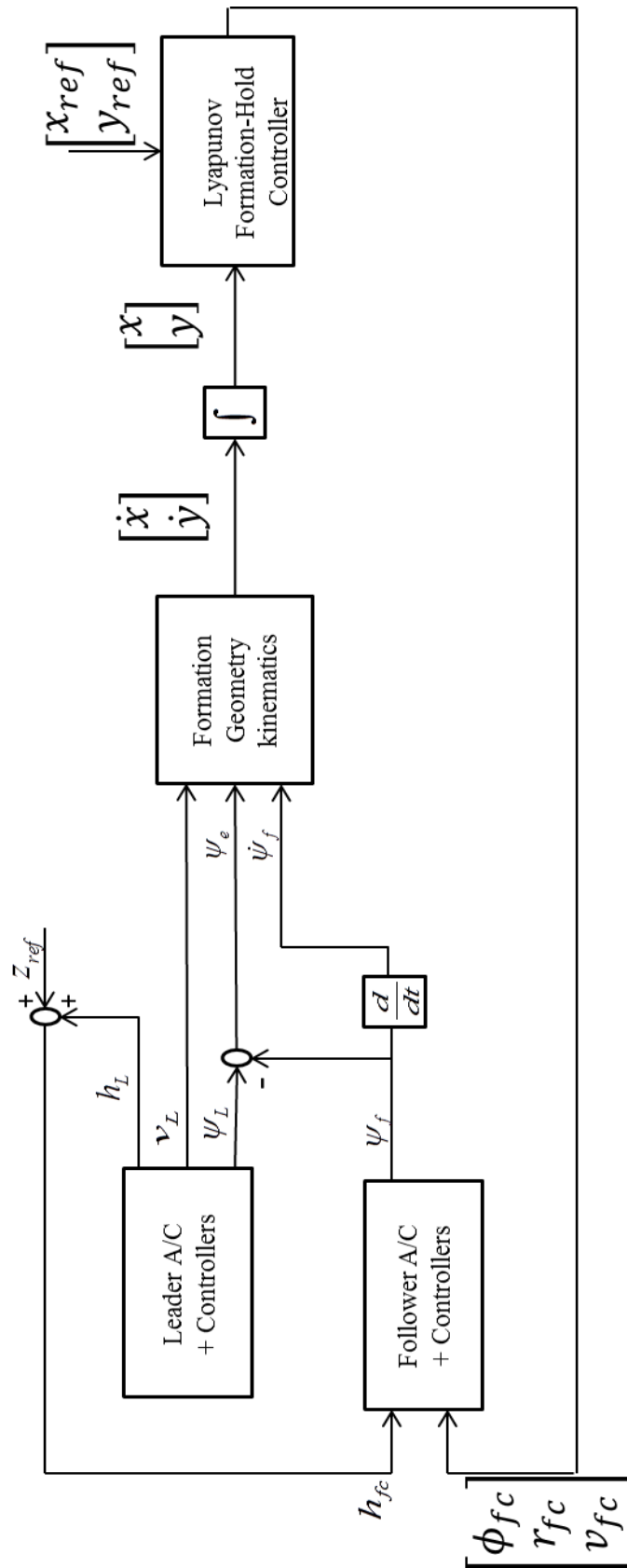
Figure 4.1: Block Diagram of the Formation Control System

4.4　　　　Results and Discussion

The formation control system using Lyapunov based guidance approcah is tested using the linearized model of the SIG RASCAL 110 model aircraft for both the leader and follower UAVs as before. For this purpose, simulation code is written in MATLAB/SIMULINK. The block diagram for the simulation code is given in Figure 2.2. To examine the effectiveness of the Lyapunov approach in realizing the desired formation geometry in spite of maneuvers carried out by the leader aircraft, three cases are considered. These cases are exactly the same as the formation flight scenarios discussed in section 3.5. The control surface deflections for the follower UAV are limited to ± 20 degrees for both the elevator and aileron and ± 15 degrees for the rudder as assumed in the previous simulations. The throttle maximum value is also constrained. The SIG RASCAL model was linearized at 1000m altitude and 20m/s velocity, and it is given in the Appendix.

Case 1: In this flight scenario, case 1, the leader UAV flies at the velocity, altitude and heading depicted in figure 4.3, 4.4 and 4.5 respectively. The leader and follower UAVs are initially flying at separation distances of $(x_{ini}, y_{ini}, z_{ini}) = (9, 8, 0)$ m. It is desired that the follower's relative position be brought to $(x_{ref}, y_{ref}, z_{ref}) = (6, 4, 5)$ m.
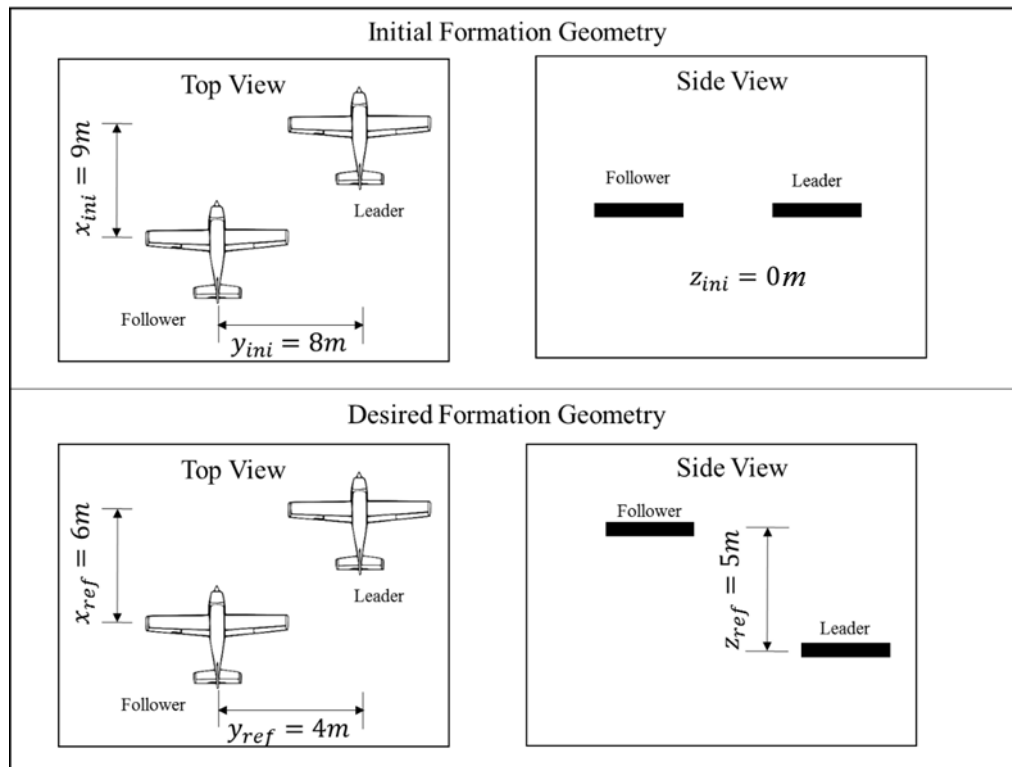
Figure 4.2: Initial and Desired Formation Geometries, Case 1, Lyapunov

76
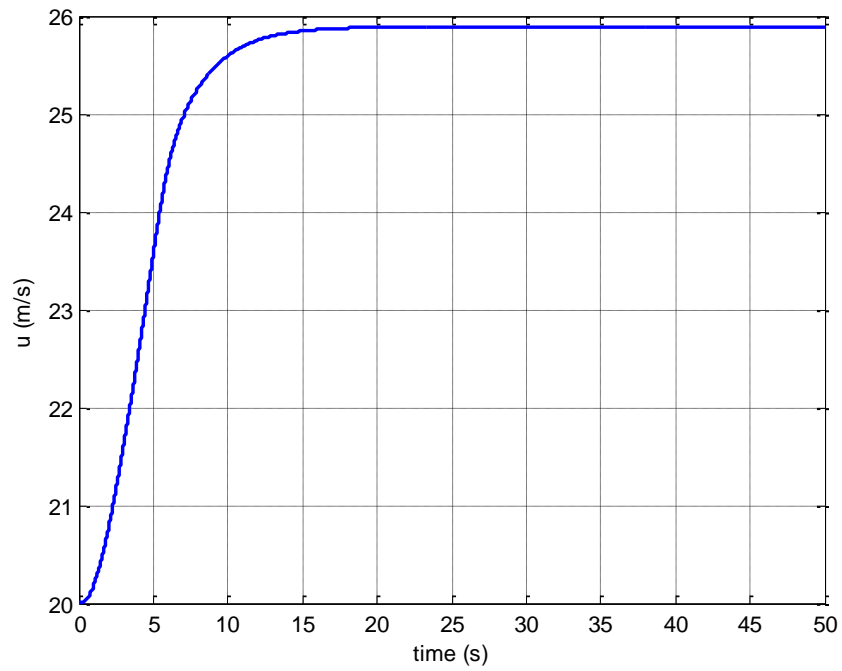
Figure 4.3: Time history of the leader UAV's velocity, Case 1, Lyapunov
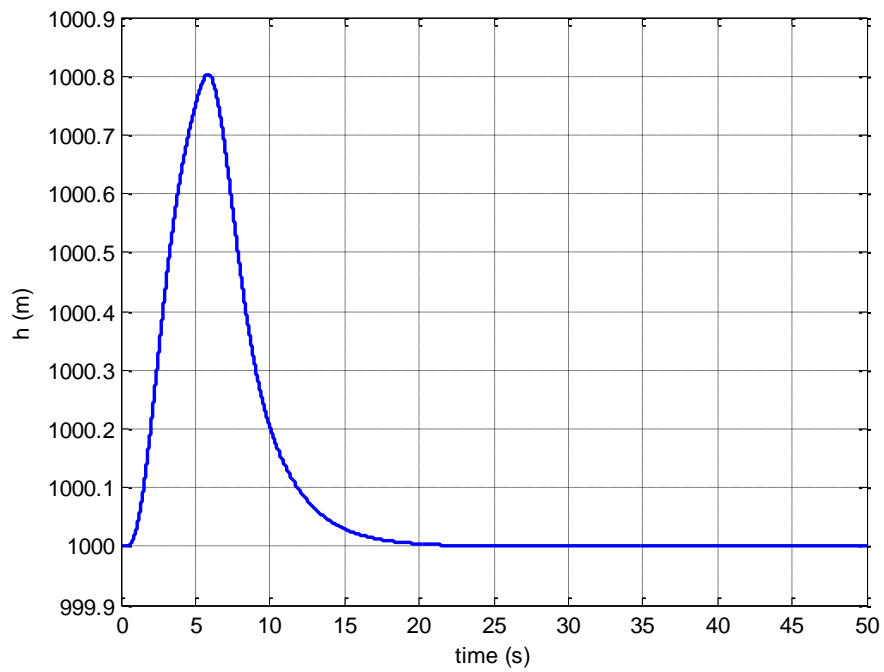
Figure 4.4: Time history of the leader UAV's altitude, case 1, Lyapunov

77
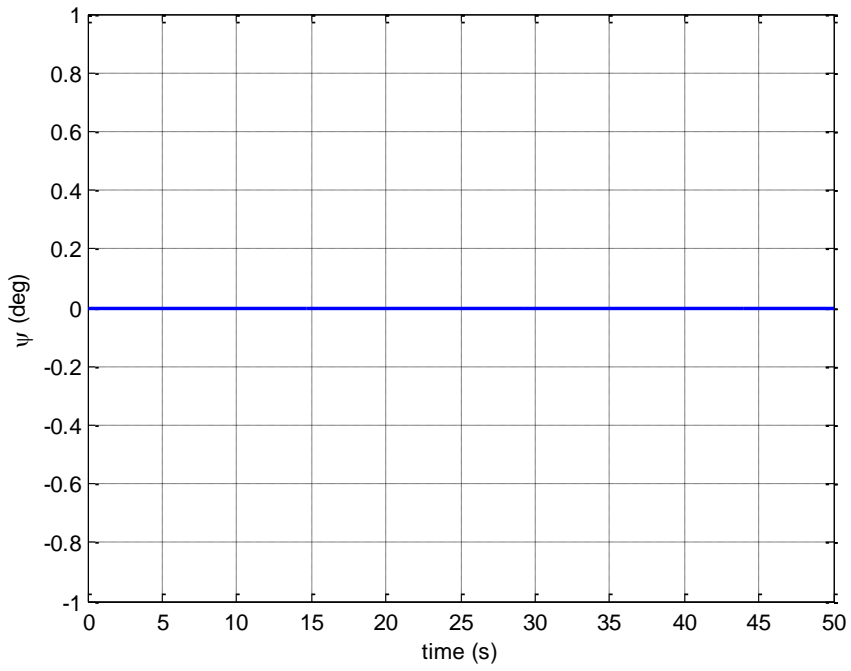
Figure 4.5: Time history of the leader UAV's heading, Case 1, Lyapunov
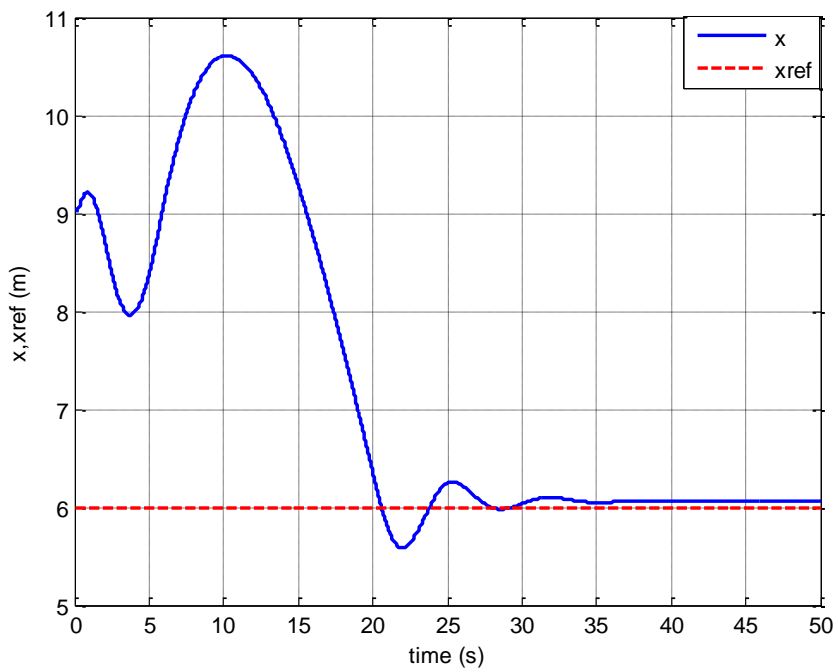
Figure 4.6: Time history of the follower UAV's relative position, x-component, Case 1,
Lyapunov

78
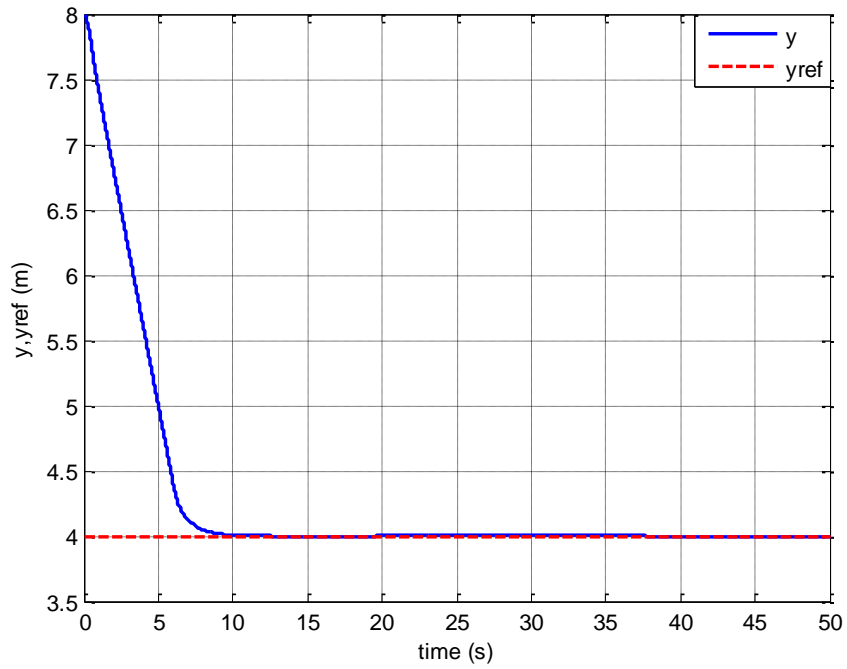
Figure 4.7: Time history of the follower UAV's relative position, y-component, Case 1, Lyapunov
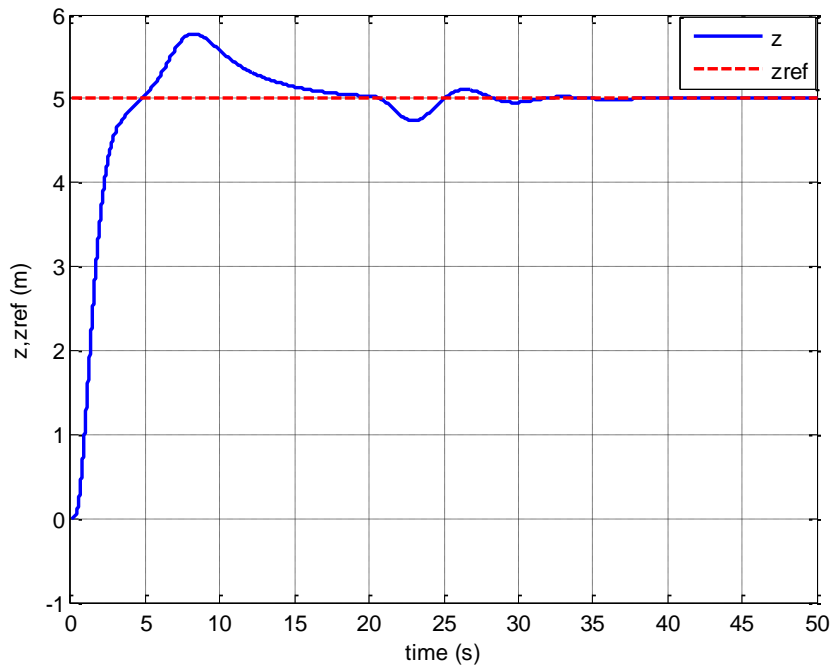
Figure 4.8: Time history of the follower UAV's relative position, z-component, Case 1, Lyapunov
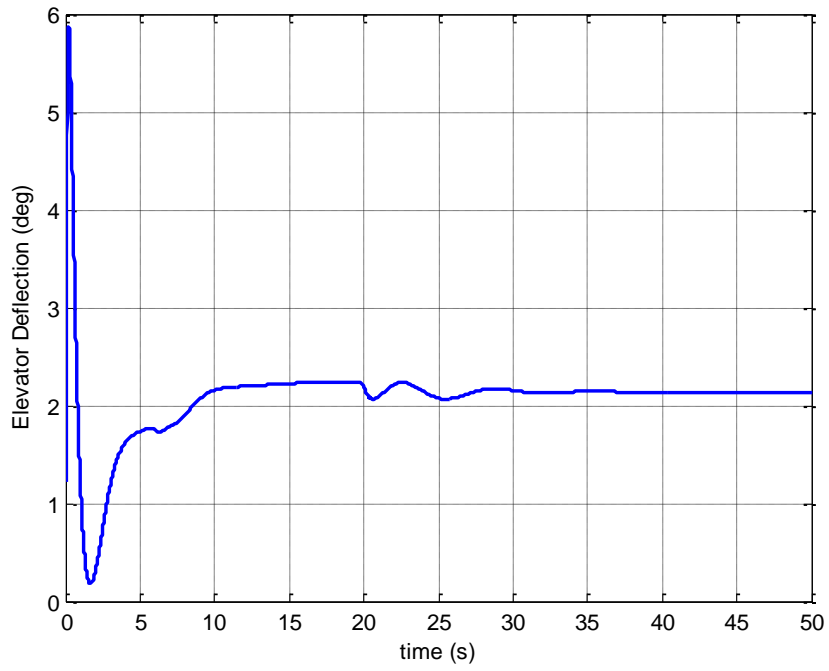
Figure 4.9: Time history of the elevator deflection, Case 1, Lyapunov
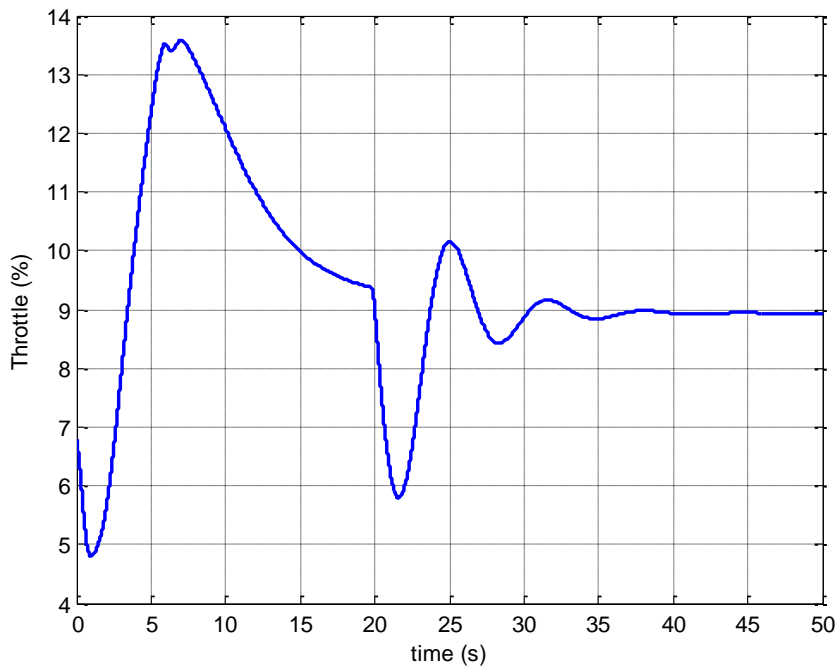
Figure 4.10: Time history of the throttle, Case 1, Lyapunov
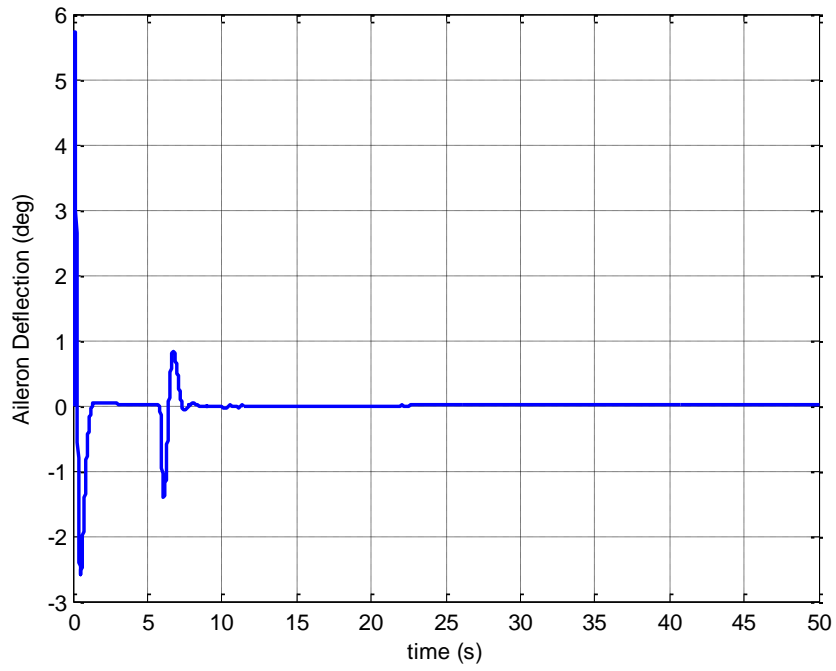
Figure 4.11: Time history of the aileron deflection, Case 1, Lyapunov
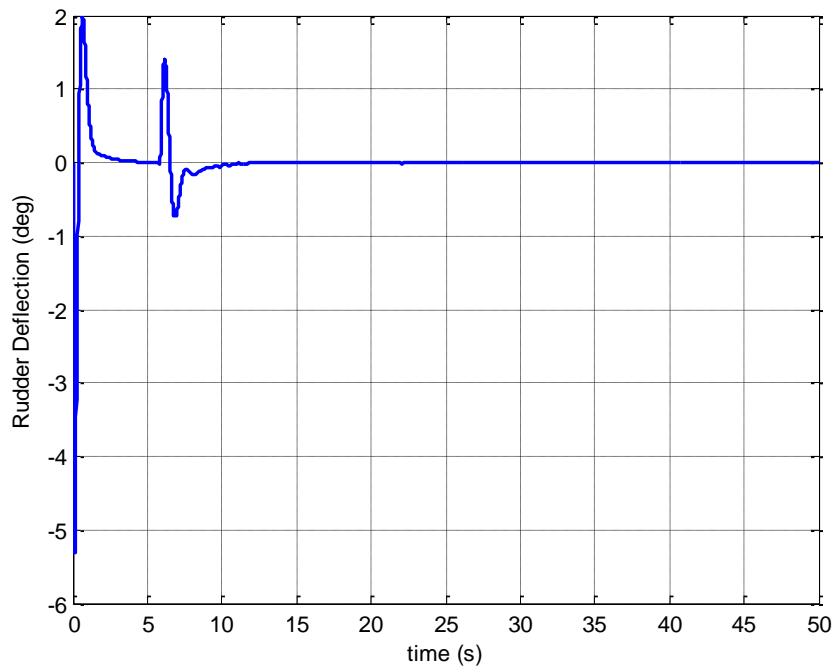

Figure 4.12: Time history of the rudder deflection, Case 1, Lyapunov
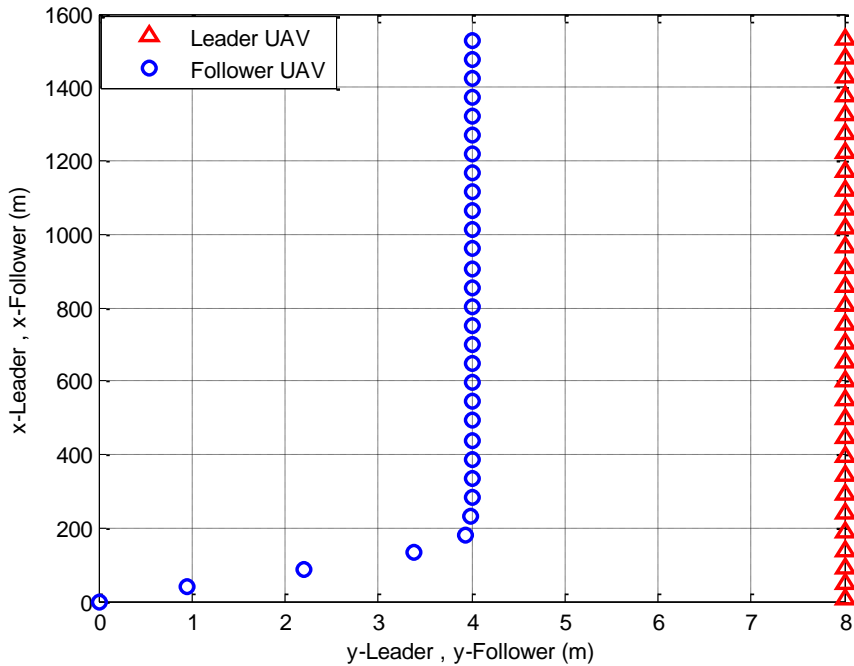
Figure 4.13: Leader UAV position vs Follower UAV position, Case 1, Lyapunov

Figure 4.3 shows the leader UAV's velocity. The velocity is increased from 20 m/s to 26 m/s albeit a steady state error of 0.09m/s due to the controller implemented on the leader. As seen in figure 4.4, the leader UAV's altitude momentarily rises to about 1000.8m and then settles at 1000m. This is as a result of the leader UAV's increase in velocity. However, a rise of 0.8m is negligible, thus in this flight scenario, we can say that the altitude is kept constant at 1000m. Figure 4.5 shows the time history of the leader UAV's heading which is kept constant at 0 degrees. We desire to see if the follower UAV can track and maintain the reference formation geometry in spite of the increase in velocity of the leader UAV. In figure 4.6, we see that the follower UAV is able to track the desired x-separation between it and the leader UAV. The initial x-separation between the leader and follower UAV is 9m and it is desired that an x-separation of 6m be maintained. In other words, we would like to reduce the x-separation between the leader and follower UAV in spite of an increase in the velocity of the leader UAV. The follower UAV is able to track the desired x-separation in about 28 seconds. A steady state error of 0.06m can be seen. This is probably as a result of the steady state error present in the design of the follower UAV controllers i.e., the inner loop controllers of our formation control system. In figure 4.7, we see that the follower UAV is also able to track the desired y-separation between it and the leader UAV. The initial y-separation between the two UAVs is 8m and a 4m separation is desired. It takes about 10 seconds for the follower UAV to track the desired y-separation without a steady state error. In figure 3.8, the follower UAV is also able to track the desired z-separation of 5m. It takes about 25 seconds for the follower UAV to track the desired z-separation. No steady state error can be seen. We can conclude then that the follower UAV is able to track the desired formation geometry since all the desired x, y and z separation distances are tracked. It took

82

28 seconds for the follower UAV to go from the initial formation geometry to the desired formation geometry. Figures 4.9 to 4.12 shows us the time histories of the deflections of the follower UAV control surfaces as the follower UAV tracks the desired formation geometry. We see no saturations in the deflection of the control surfaces. Figure 4.9 shows the deflection of the follower UAV's elevator. The highest deflection angle was about 6 degrees and the lowest was about 0 degrees. These values are way below the maximum limit of ± 20 degrees set for the elevator. Figure 4.10 is the plot of the percentage increase of the follower UAV throttle. The throttle was initially at 6.7%, it then increases to 13% before dropping back to about 9%. The increase in throttle is expected because in order for the follower UAV to reduce its x-separation from the leader in spite of the acceleration of the leader, it has to momentarily move faster than the leader. After achieving the required separation, it then has to slow down to match the leader UAV's velocity. Figure 4.11 shows the deflection of the follower UAV's aileron. The deflection angle for the aileron was within the range of -3 degrees and 6 degrees. These values are below the maximum limit of ± 20 degrees set for the aileron. Figure 4.12 shows the deflection of the follower UAV's rudder. There is no saturation in its deflection since the deflection angle for the rudder was within the range of -6 degrees and 2 degrees which is below the maximum set range limit of ± 15 degrees. Figure 4.13 shows us the positions of both the leader UAV and the follower UAV. From the figure, we see how the follower UAV changes its relative y separation from the leader UAV from 8m to 4m as desired. We can also see that the desired formation geometry is maintained. For a clearer picture of the relative x-separation between the leader and follower UAV, refer to figure 4.6.

Case 2: In this flight scenario, case 2, the leader UAV flies at the velocity, altitude and heading depicted in figure 4.15, 4.16 and 4.17 respectively. The leader and follower UAVs are initially flying at separation distances of $(x_{ini}, y_{ini}, z_{ini}) = (4, 0, 0)$ m. It is desired that the follower's relative position be maintained in spite of the change in heading of the leader UAV, i.e. $(x_{ref}, y_{ref}, z_{ref}) = (4, 0, 0)$ m. In other words, we would like to see if the follower UAV can maintain a trail formation geometry in spite of a change in heading of the leader UAV.
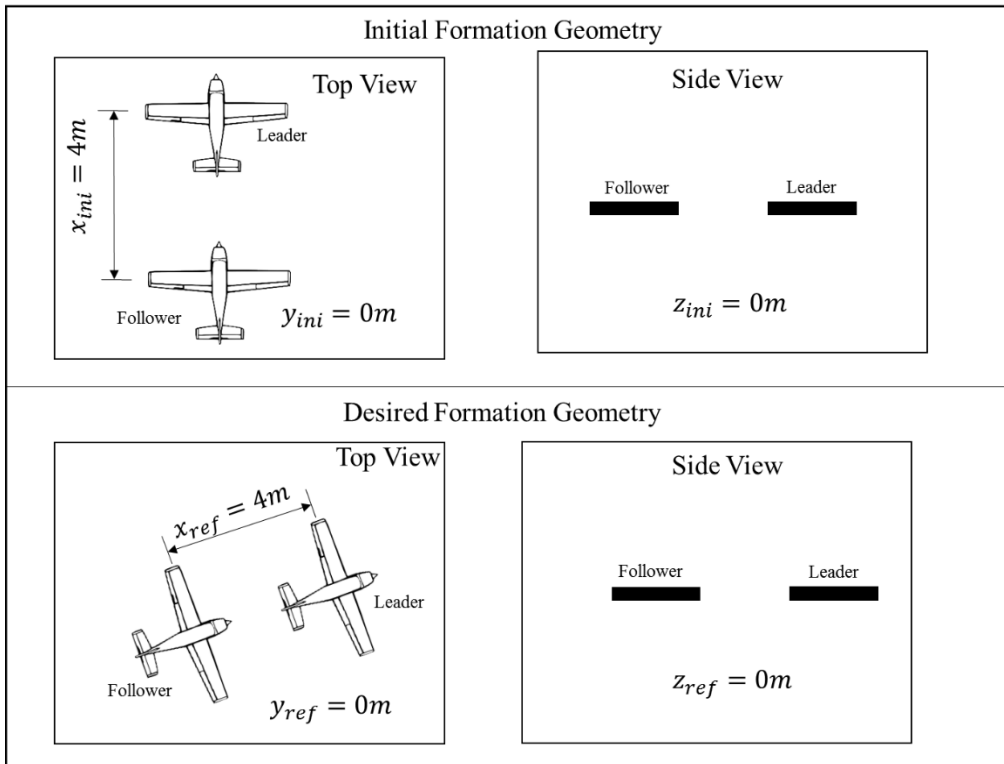
Figure 4.14: Initial and Desired Formation Geometries, Case 2, Lyapunov
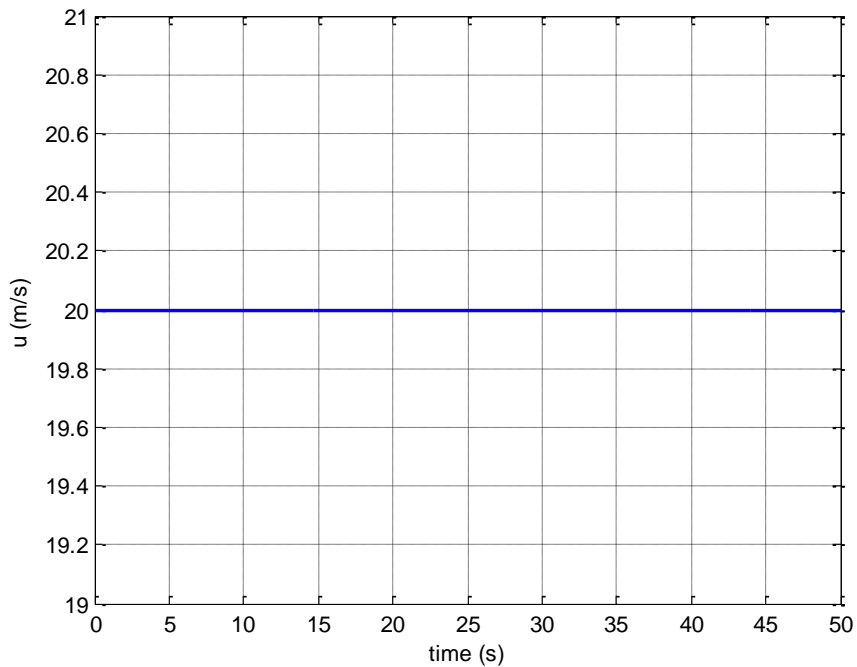
Figure 4.15: Time history of leader UAV's velocity, Case 2, Lyapunov
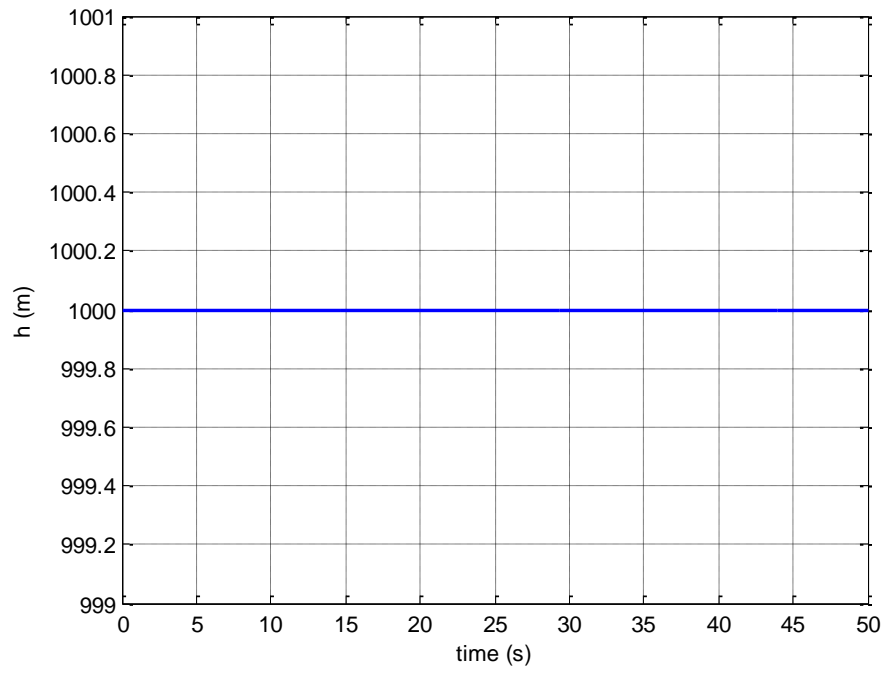
Figure 4.16: Time history of leader UAV's altitude, case 2, Lyapunov
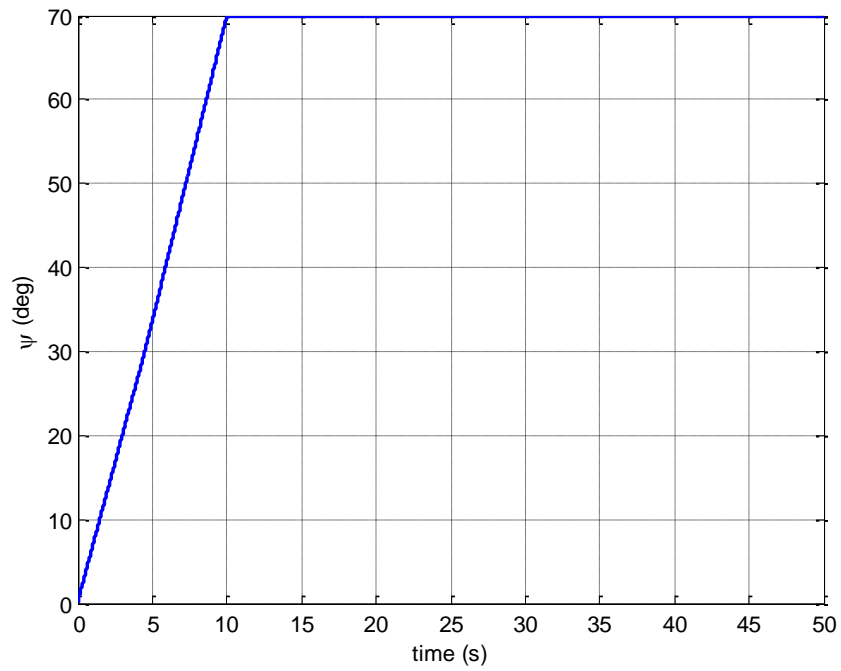
Figure 4.17: Time history of leader UAV's heading, Case 2, Lyapunov
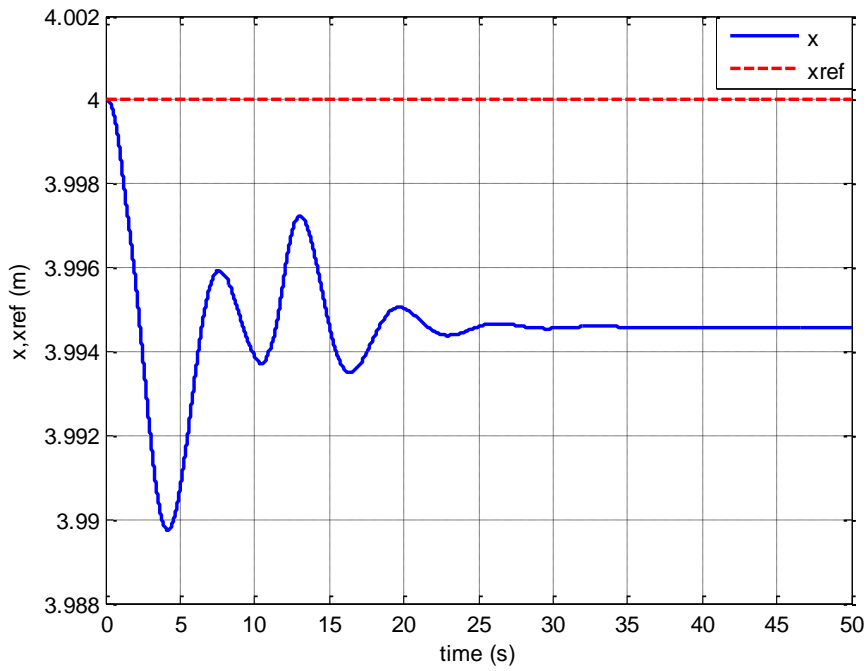
Figure 4.18: Time history of the follower UAV's relative position, x-component, Case 2, Lyapunov
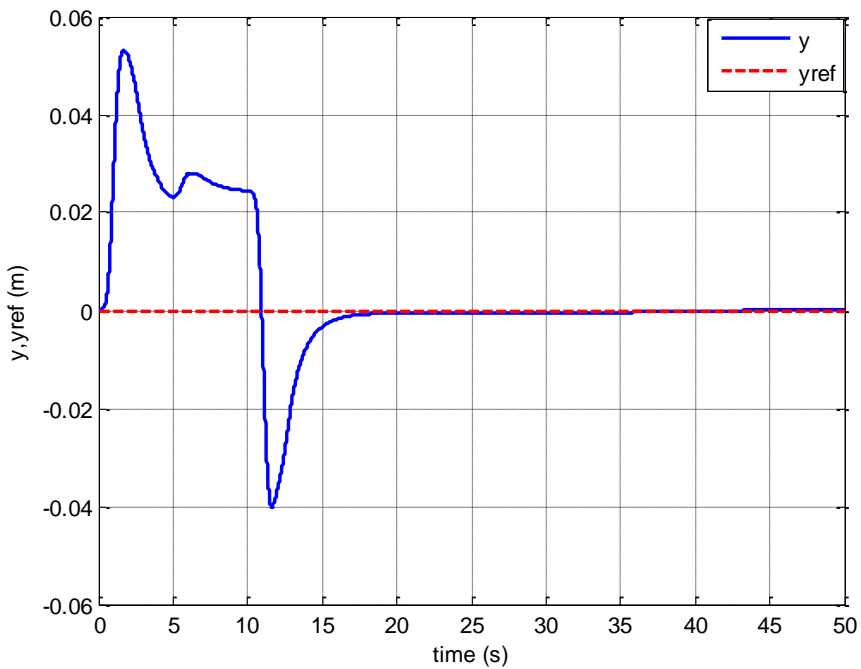
Figure 4.19: Time history of the follower UAV's relative position, y-component, Case 2, Lyapunov
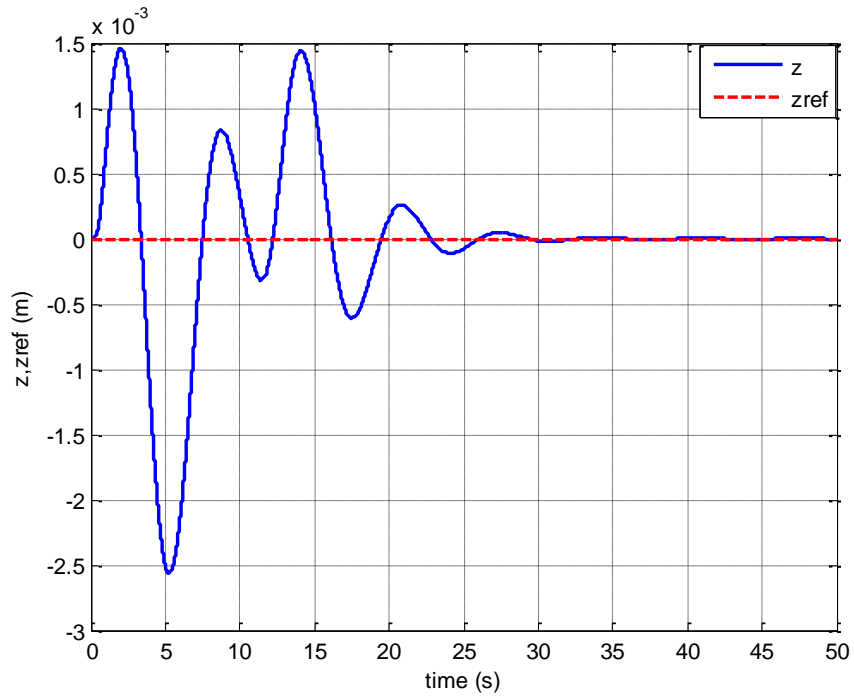
Figure 4.20: Time history of the follower UAV's relative position, z-component, Case 2, Lyapunov
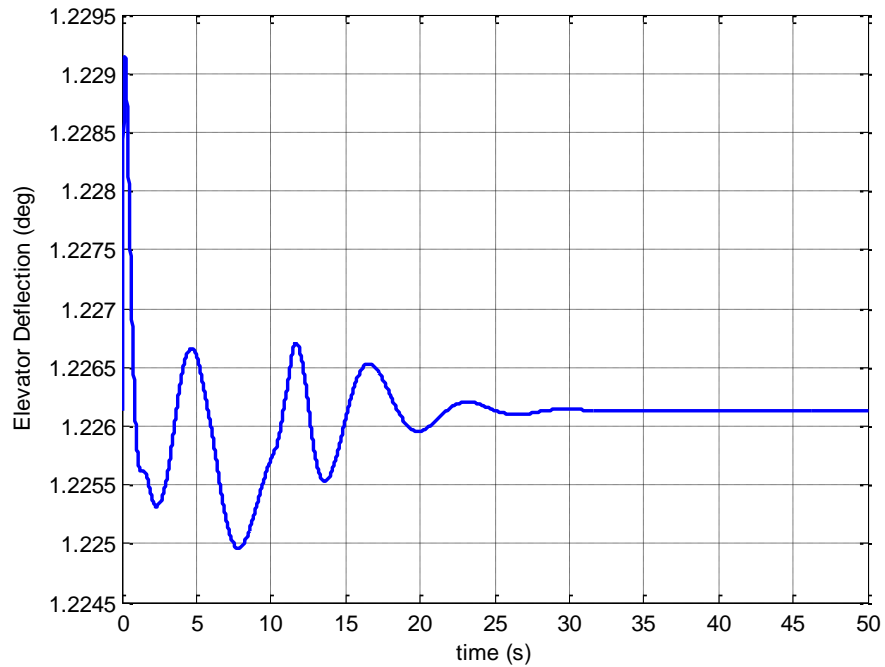
Figure 4.21: Time history of the elevator deflection, Case 2, Lyapunov
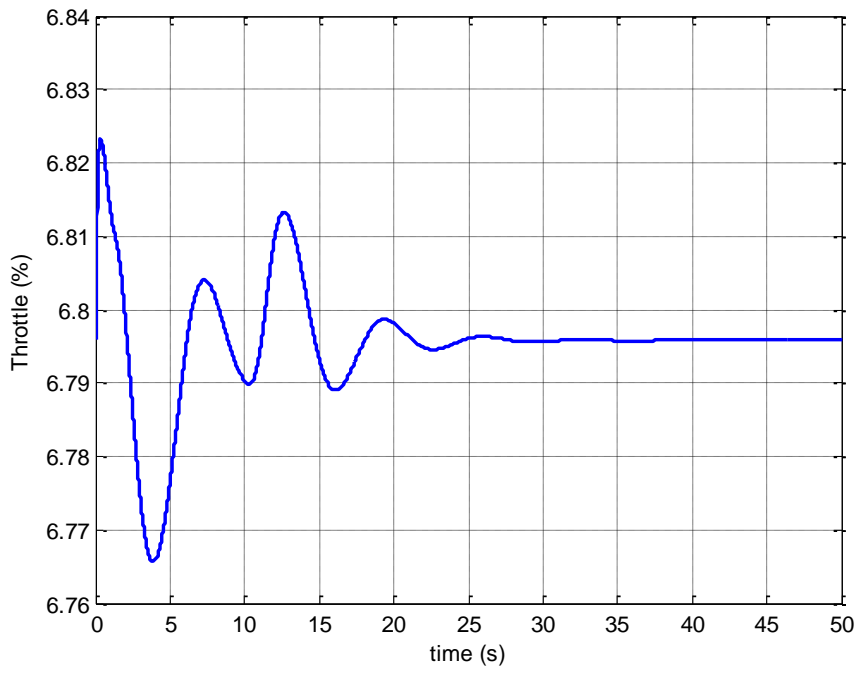
Figure 4.22: Time history of the throttle, Case 2, Lyapunov
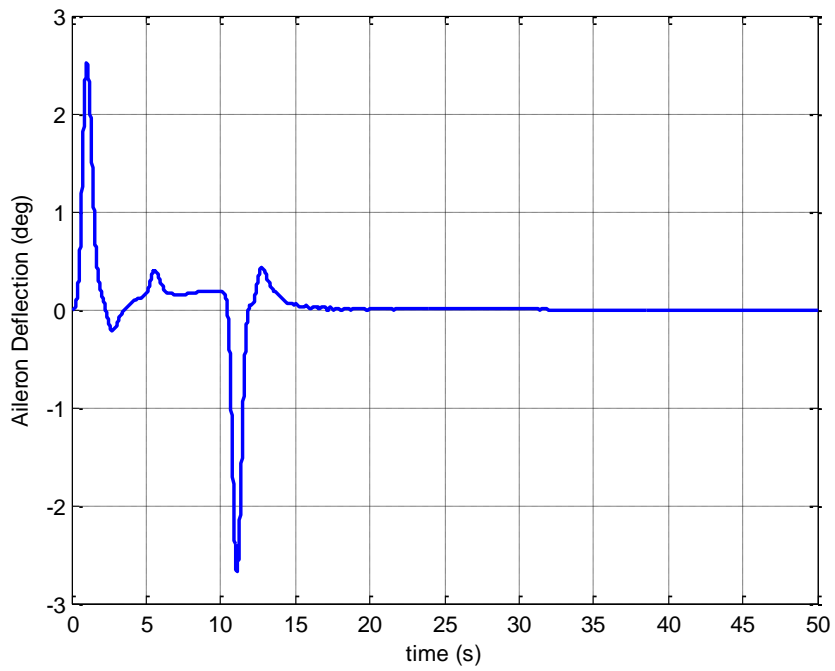
Figure 4.23: Time history of the aileron deflection, Case 2, Lyapunov

88
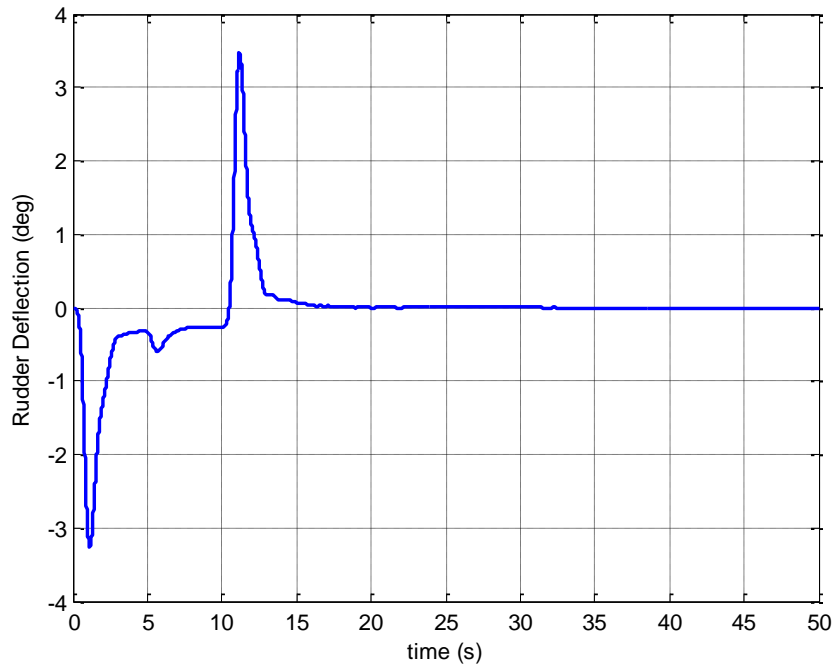
Figure 4.24: Time history of the rudder deflection, Case 2, Lyapunov
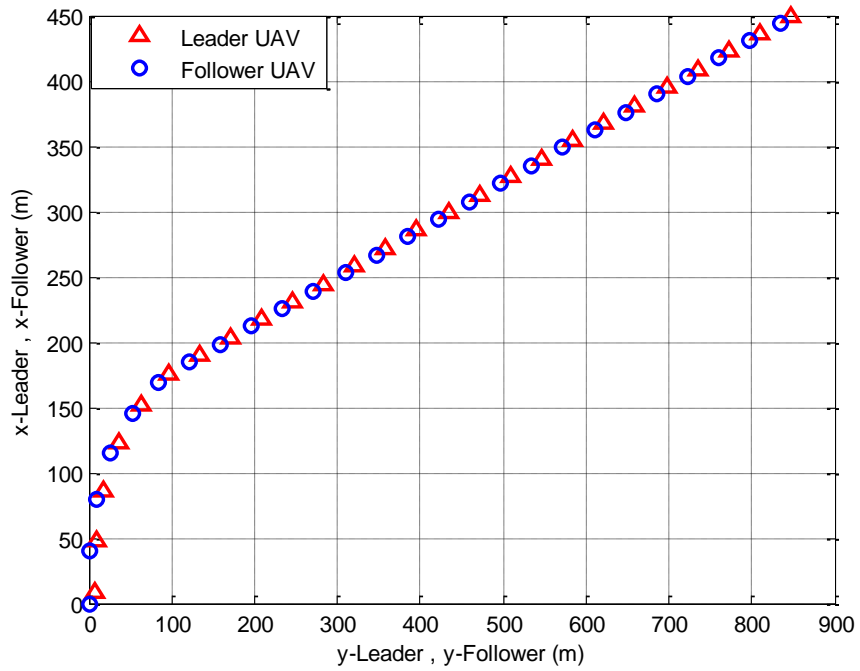
Figure 4.25: Leader UAV position vs Follower UAV position, Case 2, Lyapunov

For this formation flight scenario, the leader UAV velocity is kept constant at 20m/s, figure 4.15. The altitude is also kept constant at 1000m, figure 4.16. However, the leader UAV's heading is varied from 0 degrees to 70 degrees at a rate of 7 degrees per second, figure 4.17. It is desired that we maintain a trail formation in spite of this varying heading, figure 4.14. Figure 4.18 shows the time history of the relative x-separation between the leader and follower UAV. It is desired that this x-separation be kept constant at 4m while the leader UAV changes its heading. We see from the figure that our follower UAV was able to track the desired x-separation with a negligible error of about 6mm. We also desire that the y-separation be maintained at 0m i.e. we want the follower to fly directly behind the leader UAV as the leader UAV changes its heading. Figure 4.19, shows the time history of the relative y-separation between the leader and follower UAVs. We see from figure 4.19, that in the first 10 seconds, the follower UAV is to the left of the leader UAV by only about 6cm as the leader UAV changed its heading from 0 degrees to 70 degrees (figure 4.16). As the leader starts flying at the new heading, i.e. after 10 seconds, the follower UAV corrects its y-separation as to 0m as desired. The follower UAV veers off the desired 0m separation by an acceptable 6cm in the first ten seconds and then by about an acceptable 4 cm in the next ten seconds before settling at the desired 0m. We also desired the throughout this formation flight scenario, the leader and follower UAVs fly level with each other i.e. a z-separation of 0m be maintained. From figure 4.20, we see that our follower UAV maintains the desired z-separation. Figures 4.21 to 4.24 shows the time histories of the deflections of the control surfaces. We see no saturations in the deflections of any of the control surfaces. Figure 4.21 shows the follower UAV's elevator deflection, we see that it deflects well under the maximum set range limit of ± 20 degrees. Figure 4.22 shows the percentage change in throttle of the follower UAV. Figure 4.23 shows the time history of the follower UAV's aileron deflection as the follower UAV maintains its separation distance from the leader UAV. We see a deflection range of about ± 3 degrees which is well under the set limit of ± 20 degrees. Figure 4.24 shows the rudder deflection of the follower UAV, the rudder also deflects well under its maximum range of ± 15 degrees. From figure 4.25, we can easily see that the follower maintains the desired trail formation i.e. flies directly behind the leader UAV even as the leader UAV changes its heading.

Case 3: In this flight scenario, case 3, the leader UAV flies at the velocity, altitude and heading depicted in figure 4.27, 4.28 and 4.29 respectively. The leader and follower UAVs are initially flying at separation distances of $(x_{ini}, y_{ini}, z_{ini}) = (8, 8, 0)$ m. It is desired that these separation distances be brought to $(x_{ref}, y_{ref}, z_{ref}) = (0, 3, 0)$ m. In other words, it is desired that the leader and follower UAVs fly side by side each other while maintaining a 3m relative y-separation distance between them. An x-separation distance of 0m is desired in this flight scenario. As discussed in section 4.2, this creates a singularity problem in obtaining the control law for the Lyapunov formation-hold controller. This flight scenario is specifically tested to see if the workaround designed in section 4.2 works.
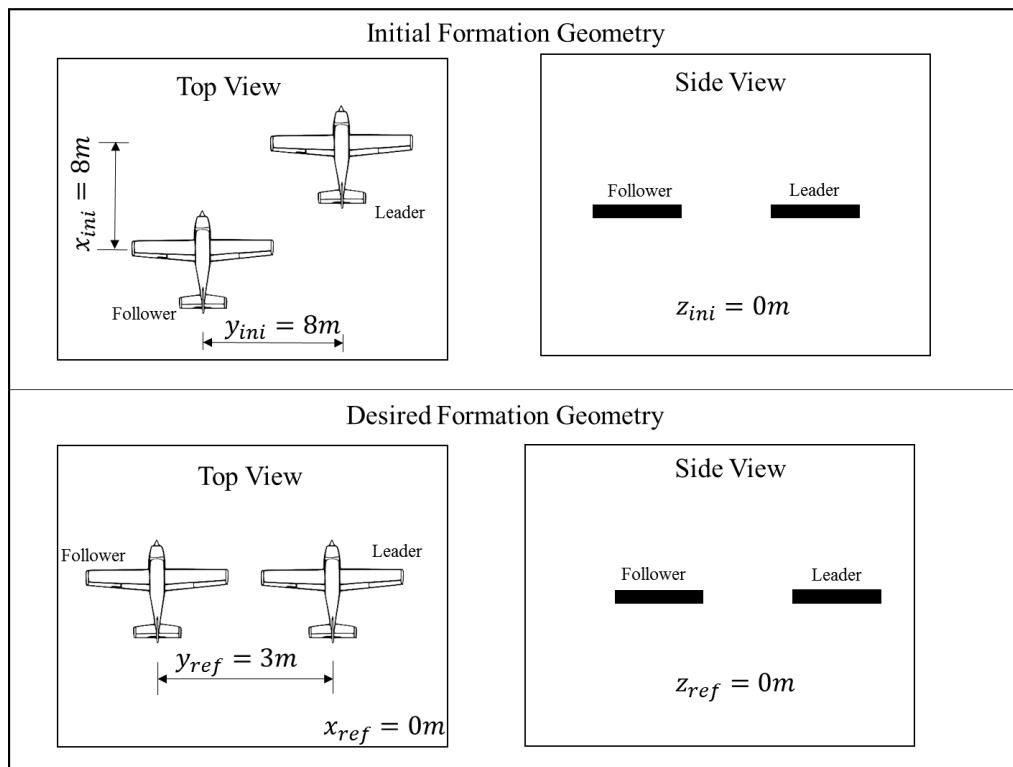
Figure 4.26: Initial and Desired Formation Geometries, Case 3, Lyapunov
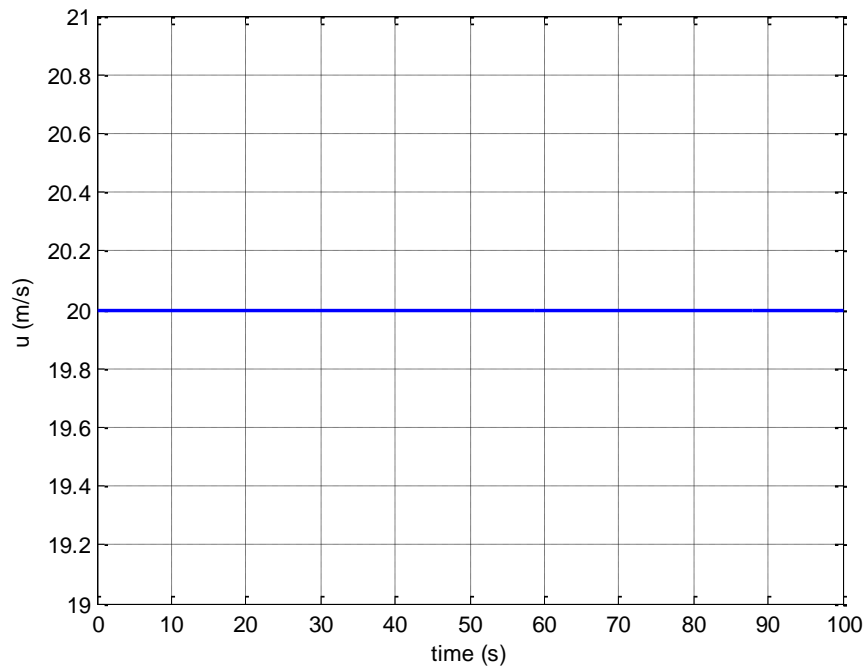
Figure 4.27: Time history of leader UAV's velocity, Case 3, Lyapunov
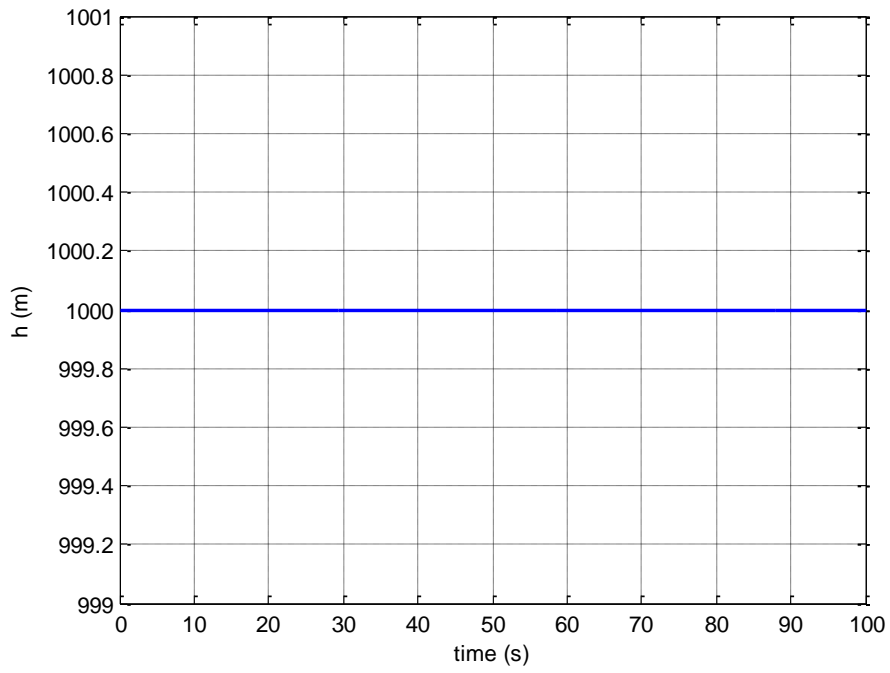
Figure 4.28: Time history of leader UAV's altitude, case 3, Lyapunov
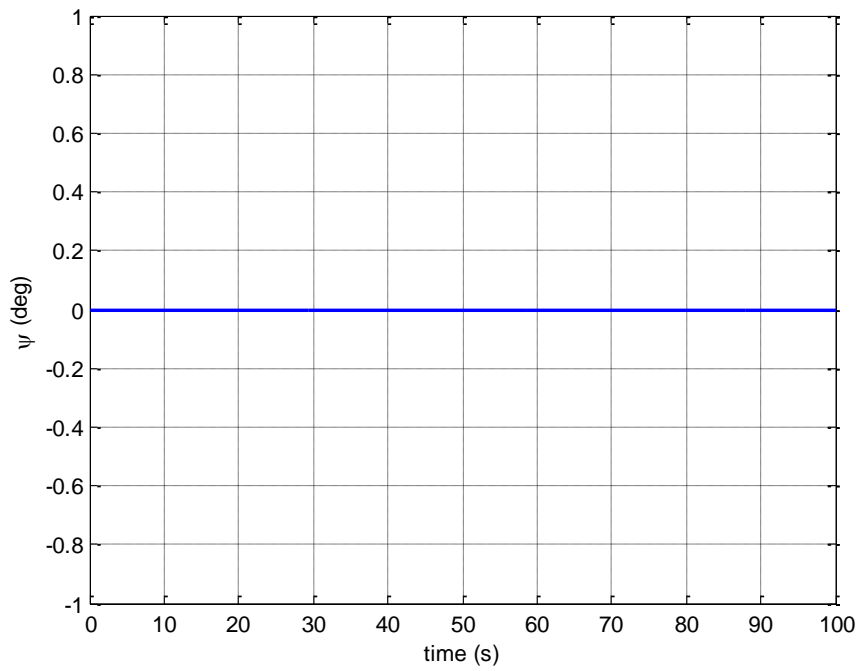
Figure 4.29: Time history of leader UAV's heading, Case 3, Lyapunov
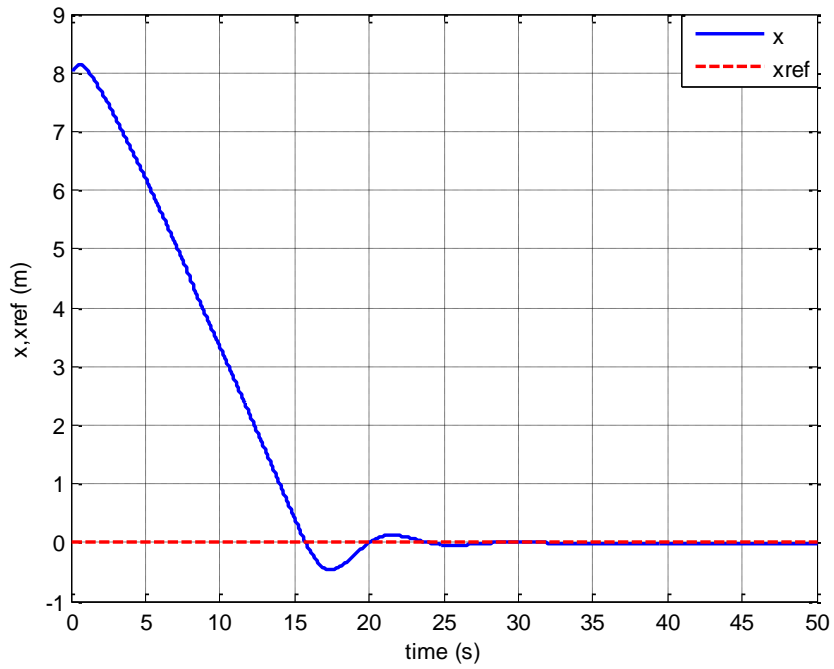
Figure 4.30: Time history of the follower UAV's relative position, x-component, Case 3, Lyapunov
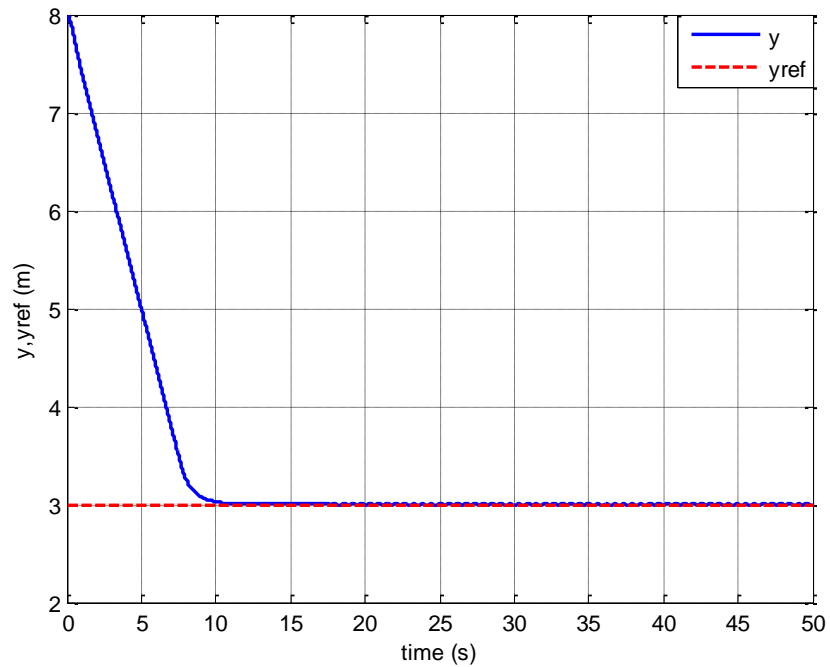

Figure 4.31: Time history of the follower UAV's relative position, y-component, Case 3, Lyapunov
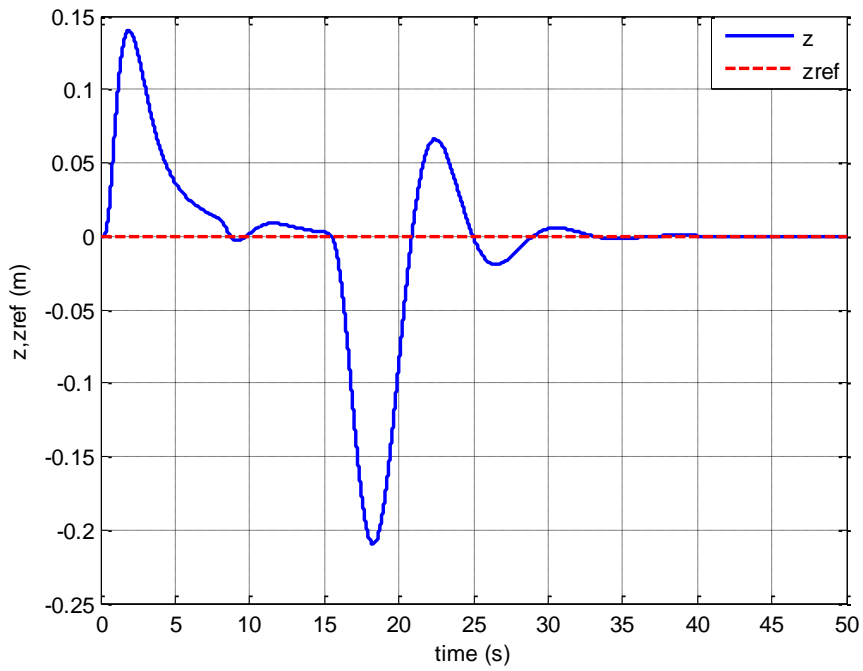
Figure 4.32: Time history of the follower UAV's relative position, z-component, Case 3, Lyapunov
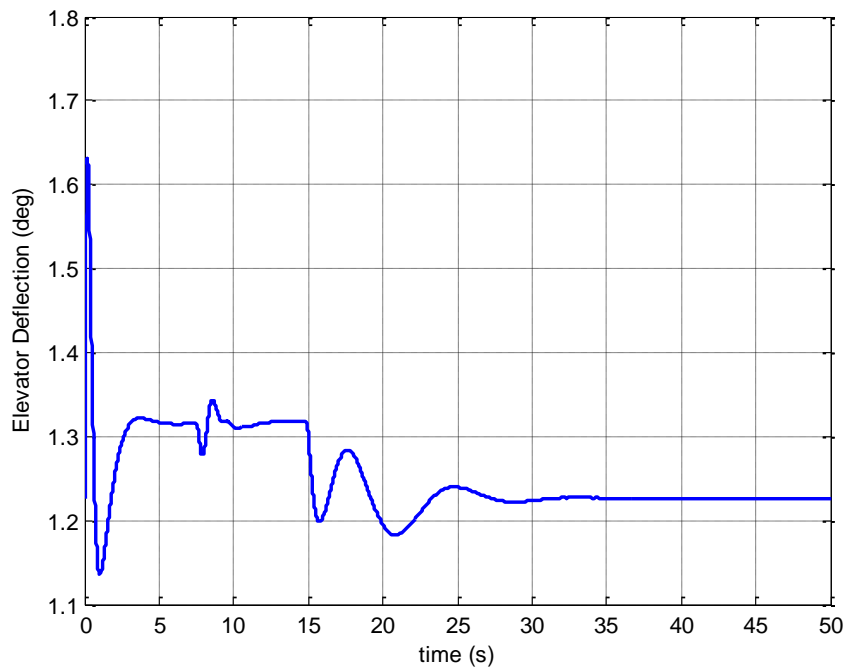
Figure 4.33: Time history of the elevator deflection, Case 3, Lyapunov

94
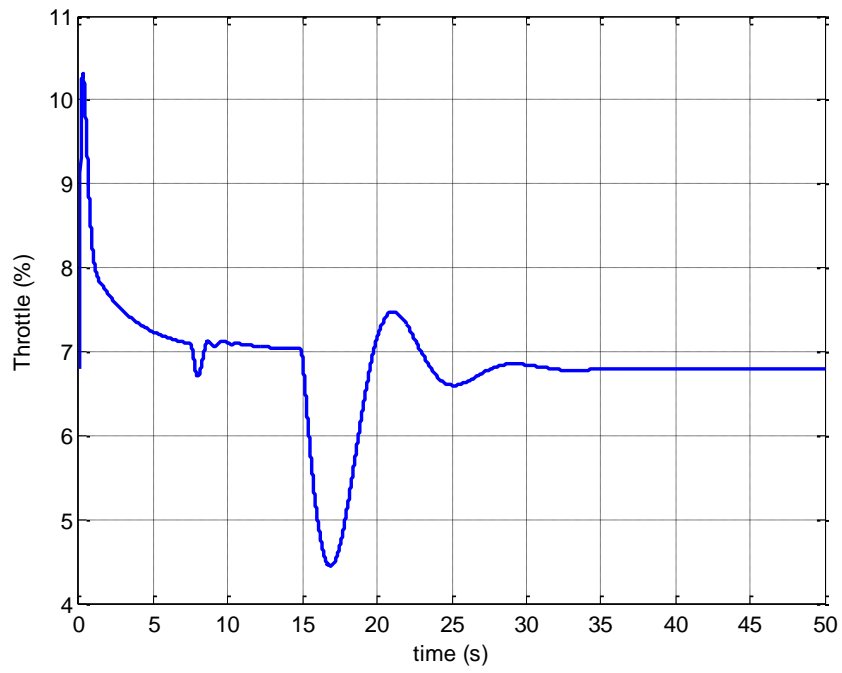
Figure 4.34: Time history of the throttle, Case 3, Lyapunov
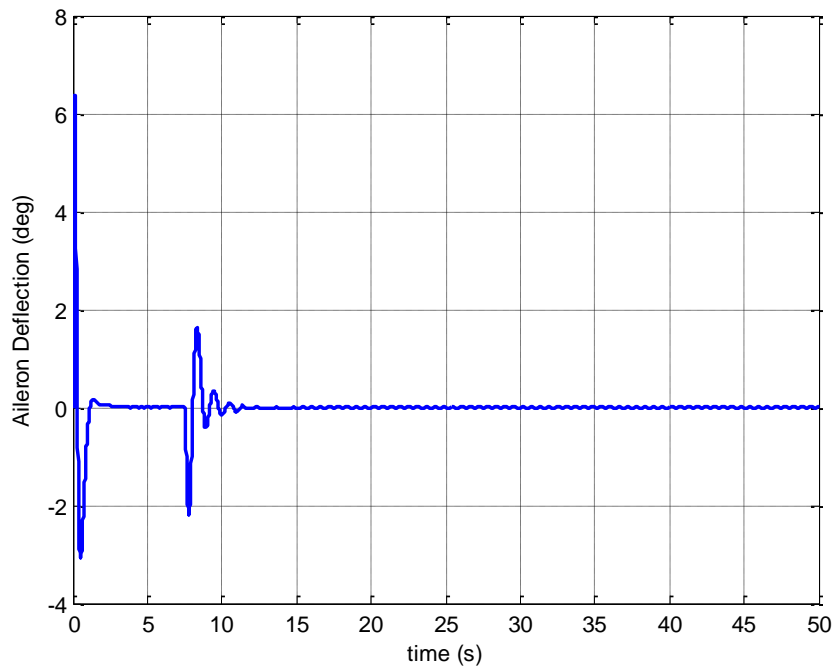
Figure 4.35: Time history of the aileron deflection, Case 3, Lyapunov

95
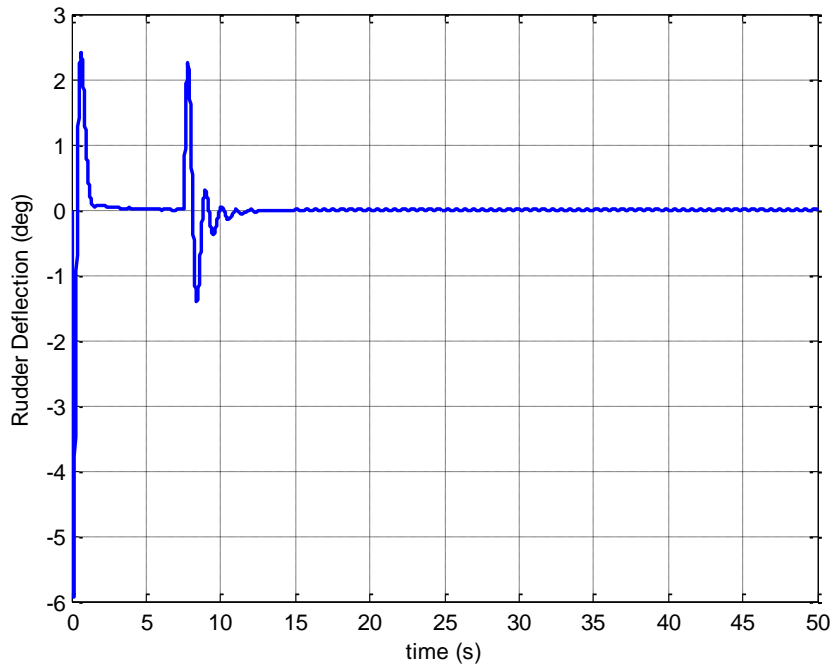
Figure 4.36: Time history of the rudder deflection, Case 3, Lyapunov
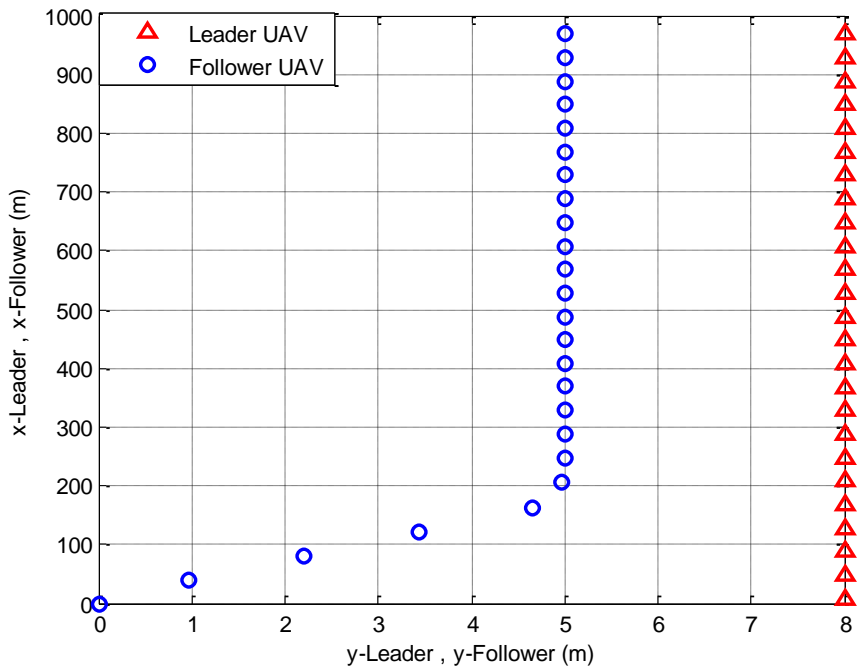
Figure 4.37: Leader UAV position vs Follower UAV position, Case 3, Lyapunov

For this formation flight scenario, the leader UAV flies at a constant velocity of 20 m/s as seen in figure 4.27. Its altitude is kept constant at a 1000m, figure 4.28 and it flies at a constant heading of 0 degrees, figure 4.29. The initial x-separation between the leader UAV and follower UAV is 8m. It is desired that this separation be brought to 0m. Figure 4.30 shows us the time history of the relative x-separation between the leader and follower UAV. From the figure, we see that the follower is able to track the desired x-separation in about 20 seconds without a steady state error. For a desired x-separation of 0m, we normally would have a singularity problem as shown in equation (57), but by using the workaround developed in section 4.2 whereby the x value in the $\begin{bmatrix} y & -1 \\ -x & 0 \end{bmatrix}^{-1}$ matrix of the Lyapunov formation-hold controller is set to 0.5 for cases where $-0.5 \leq x \leq 0.5$, we avoid this problem. The result obtained in figure 4.30 validates the efficacy of the workaround developed. Figure 4.31 shows the relative y-separation between the leader and the follower UAV, the two UAVs are initially at a y-separation of 8m. It is desired that this separation be brought to 3m. We see from the figure that the follower UAV is able to track the desired y-separation of 3m. From the figure, we have a settling time of about 10 seconds and no steady state error is seen. It is also desired that the leader and follower UAV fly level with one another i.e. they maintain a z-separation of 0m. From figure 4.32, we see that the relative z-separation between the two UAVs is practically kept at 0m. From the figure, the follower UAV veers off 0m by about 15cm in the first 10 seconds and then by about -20 cm in the next 10 seconds before settling at zero after 30 seconds of simulation . This deviations from 0m by a few centimeters is acceptable. Figures 4.33 to 4.36 show the time histories of the deflections of the control surfaces of the follower UAV as it tracks the desired formation geometry. We see no saturations in any of the deflections of the control surfaces as none of them deflect to their maximum angle limit. The deflection limit for the aileron and elevator is $\pm$ 20 degrees, and for the rudder, its $\pm$ 15 degrees. In figure 4.33, we see that the elevator deflects between 1.1 degree and 1.7 degrees. This little deflection angle is expected because the follower and leader UAV are initially flying level with each other and it is desired that they both keep flying level. Thus, a climb or descent of the follower UAV is not necessary, hence not much deflection is needed in the follower UAVs elevator. Figure 4.34 shows the percentage change in throttle. An initial rise in throttle can be seen, this is because the follower UAV needs to increase its velocity to cut its x-separation from the leader UAV from 8m to 0m. A drop in throttle is then seen since as soon as the leader approaches 0m, it needs to slow down to match the leader UAV's velocity. Figure 4.35 shows aileron deflection. From the figure, the aileron deflects within the range of -3 degrees and 6 degrees. These values are below the maximum deflection angle limit of the aileron which is $\pm$ 20 degrees. Figure 4.36 shows the rudder deflection. From the figure, the rudder deflects within the range of -6 degrees and 2 degrees. These values are also below the maximum deflection angle limit of the rudder which is $\pm$ 15 degrees. Figure 4.37 shows us the positions of both the leader UAV and the follower UAV. From the figure, we see how the follower UAV changes its relative y separation from the leader UAV from 8m to 3m as desired. We can also see that the two UAVs fly side by side each other.

From the above simulations provided in case 1, 2, and 3, we can conclude that our Lyapunov formation control system is very effective in enabling the follower UAV track a formation geometry while the leader UAV flies at a prescribed trajectory.

CHAPTER 5

PERFORMANCE COMPARISON BETWEEN THE LYAPUNOV BASED AND SDRE BASED FORMATION CONTROL SYSTEM

5.1 Lyapunov vs SDRE

In this thesis, two nonlinear control algorithms i.e. the Lyapunov control algorithm and the SDRE control algorithm were employed in the design of a formation control system for two UAVs. The control approach, implementation and performance of the SDRE based and Lyapunov based formation control systems are given in chapter 3 and chapter 4 respectively. In this chapter, comparisons between the two formation control systems will be made. To do this comparison, the two formation-hold controllers i.e. Lyapunov and the SDRE are tuned to have similar settling time in tracking a desired formation geometry. The resulting control effort for both formation control systems are then compared to each other to see which of the system require less control effort. In other words, we would like to see which of the formation control systems is less demanding on the follower UAV's control surfaces for a similar tracking performance.

The formation flight scenario in case 1 of section 4.4 is employed in testing the performance of the two formation control systems. In that formation flight scenario, the leader and follower UAVs are initially flying at separation distances of $(x_{ini}, y_{ini}, z_{ini}) = (9, 8, 0)$ m. It is desired that the follower's relative position be brought to $(x_{ref}, y_{ref}, z_{ref}) = (6, 4, 5)$ m while the leader UAV's velocity is increased from 20m/s to 26m/s and the leader UAV's altitude and heading is kept constant at 1000m and 0 degree respectively. The results for the z-component of the two formation-hold controllers is not presented here because as stated in section 2.2, the formation-hold controller only handles the x and y component of the relative position. For the z-component, an altitude controller is implemented on the follower UAV. Input to this altitude controller is the leader UAV's altitude plus the desired offset, z_{ref}.
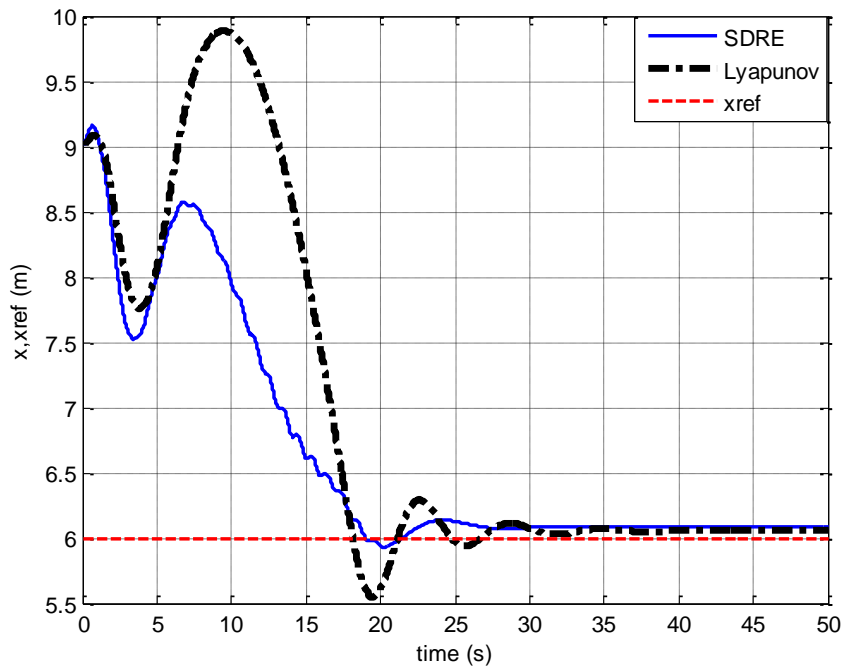
Figure 5.1: Time history of the follower UAV's relative position, x-component, Lyapunov vs SDRE
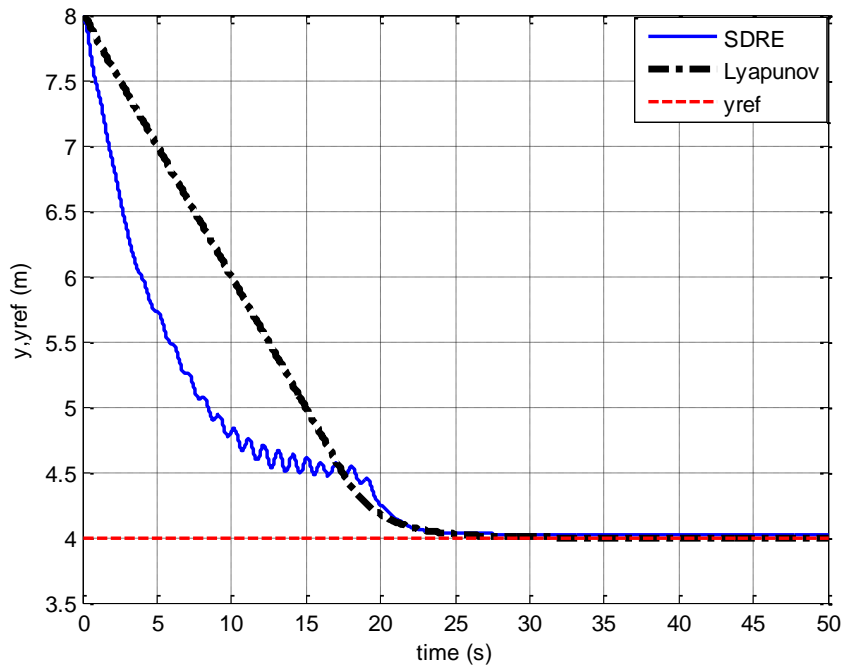
Figure 5.2: Time history of the follower UAV's relative position, y-component, Lyapunov vs SDRE

100
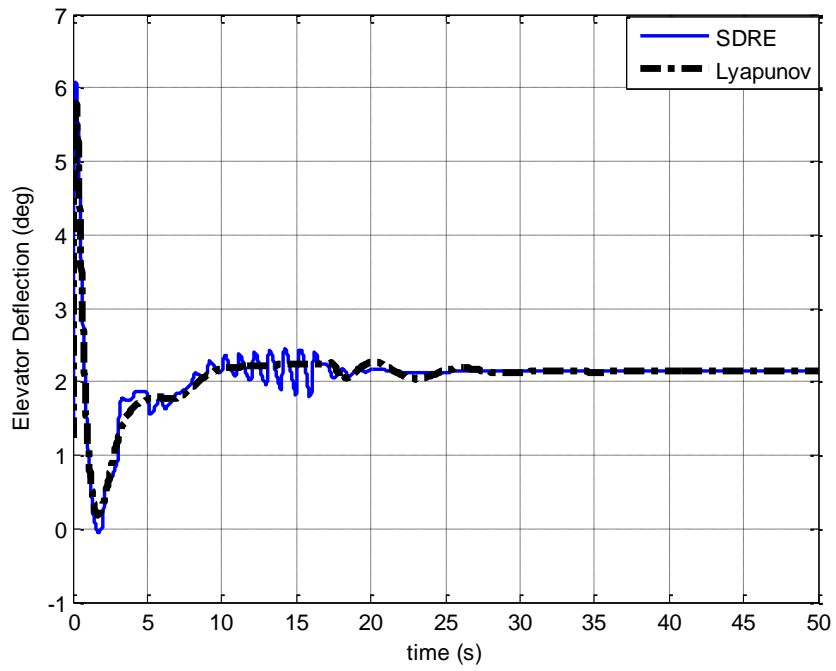
Figure 5.3: Time history of the elevator deflection, Lyapunov vs SDRE
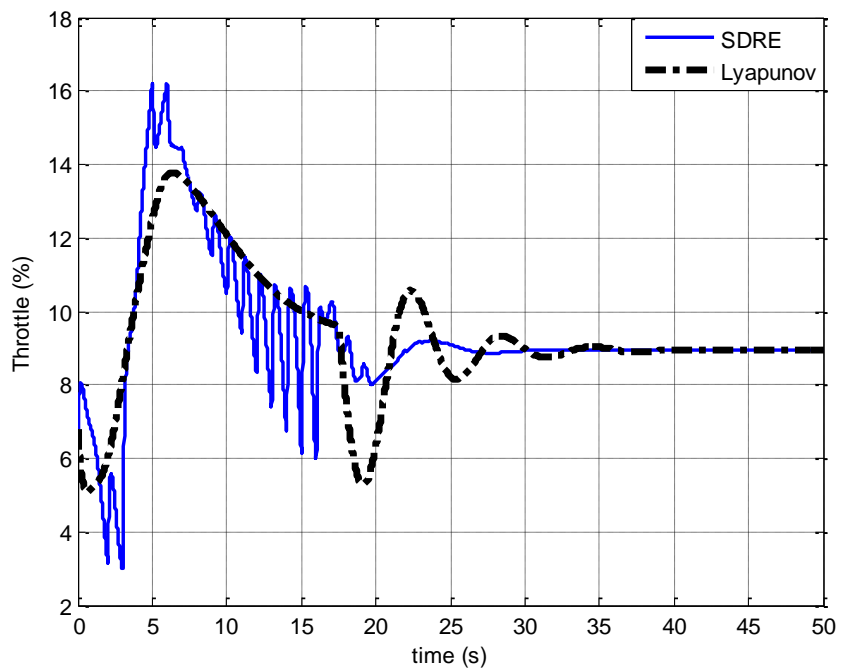
Figure 5.4: Time history of the throttle, Lyapunov vs SDRE
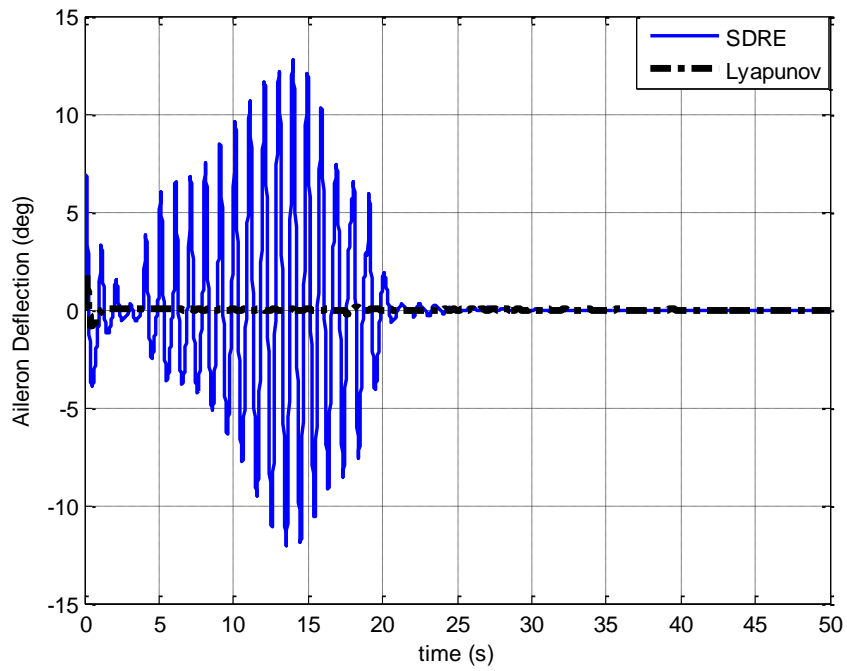
Figure 5.5a: Time history of the aileron deflection, Lyapunov vs SDRE
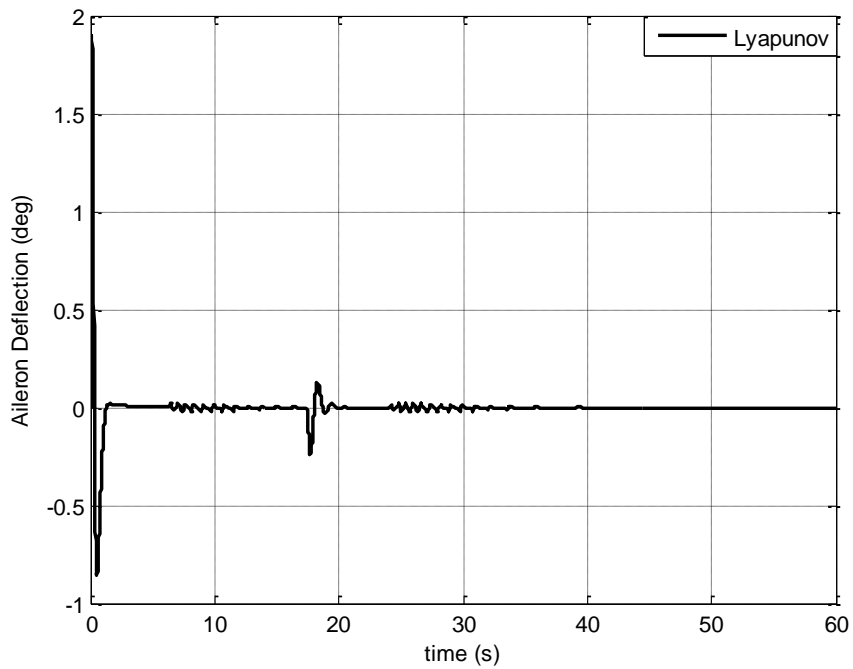
Figure 5.5b: Time history of the aileron deflection, Lyapunov
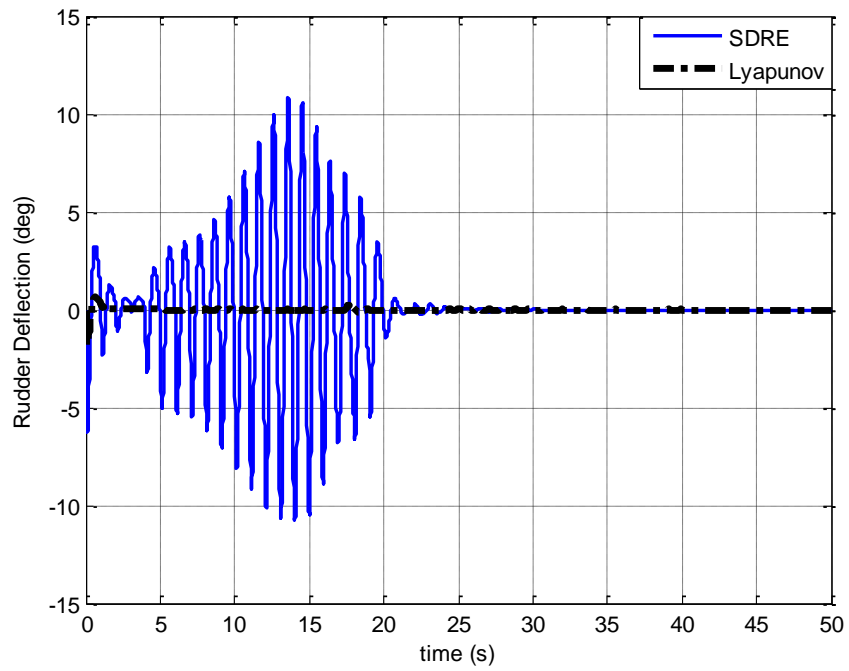
Figure 5.6a: Time history of the rudder deflection, Lyapunov vs SDRE
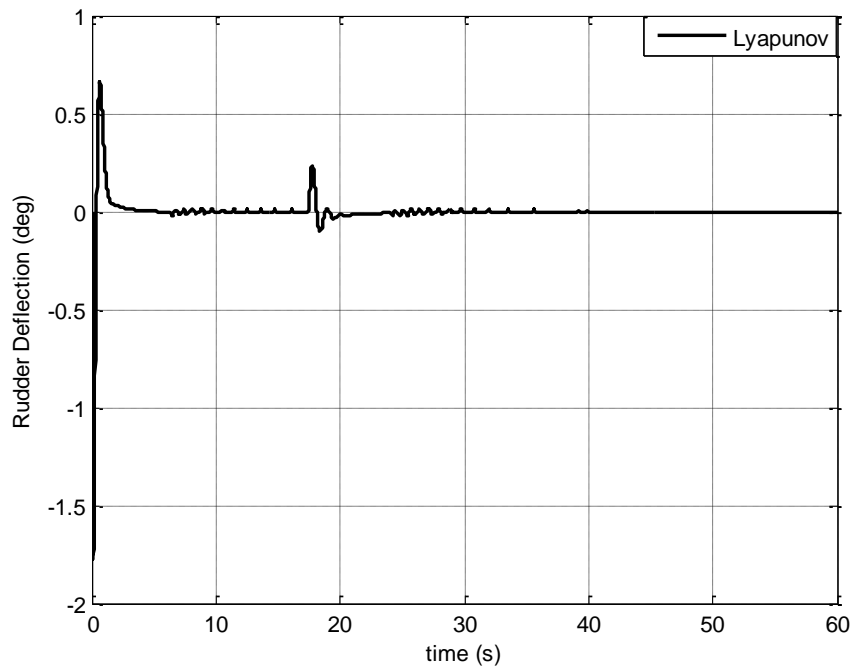

Figure 5.6b: Time history of the rudder deflection, Lyapunov

Figure 5.1 shows the time history of the x-component of the follower UAV's relative position to the leader UAV for both the Lyapunov formation control system and the SDRE formation control system. The two formation control systems were tuned to have similar tracking performances, specifically, similar settling times. From the figure, the SDRE system has a settling time of about 25 seconds while the Lyapunov system has a settling time of about 26 seconds. Figure 5.2 shows the time history of the y-component of the follower UAV's relative position to the leader UAV for both the Lyapunov formation control system and the SDRE formation control system. The settling time for the two systems is about 22 seconds. However, the Lyapunov system has a smoother performance as compared to the SDRE system. We see oscillations in the response of the SDRE system between 10 seconds are 20 seconds which are absent in the response of the Lyapunov system. Having tuned the two formation control systems to have similar settling times, we now compare the control effort for both systems by looking at the deflections of the control surfaces in both systems. Figure 5.3 shows the time history of the elevator deflection for both systems. The elevator for both systems deflected in a very similar manner. The deflection angles of the elevator are practically the same for both systems. However, between 10 seconds and 20 seconds of simulation, the deflection of the elevator for the SDRE based system is more oscillatory than that of the Lyapunov based system. Figure 5.4 shows the time history of the throttle for both systems. The percentage change in throttle for the Lyapunov based system is a lot smoother than that of the SDRE based system. However, magnitude wise, the percentage change is throttle for both systems is similar. The time history of the aileron deflection for both systems can be seen in figure 5.5a. The Lyapunov based system outperforms the SDRE based system. We can see from the figure that the demand on the aileron for the SDRE based system is a lot higher than that of the Lyapunov based system. The aileron in the Lyapunov based formation control system only deflects between -1 degrees and 2 degrees while the aileron in the SDRE formation control system deflects between $\pm$ 12 degrees. The aileron deflection for the SDRE system is also a lot more oscillatory than that of the Lyapunov based system. Figure 5.6a shows the rudder deflection for both the SDRE based and the Lyapunov based formation control system. The Lyapunov based system aslo outperforms the SDRE based system in this aspect. The rudder deflection in the SDRE based system is a lot more oscillatory than that of the Lyapunov based system. The demand on the rudder in the SDRE based system is higher than the demand on the rudder in the Lyapunov based system. In figure 5.6a, we see that the rudder in the SDRE based system deflects between ± 10 degrees, while in figure 5.6b, we see that the rudder for the Lyapunov based system deflects between -1.7 degrees and 0.7 degree. Thus, we can conclude that for a similar tracking performance, the Lyapunov based system requires less control effort than the SDRE based system and hence, has a better overall performance.

The results presented above and the conclusions made are for the particular formation flight scenario in case 1 of section 4.3, but in general, it is expected that response of the SDRE based system will be more oscillatory than the response of the Lyapunov based system. It is also generally expected that the control effort of the SDRE based system will be higher than that of the Lyapunov based system. The oscillations in the response of the SDRE based system as well as the increased control effort is as a result of the SDRE feedback gain update rate. Every time the feedback gain is updated, the control surfaces will have to deflect to track the new control signals gotten thereby increasing the demand on the control surfaces.

The shorter the interval between gain update rates, the higher the deflection rate of the control surfaces but the better the tracking performance.

CHAPTER 6

CONCLUSION AND FUTURE WORK

6.1   Conclusion

In this thesis, an algorithm for the autonomous formation flight of two UAVs is designed. From the literature survey, we found out about the various approaches to solving the autonomous formation flight problem. The leader-follower approach to formation flight is employed in this thesis because of the ease in implementing it and also because its approach is similar the approach employed in real life manned formation flights. In the Leader-follower approach to formation flight, the leader maintains a prescribed trajectory while the followers track a fixed relative distance from the neighboring aircraft. To solve the formation control problem associated with the leader-follower approach, two nonlinear controllers were designed. An SDRE based controller and a Lypunov based controller. Nonlinear controllers were used because the associated formation kinematic equations of the relative distances of the two UAVs are nonlinear. These nonlinear controllers which are the formation-hold controllers generate the required guidance laws to enable the follower UAV track the desired formation geometry.

The formation control system designed in this thesis is a two-loop structured control system. In the outer loop, the formation-hold controller, or the guidance algorithm is implemented. The actual relative position of the follower UAV with respect to the leader UAV as well as the desired formation geometry i.e., the desired relative position of the follower UAV with respect to the leader UAV are sent to the formation-hold controller. The formation-hold controller determines the required guidance laws the follower UAV need to track to be able to maintain the desired formation geometry. These guidance laws are sent into the inner loop of our formation control system. In the inner loop, LQT controllers were designed to enable the follower UAV to track the respective signals i.e. guidance laws it receives from the formation-hold controller.

Simulations were carried out using MATLAB/SIMULINK software. To test the efficacy of our formation-hold control system, three formation flight scenarios were investigated for both controllers i.e., the SDRE based nonlinear controller and the Lyapunov based nonlinear controller. From the simulations, we see that both nonlinear controllers generated the required guidance laws to enable the follower UAV maintain the desired formation geometry in spite of maneuvers carried out by the leader UAV in all three flight scenarios.

From our simulation results, we arrived at the following conclusions:

- For a smoother tracking while using SDRE, a high update rate is needed but at the cost a higher deflection rate of the control surfaces which might not always be feasible. A lower gain update rate reduces the control surfaces deflection rate but at the sacrifice of tracking performance. Depending on the mission profile, a trade off would have to be made between tracking performance and the load on the control surfaces.

- By comparing the inner loop and outer loop eigenvalues of the SDRE formation control system, we found out that it is not absolutely necessary to ensure that all the outer loop eigenvalues are slower than the inner loop eigenvalues. The outer loop eigenvalues can be faster than a few of the inner loop eigenvalues.

- The Lyapunov based formation control system has a better overall performance than the SDRE based formation control system in the sense that it is less demanding on the control surfaces of the follower UAV.

- The Lyapunov based formation control system provide a smoother response than the SDRE based sytem in tracking the desired formation geometry. The SDRE based system is more oscillatory than the Lyapunov based system as a result of feedback gain update rate.

6.2   Future Work

Due to the fact that our formation geometry is specified in terms of relative distance, collision among the individual members of the formation flight can be easily avoided. However, the designed algorithm in this thesis does not take into account the presence of obstacles in the flight path of the formation. In future works, a scheme to enable the formation avoid obstacles in its path may be designed.

The formation kinematic equations used are only valid for a planar formation flight. In the future, a more general kinematic relation may be derived.

Simulations were carried out using linear models of UAVs. In the future, nonlinear models may be used to test the efficacy of our algorithm.

Due to the ease of implementation, the leader-follower approach was used. However, the downside of this approach is that it is not robust to leader failure. A different approach may be used in the future.

All the tests carried out were all software based. In the future, this algorithm may be implemented on actual UAVs.

REFERENCES

[1] David, G. *Unmanned Aerial Vehicles: Implications for Military Operations*, Occasional Paper No.16, Center for Strategy and Technology, Air War college, Air University, Maxwell Air Force Base, Alabama, July 2000.

[2] Sarris, Z. *Survey of UAV Applications in Civil Markets*, Technical University Crete, 2001.

[3] Ray, R.J., Cobleigh, B.R., Vachon, M.J. and John, C.S., *Flight Test Techniques Used To Evaluate Performance Benefits During Formation Flight*, NASA Dryden Flight Research Center, California, August 2002.

[4] Fowler, J. M., Andrea, R. D., "Distributed Control of Closed Formation Flight", *Proceedings of the Conference of Decision & Control*, Las Vegas, Nevada USA, December 2002.

[5] Patcher, M., D'Azzo, J.J., and Dargan, J., "Automatic Formation Flight Control," *Journal of Guidance, Control and Dynamics,* Vol. 17, No. 6, November-December 1994, pp. 1380-1383.

[6] Chiaramonti, M.; Giulietti, F.; Mengali, G., "Formation Control Laws for Autonomous Flight Vehicles," *Control and Automation, 2006. MED '06. 14th Mediterranean Conference on* , vol., no., pp.1,5, 28-30 June 2006.

[7] Van den Broek, T. H A; Van de Wouw, N.; Nijmeijer, H., "Formation control of unicycle mobile robots: a virtual structure approach," *Decision and Control, 2009 held jointly with the 2009 28th Chinese Control Conference. CDC/CCC 2009. Proceedings of the 48th IEEE Conference on,* vol., no., pp.8328, 8333, 15-18 Dec. 2009

[8] Kar-Han Tan; Lewis, M.A., "Virtual structures for high-precision cooperative mobile robotic control," *Intelligent Robots and Systems '96, IROS 96, Proceedings of the 1996 IEEE/RSJ International Conference on* , vol.1, no., pp.132,139 vol.1, 4-8 Nov 1996.

[9] Zhou Chao; Lei Ming; Zhou Shaolei; Zhang Wenguang, "Collision-free UAV formation flight control based on nonlinear MPC," *Electronics, Communications and Control (ICECC), 2011 International Conference on* , vol., no., pp.1951,1956, 9-11 Sept. 2011.

[10] Giulietti, F., Pollini, L., and Innocenti, M., "Formation Flight Control: A behavioral Approach," *AIAA Guidance, Navigation and Control Conference,* AIAA paper 2001-4239, Montreal, Canada, August 2001.

[11] Yunfei Zou, Prabhakar R. Pagilla, and Ryan T. Ratliff. "Distributed Formation Flight Control Using Constraint Forces", *Journal of Guidance, Control, and Dynamics*, Vol. 32, No. 1 (2009), pp. 112-120.

[12] Paul, T.; Krogstad, T.R.; Gravdahl, J.T., "UAV formation flight using 3D potential field," *Control and Automation, 2008 16th Mediterranean Conference on* , vol., no., pp.1240,1245, 25-27 June 2008.

[13] Galzi, D.; Shtessel, Y., "UAV formations control using high order sliding modes," *American Control Conference, 2006* , vol., no., pp.6 pp.,, 14-16 June 2006.

[14] Sattigeri, R, Calise, A.J. and Evers, J., "An Adaptive approach to Vision-based Formation Control," *AIAA-2003-5727 Guidance, Navigation and Control Conference,* Austin, TX, August 2003.

[15] çinem, T., "State Dependent Ricatti Equation(SDRE) Control: A survey", *proceedings of the 17th World congress, The International Federation of Automatic Control,* Seoul, Korea. July 16-18, 2008

[16] Pearson, J.D., "Approximation methods in optimal control". *Journal of Electronics and Control*, 13, 453-469, 1962.

[17] Wernli, A., Cook, G., "Suboptimal control for the nonlinear quadratic regulator problem". *Automatica*, 11, 75-84, 1975.

[18] Mracek, C.P. and J.R. Cloutier, "Control designs for the nonlinear benchmark problem via the state-dependent Riccati equation method". *International Journal of Robust and Nonlinear Control*, 8, 401-433, 1998.

[19] Dargan, J.L, *Proportional plus Integral Control of Aircraft for Automated Maneuvering Formation Flight* M.S Thesis, AFIT/GE/ENG/91M-03, Air force Inst. Of Technology, Wright-Patterson AFB, OH, March 1991.

[20] Desineni Subbaram Naidu, *Optimal Control Systems,* CRC Press LLC, 2003.

[21] Sinem Işık*, Flight Control System Design for an Over Actuated UAV against Actuator Failures*, M.S Thesis, Middle East Technical University, February 2010.

[22] Anderson, B.D.O and Moore, J.B. *Optimal Control Linear Quadratic Methods*, Dover Publications, 2007.

[23] Mclean, D. *Automatic Flight Control Systems*, Prentice Hall, New York, 1990.

[24] Khalil, H.K., *Nonlinear Systems*, Prentice Hall, 2002.

APPENDIX A

SIG RASCAL 110 LINEARIZED SYSTEM MATRICES

A.1 Longitudinal Dynamics of the Leader and Follower UAVs

$$
Along = \begin{bmatrix}
-0.0893 & 0.1064 & 0.3701 & -9.8039 & -0.0001 \\
-1.1273 & -7.4207 & 17.7733 & 0.2041 & -0.0010 \\
0.0406 & -0.3144 & -8.0281 & 0 & 0 \\
0 & 0 & 1 & 0 & 0 \\
0.0208 & 0.9988 & 0 & -20.0043 & 0
\end{bmatrix}
$$

$$
Blong = \begin{bmatrix}
-0.5302 & 0.1135 \\
-9.8269 & -0.0001 \\
-33.0768 & -0.0003 \\
0 & 0 \\
0 & 0
\end{bmatrix}
\quad
Xlong = \begin{bmatrix}
u \\ w \\ q \\ \theta \\ h
\end{bmatrix}
\quad
ulong = \begin{bmatrix}
\delta elev \\ \delta th
\end{bmatrix}
$$

A.2 Lateral Dynamics of the Leader and Follower UAVs

$$
Alate = \begin{bmatrix}
-0.4807 & -0.6362 & -20 & -9.8039 & 0 \\
-0.9700 & -8.2639 & 0.1482 & 0 & 0 \\
0.2808 & -0.3477 & -0.5848 & 0 & 0 \\
0 & 1 & -0.0208 & 0 & 0 \\
0 & 0 & 1.0002 & 0 & 0
\end{bmatrix}
$$

$$
Blate = \begin{bmatrix}
0 & 2.3139 \\
55.7042 & 1.0549 \\
-3.5463 & -7.8857 \\
0 & 0 \\
0 & 0
\end{bmatrix}
\quad
Xlate = \begin{bmatrix}
v \\ p \\ r \\ \phi \\ \psi
\end{bmatrix}
\quad
ulate = \begin{bmatrix}
\delta ail \\ \delta rud
\end{bmatrix}
$$

APPENDIX B

SIMULATION MODELS
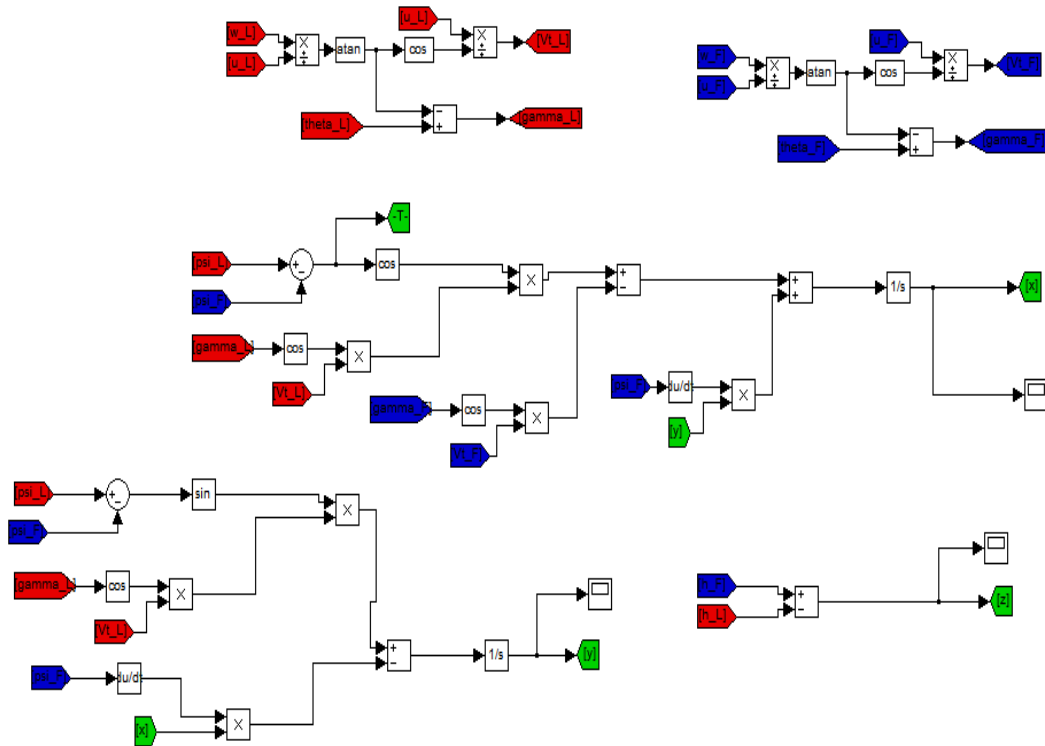
Figure B.1: Formation kinematics Model
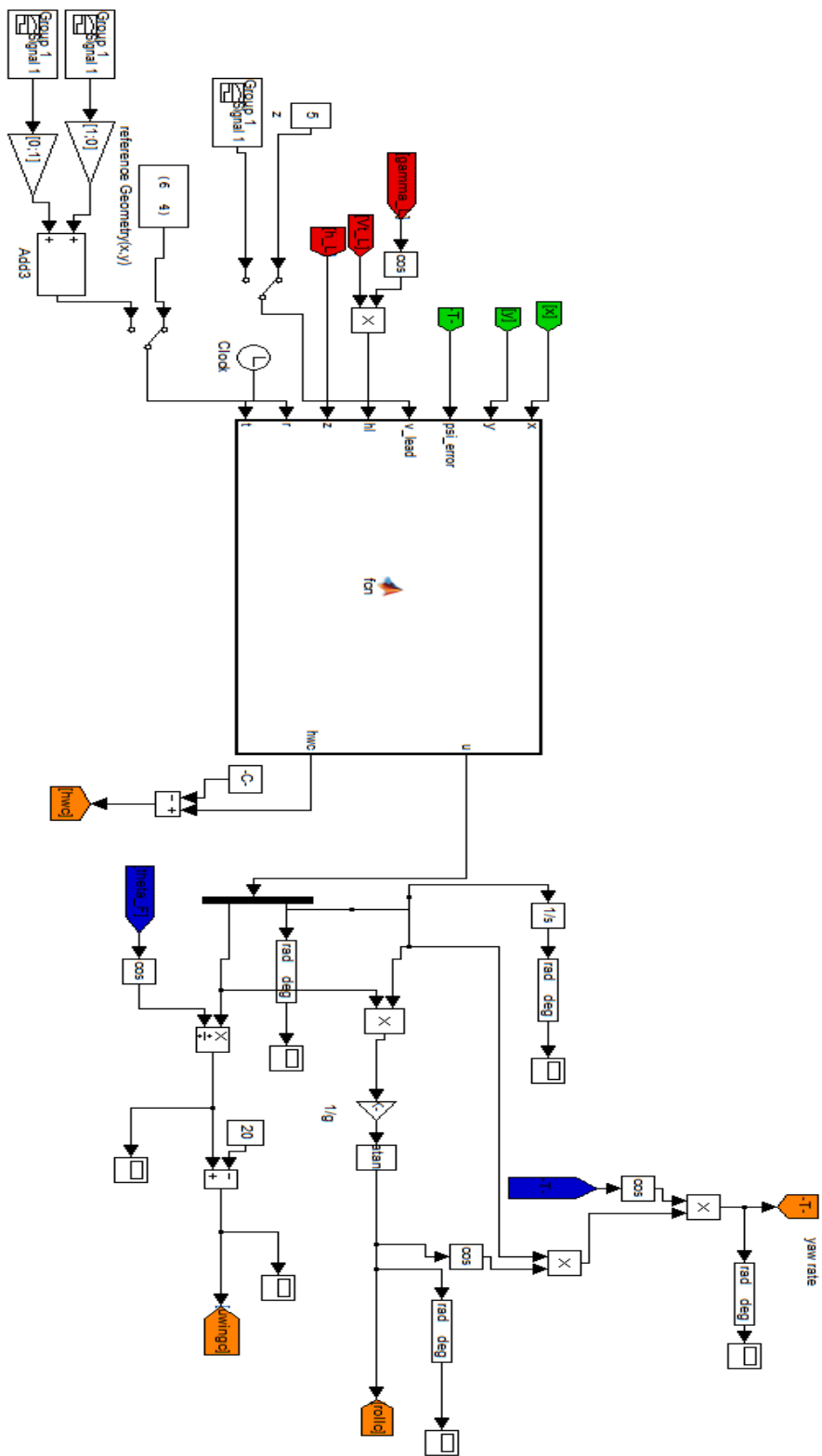
Figure B.2: Lyapunov/SDRE Formation-hold Controller Model